SYNTHESIS AND CHARACTERIZATION OF PERYLENE TETRACARBOXYLIC PROPARGYL ESTERS AS PRECURSOR MATERIALS FOR LIGHT-HARVESTING PERYLENE DERIVATIVES IN ORGANIC PHOTONIC APPLICATIONS

A THESIS SUBMITTED TO
THE BOARD OF GRADUATE PROGRAMS
OF
MIDDLE EAST TECHNICAL UNIVERSITY, NORTHERN CYPRUS CAMPUS

BY

MOHAMAD SAWALHA

IN PARTIAL FULFILLMENT OF THE REQUIREMENTS
FOR
THE DEGREE OF MASTER OF SCIENCE
IN SUSTAINABLE ENVIRONMENT AND ENERGY SYSTEMS PROGRAM

SEPTEMBER 2021

Approval of the Board of Graduate Programs

Prof. Dr. Cumali Sabah

Chairperson

I certify that this thesis satisfies all the requirements as a thesis for the degree of Master of Science

Assoc. Prof. Dr. Ceren Ince

Program Coordinator

This is to certify that we have read this thesis and that in our opinion it is fully adequate, in scope and quality, as a thesis for the degree of Master of Science.

Asst. Prof. Dr. Mustafa Erkut Özser

Supervisor

Examining Committee Members

Asst. Prof. Dr. İme Akanyeti	Environmental Engineering Dept. CIU	
Asst. Prof. Dr. Mustafa Erkut Özser	Chemistry Group. METU NCC	
Assoc. Prof. Dr. Murat Fahrioğlu	EEE Program. METU NCC	

I hereby declare that all information in this document has been obtained and presented in accordance with academic rules and ethical conduct. I also declare that, as required by these rules and conduct, I have fully cited and referenced all material and results that are not original to this work.

Name, Last name : Mohamad Sawalha

Signature :

ABSTRACT

SYNTHESIS AND CHARACTERIZATION OF PERYLENE TETRACARBOXYLIC PROPARGYL ESTERS AS PRECURSOR MATERIALS FOR LIGHT-HARVESTING PERYLENE DERIVATIVES IN ORGANIC PHOTONIC APPLICATIONS

Sawalha, Mohamad
Master of Science, Sustainable Environment and Energy Systems Program
Supervisor: Asst. Prof. Dr. Mustafa Erkut Özser

SEPTEMBER 2021, 95 pages

In this study, two isomerically pure perylene tetracarboxylic propargyl ester derivatives (P4 and P11) were synthesized and characterized to be used as intermediate compounds for bipolar perylene derivatives. The synthesized intermediates are extremely valuable and versatile building blocks, and their optical, photophysical, and electrochemical properties can be further tuned by the attachments of suitable electron-donating groups at the peri or bay positions.

Electron-donor azidofluorene was combined with the electron-acceptor perylene tetracarboxylic propargyl ester derivatives (P4 and P11) and new D-A type bipolar molecules (P6 and P12) were obtained. Photophysical, electrochemical, and thermal properties of the synthesized molecules were studied. UV-Vis and emission spectra, fluorescence quantum yield, lifetime, and HOMO-LUMO energy levels were determined and discussed. The synthesized molecules have a great potential to be utilized in organic photonic applications such as dye-sensitized solar cells (DSSCs) and organic light-emitting diodes (OLEDs) owing to their charge transfer and light-harvesting abilities.

Keywords: Perylene imides, Organic Photovoltaics, DSSC, Light-harvesting molecules, Photophysics.

ÖZ

ORGANİK FOTONİK UYGULAMALARDA IŞIK HASADI YAPAN PERİLEN TÜREVLERİ İÇİN ÖNCÜ MATERYAL OLARAK PERİLEN TETRAKARBOKSİLİK PROPARGİL ESTERLERİN SENTEZİ VE KARAKTERİZASYONU

Sawalha, Mohamad
Yüksek Lisans, Sürdürülebilir Çevre ve Enerji Sistemleri
Tez Yöneticisi: Yrd. Doç. Dr. Mustafa Erkut Özser

Eylül 2021, 95 pages

Bu çalışmada iki izomerik olarak saf perilen tetrakarboksilik propargil ester türevi (P4 ve P11) sentezlenmiştir. Sentezlenen moleküller bipolar perilen türevlerinin elde edilmesinde kullanılabilecek önemli ara ürünlerdir. Ara ürün olarak elde edilen moleküllerin peri ve körfez pozisyonlarına uygun elektron-verici grupların bağlanması ile bipolar yapıda farklı materyaller elde edilebilmekte ve elektron-verici grupların değiştirilmesi ile farklı optik, fotofiziksel ve elektrokimyasal özelliklere sahip materyaller elde edilebilmektedir.

Sentezlenen perilen tetrakarboksilik propargil ester türevleri (P4 ve P11), elektron-verici azidofloren grubu ile bir araya getirilerek, donor-akseptör (D-A) tipi bipolar moleküller (P6 ve P12) elde edilmiştir. Sentezlenen moleküllerin fotofiziksel, elektrokimyasal ve termal özellikleri araştırılmıştır. UV-Vis ve emisyon spektrumları, floresans kuantum verimi, floresans ömrü ve HOMO-LUMO enerji seviyeleri belirlenmiş ve tartışılmıştır. Sentezlenen moleküller, yük transferi ve ışık toplama yetenekleri nedeniyle boya duyarlı güneş pilleri (DSSC) ve organik ışık yayan diyotlar (OLED) gibi organik fotonik uygulamalarda kullanılmak üzere büyük bir potansiyele sahiptir.

Anahtar Kelimeler: Perilen imidler, organik fotovoltaikler, DSSC, ışık hasad edici moleküller, fotofizik

.

Every achievement requires self efforts as well as guidance and support from people, especially those who are very close to our hearts. This dissertation is dedicated to my loving family, whose encouragement made me able to complete this work successfully.

ACKNOWLEDGEMENTS

I would like to express my deepest gratitude to my supervisor Asst. Prof. Dr. Mustafa Erkut Özser, whose expertise, generous guidance, and support throughout my research made it possible for me to complete this dissertation successfully. I am also grateful to Dr. Saliha Öner, who helped me in every step during my laboratory work as well as my thesis writing. It was a pleasure working with them. I would also like to thank the jury members, Asst. Prof. Dr. İme Akanyeti, and Assoc. Prof. Dr. Murat Fahrioğlu for their suggestions and comments.

I sincerely thank all my teachers in the SEES program, the staff of the Chemistry group, my colleague teaching assistants, and all of my friends in METU-NCC especially Mehmet Tufan Kuvvet, who helped me in the laboratory work during my first academic year. Also, I gratefully acknowledge the support of METU-Ankara for the NMR analysis, and Dr. Hakan Bilgili for the optical and electrochemical measurements.

Finally, I am very grateful to my parents, Abdul Hakim Sawalha and Hana Al-Farran, my siblings, Hasan, Ghaida, Roaa, and Raghad for their love and support throughout my studies.

TABLE OF CONTENTS

LIST OF TABLES

TABLES

LIST OF FIGURES

FIGURES

LIST OF ABBREVIATIONS

ABBREVIATIONS

Btu	British thermal unit
$CDCl_3$	Deuterated chloroform
DCM	Dichloromethane
DMF	Dimethylformamide
DSSC	Dye-Sensitized Solar Cell
e^-	Electron
EET	Excited Energy Transfer
EIA	Energy Information Administration
EPA	Environmental Protection Agency
E_g	Optical band gap energy
$E_{1/2\ ox}$	Oxidation potential
$E_{1/2\ red}$	Reduction potential
FTIR	Fourier Transform Infrared
GHGs	Greenhouse gases
HOMO	Highest Occupied Molecular Orbital
IRENA	International Renewable Energy Agency
LUMO	Lowest Unoccupied Molecular Orbital
NMR	Nuclear Magnetic Resonance
UV-VIS	Ultraviolet-Visible

The text explains other symbols and abbreviations.

CHAPTER 1

INTRODUCTION

1.1 Background Statement

Energy is essential for developing economically, socially, and improving life quality all around the globe. Most of the world's energy is produced by traditional methods, consuming fossil fuels and producing greenhouse gases (GHGs). The enormous amounts of GHGs released from the energy sectors have raised a vital, challenging problem which is global warming. According to the United States Environmental Protection Agency (EPA), electricity and heat production have the highest amount of GHG emissions (United States Environmental Protection Agency, 2019).

Figure 1.1 shows the percentage of GHG emissions related to each sector. Electricity and heat production counts for 25% of the total GHG emissions, agriculture, forestry, and other land use comes second, counting for 24%, while industry, transportation, and others are responsible for 21,14 and 10 percent of the emissions, respectively.

The negative effects of global warming on climate change, human health, biodiversity, and many other aspects have been studied in the last years (Botkin et al., 2007; McMichael et al., 2006; Park et al., 2018). Even though some of the forecasts are uncertain, there is a huge concern and understanding of the negative effects of global warming. These concerns have raised the demand for developing and utilizing clean and renewable energy sources such as solar, wind, hydro, biomass, wave, and tidal energy (Panwar et al., 2011).

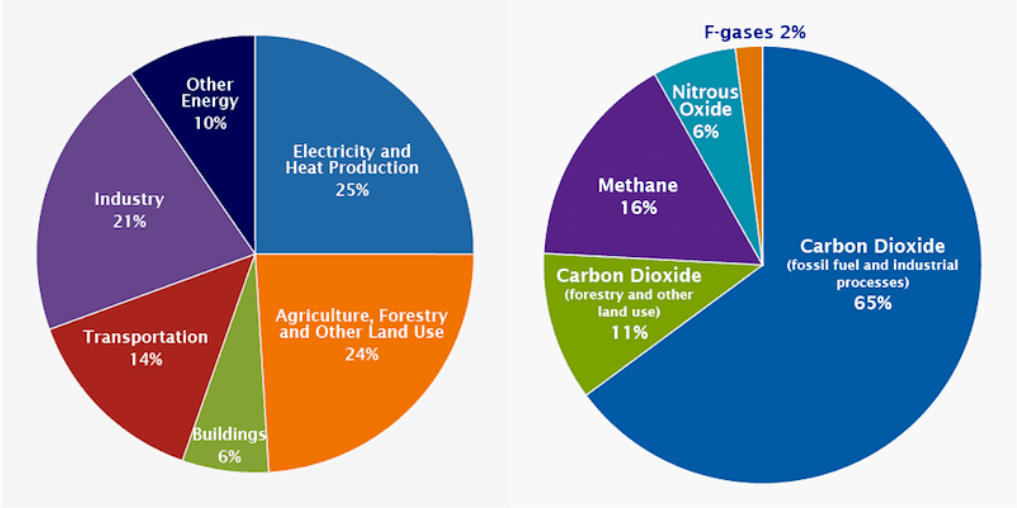

Figure 1.1. Sources of greenhouse gases emissions (United States Environmental Protection Agency, 2019).

The worldwide increasing demand for energy coupled with the depletion of fossil fuels reserves has raised the attention to find a new alternative to produce energy. The U.S. Energy Information Administration (EIA) predicts that the world energy demand will grow by 50% within the next 30 years (Newell et al., 2019). Figure 1.2 shows the dramatic increase in the global energy demand. In 2010, the global energy demand was around 530 quadrillion Btu and the demand is predicted to be around 900 quadrillion Btu in 2050. To meet this demand in a sustainable and environmentally friendly way, a mixture of renewable energy technologies is the solution for our future.

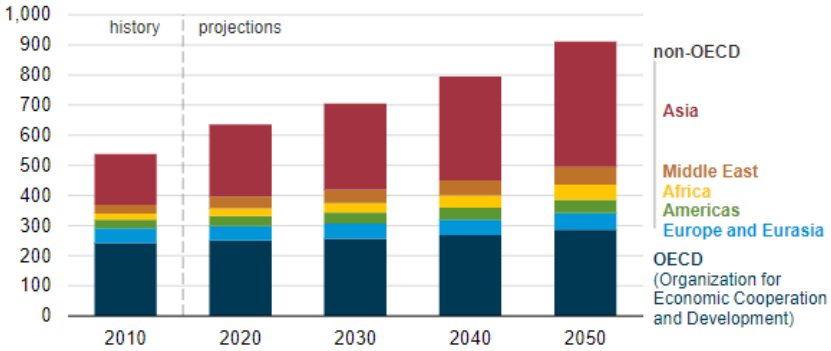

Figure 1.2. Energy consumption by region between the years 2010 and 2050 (quadrillion Btu) (Newell et al., 2019).

The worldwide usage of renewable energy is predicted to show a huge increase in the coming years. EIA predicted that the consumption of renewable energy will increase by 3.1% per year between 2018 and 2050, making renewable energy the major source of energy worldwide in 2050. Figure 1.3 shows that the worldwide consumption of renewable energy will increase from around 50 quadrillion Btu in 2018 to 250 quadrillion Btu in 2050. Renewable energy counts for 15% of the total energy consumption in 2018, rising to 28% in 2050 (Newell et al., 2019).

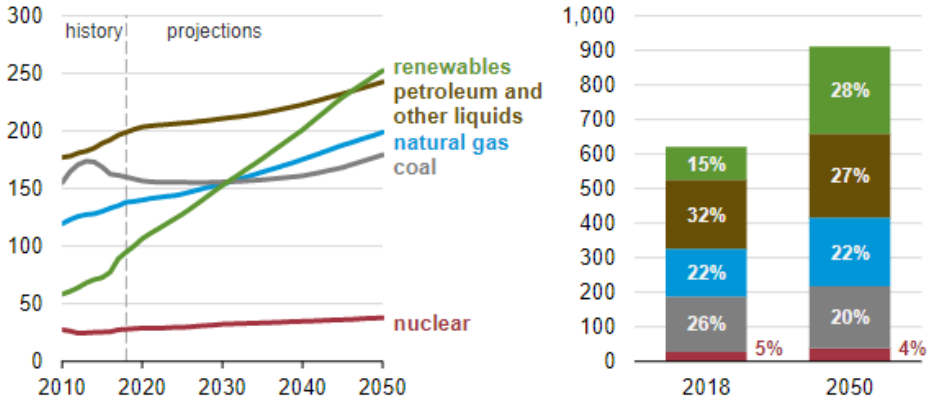

Figure 1.3. Worldwide energy consumption by energy source (quadrillion Btu)(Newell et al., 2019).

Renewable energy resources are proposed to be the most effective and efficient solution for global warming. However, to test whether these sources have a great potential for implementation, the economic, social, and environmental aspects should be considered. Among all the renewable resources, solar energy is the most promising technology to fulfill a worldwide increasing demand for energy (Kabir et al., 2018). The sun is the most abundant source of free energy for our planet. However, many obstacles stand in the way of implementing solar power technologies, including the low solar cell efficiencies, high cost, and environmental effect of disposal after the solar cells become obsolete (Kabir et al., 2018).

1.2 Problem Statement

The low efficiency of solar cells has been a major concern for the last few decades. The first silicon photovoltaic (PV) technology was invented in the United States with a 6% efficiency (Blandford and Watkins, 2009). Currently, new technologies are being employed to harvest solar radiation and generate electricity from it. Today's most efficient solar cells can reach efficiencies up to 39%. However, the high cost of these technologies makes it impossible to be commercially available (Dimroth, 2006). Most of the economically feasible and commercially available solar cells have efficiencies between 16 and 25% (Blakers et al., 2013; Lee, 2009). The capital cost of silicon-based photovoltaics is still quite expensive and the use of a toxic chemical in the manufacturing of photovoltaics is another concern. These aspects allowed the emerging of a new solar power technology called Dye-Sensitized Solar Cells (DSSC).

Dye-sensitized solar cells imitate the photosynthesis process used by plants. DSSCs use special dyes to harvest the photons coming from the sun. Dye molecules are sintered together on a mesoporous oxide layer of nanometer-sized particles. Photoexcitation of the dye allows the injection of an electron into the conduction band of the titanium oxide (TiO_2). Then, the dye is restored to its initial state by donating electrons from the electrolyte. The DSSC contains a redox system, usually iodine/triiodide couple to regenerate the sensitizer. Overall, the system generates electricity without suffering any permanent chemical transformation (Grätzel, 2003). The manufacturing of DSSCs is relatively easier than silicon-based solar cells. It is environmentally friendly and has a lower cost compared to silicon-based photovoltaics (Wu et al., 2011). The main disadvantage of DSSC is the low efficiency. Many researchers have reported DSSC efficiencies between 10% and 13% (Chiba et al., 2006; Ito et al., 2008; Mathew et al., 2014). One way to improve the DSSC efficiencies is to design and synthesize new & efficient dye molecules.

In this study; synthesis, characterization and study of the optical, photophysical and electrochemical properties of different perylene tetracarboxylic derivative sensitizers

are presented. Synthesized materials can be utilized as sensitizers in DSSC applications. Also, they have a potential to be used as emitter materials in other photonic applications such as OLEDs. The detailed literature review based on perylene-based dye molecules is presented in subchapter 2.3.

CHAPTER 2

LITERATURE REVIEW

2.1 Solar Energy

The sun is the largest inexhaustible source of energy for our planet Earth. Energy from the sun in the form of radiant light and heat supports almost all life on Earth. The amount of energy coming from the sun is larger than all of the other renewable and fossil-fuels based energy combined. One hour of sunlight is more than enough to supply energy for a whole year to the globe (Lewis, 2007). Solar energy can be harnessed via natural and man-made processes. The most important process is photosynthesis which is done by plants by harvesting solar radiations and converting them to chemical form. Synthetic processes to harvest solar energy involve a range of ever-developing technologies such as photovoltaics, concentrated solar panels, solar thermal energy, solar heating, and artificial photosynthesis. The most considerable advantage of solar energy is that it is a clean and sustainable energy source that can be supplied without causing any harm to the environment (Kalogirou, 2004). During the last century, most of our energy was supplied by fossil fuels because these are less costly and more convenient than other sources. However, with the recent concern about environmental pollution and global warming, renewable sources are the new alternative for energy production.

2.2 Photovoltaics

Photovoltaics (PV) technology is receiving great attention as a new approach to widespread sustainable energy production with increasing attention towards emission-free and sustainable energy production. Photovoltaic devices convert

radiant light coming from the sun into direct current (DC) electricity (Quaschning, 2014). Over the last decades, photovoltaic technology went through significant improvements regarding efficiency. Also, the cost of photovoltaic cells has received an incredible decrease in the last years, making it a more competitive source of energy to supply the increasing energy demand (Green, 2016).

It is important to look at the history of PV cells because there are lessons to be learned to help us improve the future of PV cells. In 1954, the first practical silicon solar cell was invented by Daryl Chapin in Bell Labs in the United States. The conversion efficiency of the solar cell was around 6% which was too inefficient to be used (Blandford and Watkins, 2009). Three years after his invention, Daryl Chapin and his colleagues received a patent for a new solar cell with an efficiency of 8%. In 1958, Hoffman Electronics created 9% efficient n-on-p silicon solar cells and they also commercialized a 10% efficient solar cell in the next year. Hoffman Electronic improved their solar cells to achieve an efficiency of 14% in 1960. Throughout the years, PV cells performance improved dramatically until 1985, when 20% efficient silicon solar cells were made by the Centre for Photovoltaic Engineering at the University of New South Wales. Photovoltaic Engineers at the University of New South Wales kept experimenting and developing new solar cells and in 2016, they successfully had a new world record for unforced sunlight conversion to electricity with an efficiency of 34.5%. A few years ago, First Solar created a commercial solar panel with 22.1% efficiency and it is currently the most dominant technology in the worldwide solar power market (Fraas and Fraas, 2014).

The cost of solar cells hindered the widespread of solar panels in the last few decades. However, the prices of photovoltaics have fallen dramatically in the last few years. In 2009, the installation cost of a solar panel was $8.50/watt. With the improvement in the efficiency and manufacturing processes, the price of solar panels has fallen by more than 65% in the last 10 years. Figure 2.1 shows that the cost of solar panels in the first half of 2015 was $3.79/watt, decreasing by 22% to reach $2.96/watt in the second half of 2019 (“solar panel cost and efficiency,” 2020). The prices of solar panels are projected towards a dramatic decrease, as the International Renewable

Energy Agency (IRENA) forecasts that the solar PV price will be reduced by 59% by 2025 ("IRENA Forecasts 59% Solar PV Price Reduction By 2025", 2020). These reductions and forecasts have driven the widespread installation of solar panels to make them the major source of energy in the future.

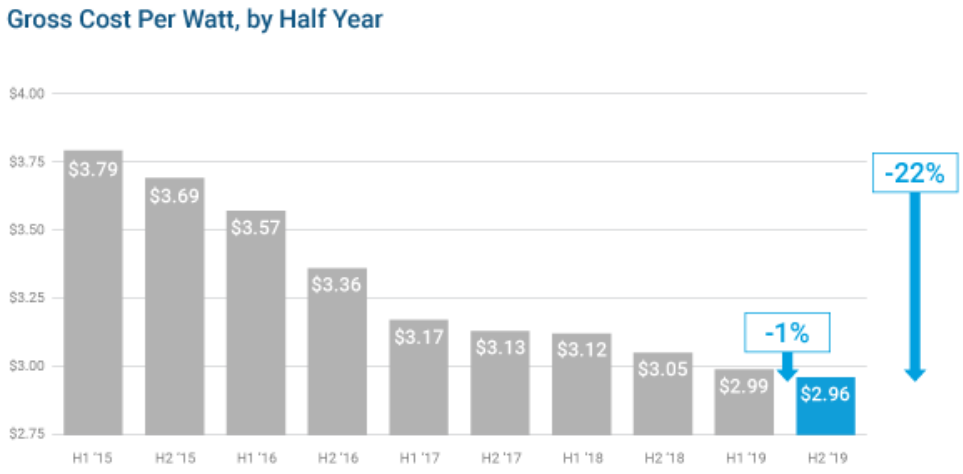

Figure 2.1. Cost of solar panels by half-year between 2015 and 2019 ("solar panel cost and efficiency," 2020)

Photovoltaics can be categorized into organic and non-organic (silicon-based) photovoltaics. The main difference between silicon solar cells and organic solar cells is the semiconductor material used. Silicon solar cells use silicon derivatives, while organic solar cells use carbon-based organic compounds to convert solar radiations into electricity. Each type has its advantages and disadvantages that will be discussed in the coming subchapters.

2.2.1 Silicon-based photovoltaic

Silicon-based solar cells are currently the most common solar power technology in the world. The widespread of silicon solar cells is driven by the ongoing improvement to both performance and cost. A silicon solar cell is composed of p-type and n-type semiconductor materials (i.e. silicon) placed together in physical

contact. When the photons coming from the sun is absorbed by the n-region, electrons are excited and move from n-type to p-type generating a hole in the n-region. This process is called exciton generation. Then, the exciton travels in the direction of p-n-junction, creating an electric field that can be collected by metallic contact, as illustrated in Figure 2.2 (Nelson, 2003; "Photovoltaic or solar cell," 2020). The efficiency of this type of solar cell depends mainly on the type of silicon used which limits the advancement of this technology to some level.

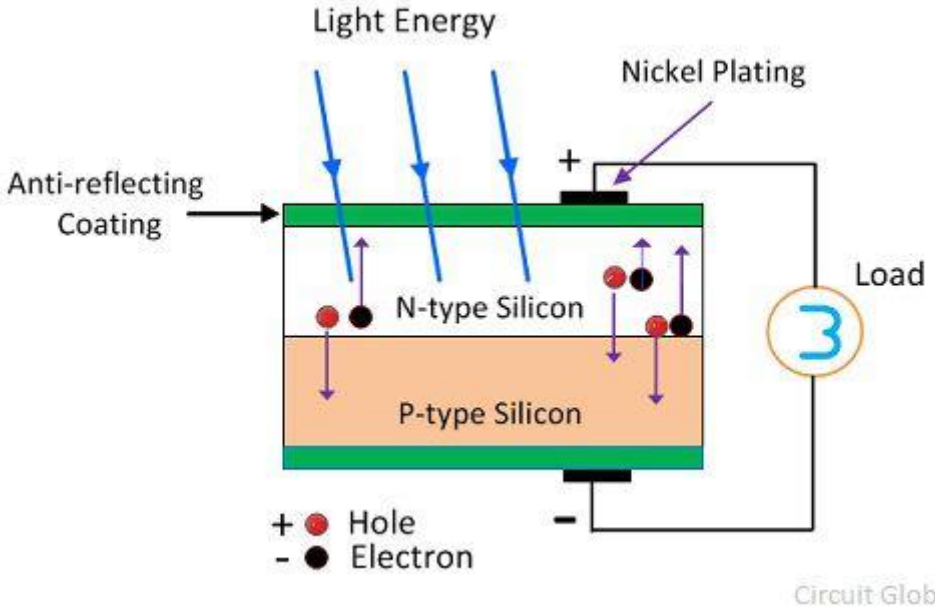

Figure 2.2. Mechanism of a silicon-based solar cell ("Photovoltaic or solar cell," 2020).

2.2.2 Organic photovoltaic

An organic photovoltaic (OPV) is a type of photovoltaic that utilizes organic semiconductors (OSC) - typically polymers or small molecules. This type of photovoltaics received significant attention due to promising qualities such as low manufacturing cost, lightweight, flexibility, and use of environmentally friendly raw materials (Hoppe and Sariciftci, 2004). When the light is absorbed by the OSC, the electrons are excited from the highest occupied molecular orbital (HOMO) to the

lowest unoccupied molecular orbital (LUMO), leaving a positively charged space called a 'hole'. The hole and electron become attracted because of their opposite charge creating an electron-hole pair known as an exciton. Then, the exciton diffuses to the donor-acceptor interface, where exciton dissociation happens. At the interface, the electron will move to the acceptor material while the hole will stay on the donor material. Lastly, the electrons will transfer to the cathode and the holes to the anode, and they are collected in an external circuit to produce electric current, as shown in Figure 2.3 (Ranabhat et al., 2016).

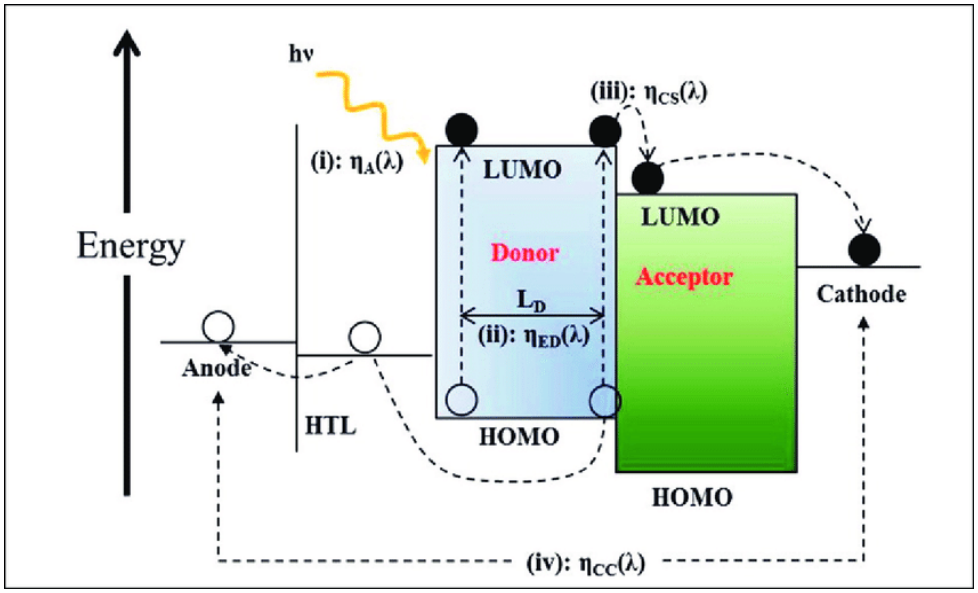

Figure 2.3. Mechanism of an organic solar cell (Ranabhat et al., 2016).

2.2.3 Dye-sensitized solar cells (DSSC)

A dye-sensitized solar cell is a branch of organic solar cells. DSSC has drawn more attention in the last years due to several attractive features such as ease of manufacturing, low cost of raw materials, using environmentally friendly materials, flexibility and semi-transparency. A DSSC is composed of a layer of TiO_2 nanoparticles, covered with a molecular organic dye that absorbs sunlight. Figure 2.4 illustrates the working principle of a DSSC. When the light is absorbed by the dye, the photosensitizers are excited from the ground state (S) to the excited state (S*).

Then, the excited electrons are injected into the conduction band of the TiO_2 electrode. The electrons travel from the TiO_2 to the counter electrode through an electric circuit, creating a current. The oxidized sensitizer accepts electrons from the iodide ion (I^-) in the electrolyte. The iodide (I^-) and triiodide (I_3^-) ions go through a continuous redox reaction and regenerate the sensitizer as shown by formulas (1) and (2) (Sharma et al., 2018).

(1) $S^* + e^- \rightarrow S$

(2) $I_3^- + 2e^- \rightarrow 3I^-$

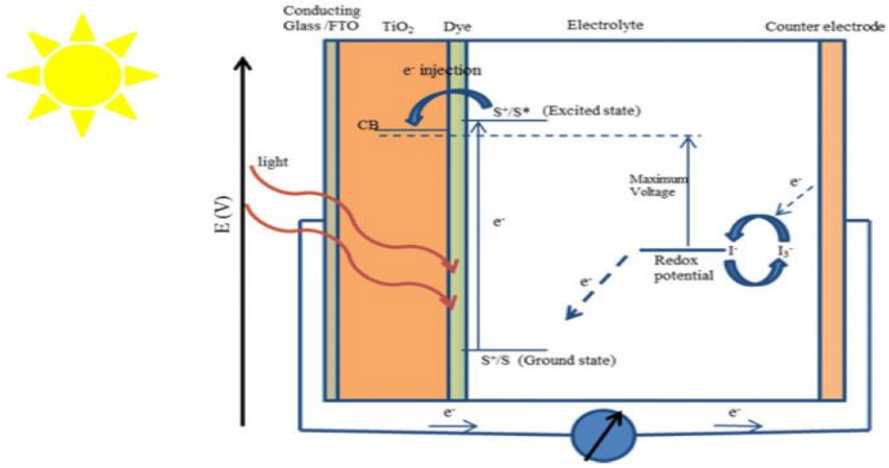

Figure 2.4. Working principle of a DSSC (Sharma et al., 2018).

2.3 Organic light-emitting diodes (OLEDs)

Over the past few years, organic light-emitting diodes (OLEDs) have been implemented in lights, mobile phones, and televisions due to the continued enhances in both performance and lifetimes. OLEDs consist of multiple layers namely; the cathode, emissive layer, conductive layer, anode, and substrate as shown in Figure 2.5. Each layer has a distinct function involving charge injection, charge transport, and light emission. The color and maximum efficiency of OLEDs are determined by the emissive layer, which can be created by using organic molecules or polymers as core components (Dayneko et al., 2020).

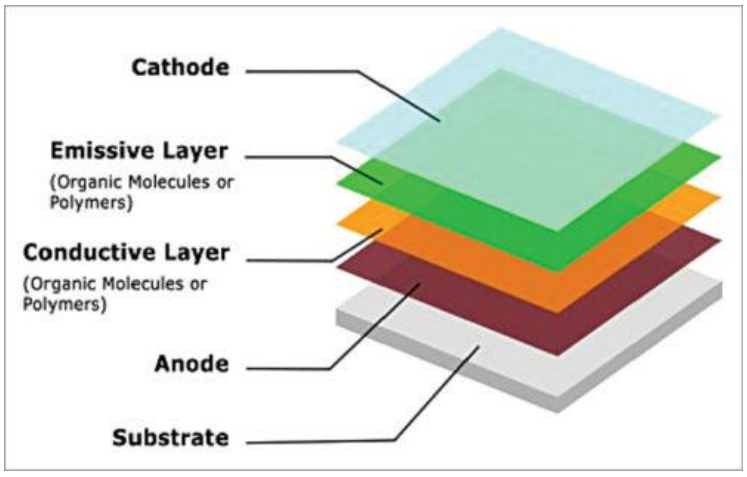

Figure 2.5. OLED architecture

Perylene derivatives are the most promising building block candidates to be used as an efficient emitter material in OLEDs among fluorescent organic molecules. This is due to their excellent quantum yield photoluminescence, high charge carrier mobility, and high thermal and photochemical stability (Dayneko et al., 2020; Bala et al., 2020; Dayneko et al., 2021; Gupta et al., 2018).

Dayneko et al. (2020) presented electrically pumped, solution-processed red OLEDs based on N-annulated perylene diimide dimer as the emitting material as shown in Figure 2.6. They concluded that the N-annulated perylene diimide-based materials have a great potential to be utilized in advanced lighting devices owning to their enhanced emission properties, power efficiency, and external quantum efficiency. Moreover, Dayneko et al. (2021) reported the design, synthesis, and characterization of a series of N-annulated perylene diimide with sterically bulky alkyl-substituted benzyl side chains to be used as emitters in OLEDs. The synthesized perylene diimide dimers showed high photoluminescence quantum yield, which is a favored property for the emitter material. Also, Dayneko et al. (2021) demonstrated that all OLED devices based on the synthesized PDI molecules exhibited good performance.

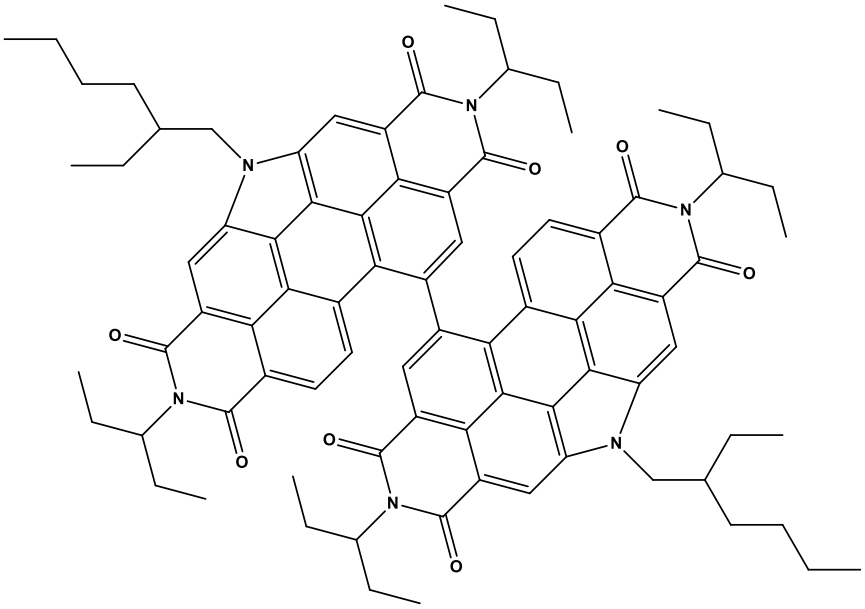

Figure 2.6. N-annulated perylene diimide dimer, red emitting molecule

Bala et al. (2020) demonstrated the design, synthesis, and characterization of various perylene tetraester based columnar liquid crystals as shown in Figure 2.7. Perylene columnar liquid crystals were employed as an emitting material in OLEDs due to their excellent physical properties and high charge transport properties. Bala et al. (2020) concluded that the attainment of materials with both high mobility and strong fluorescence emissions is beneficial for good optoelectronic materials. Furthermore, Gupta et al. (2018) presented a star-shaped triazine-perylene conjugate that can be used as an emitter in OLEDs as shown in Figure 2.8. In their research, the HOMO and LUMO energy levels were visualized, and the changes in the singlet, triplet energies, and the small energy bandgap concerning the molecular structure were calculated. The star-shaped compound had a great potential to be utilized in OLED applications due to its high brightness, current efficiency, power efficiency, and external quantum yield.

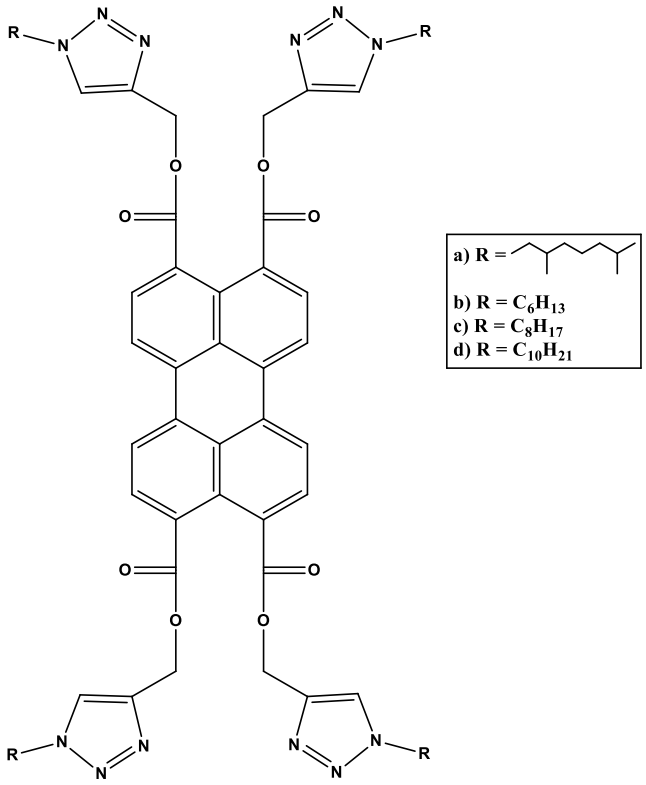

Figure 2.7. Perylene tetraester based columnar liquid crystals

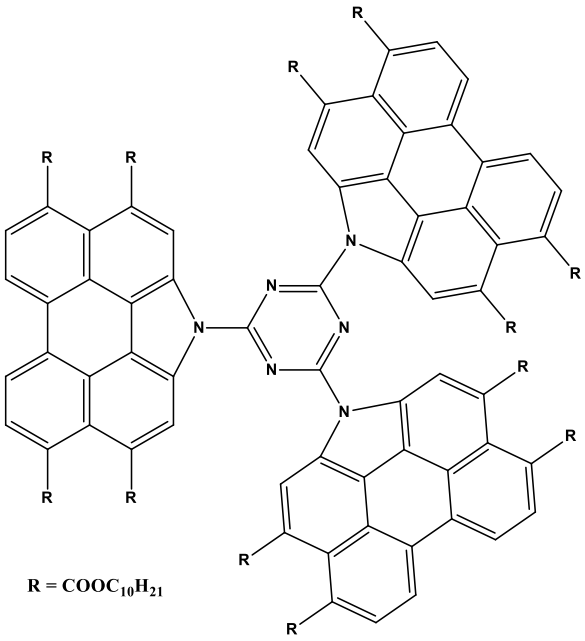

Figure 2.8. Perylene-triazine-based star-shaped green light emitter

2.4 Perylene tetracarboxylic acid derivatives

Perylene-3,4,9,10-tetracarboxylic acid (PTCA) derivatives are one of the most important classes of functional dyes. In the last decade, PTCAs were extensively studied and integrated with both academic and industrial research. With their exceptional properties such as versatile absorption, chemical robustness, photo- and thermal stability, fluorescence, perylene bisimides were intensively explored in the field of functional organic materials. In the last 30 years, many PTCA derivatives have been synthesized and utilized in various applications. These perylene derivatives have improved electrochemical and optical properties and provided great stability and robustness, moderate solubility, and high fluorescence quantum yield.

There are 12 functional positions in the perylene core as shown in Figure 2.9, positions 1,6,7,12 are known as bay positions, 2,5,8,11 are known as ortho positions, and 3,4,9,10 are known as peri positions. Structural modification of perylene tetracarboxylic acid derivatives at the ortho or bay positions by the attachment of different functional groups was reported in many studies (Sengupta et al., 2014).

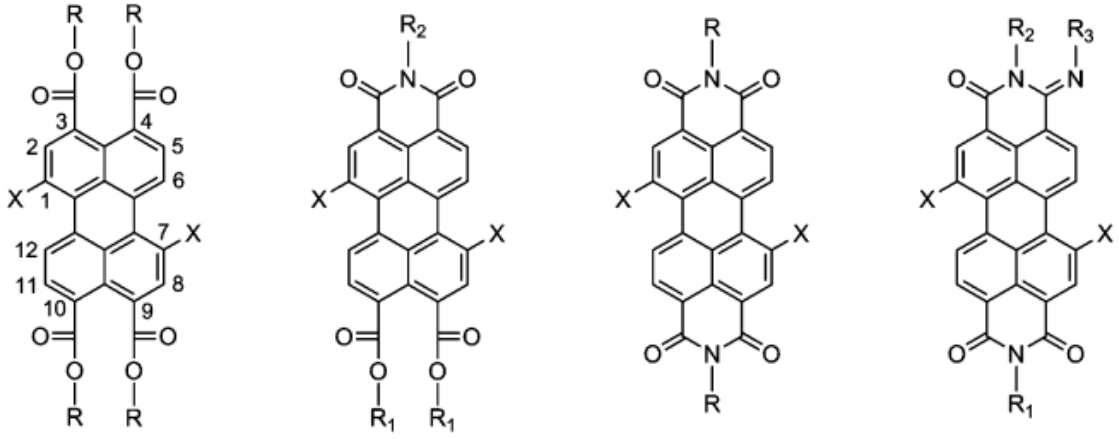

Figure 2.9. Perylene tetracarboxylic acid derivatives (Sengupta et al., 2014).

Dubey et al. (2020) designed and synthesized antenna molecules based on naphthalene monoimide as electron-donor and PTCA as electron-acceptor, which

had a good absorption for a wide range of the solar spectrum (400-600 nm). The group presented a new approach to avert the undesired intermolecular charge transfer in perylene imide-based light-harvesting antenna system by attaching naphthalene monoimide as electron-donor at the imide position rather than the bay position. The attachment at the imide-position was proven to have a notably faster excitation energy transfer than the antenna system bearing the donor group at the bay positions. Nevertheless, the attachment of naphthalene monoimide which is a large energy-donor at the imide-positions induced an additional slow quenching process for the perylene's singlet excited state. It was concluded that antenna molecules **1** and **2** (Fig. 2.10-2.11) are appropriate light-harvesting antenna systems for use in artificial photosynthesis.

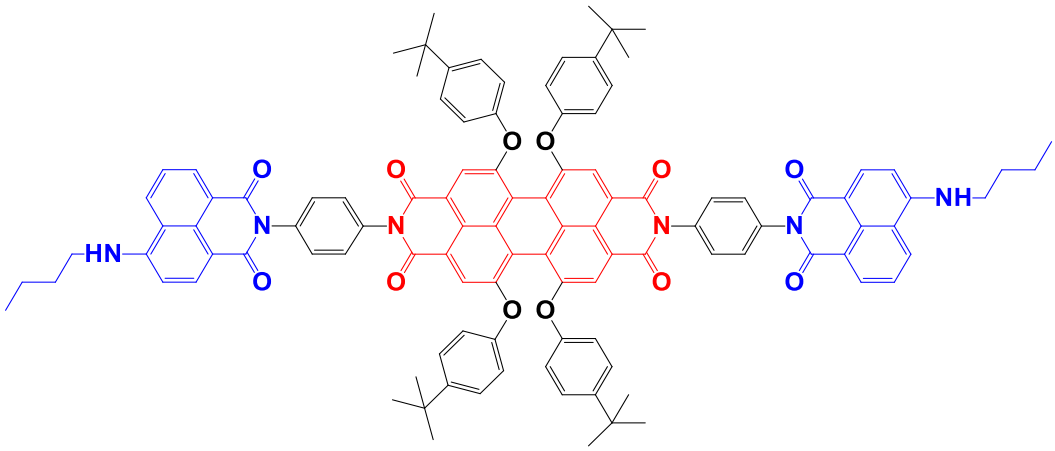

1

Figure 2.10. Imide functionalized antenna system **1** (Dubey et al., 2020).

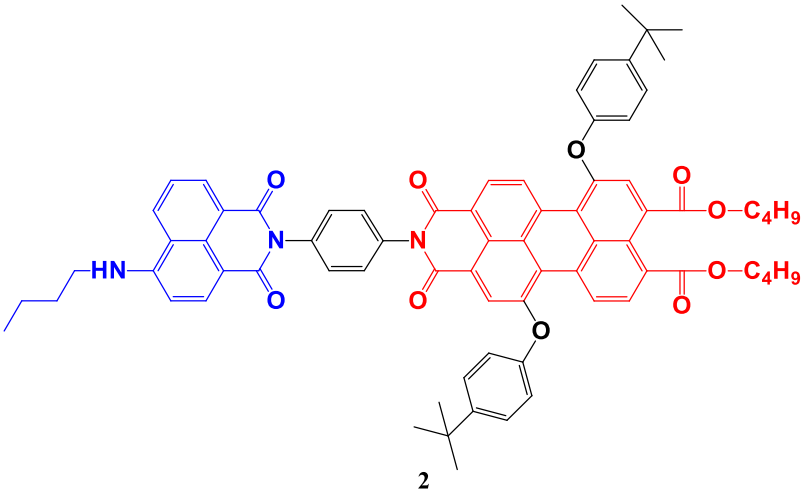

Figure 2.11. Imide functionalized antenna system **2** (Dubey et al., 2020).

Sengupta et al. (2014) found a new method to synthesize isomerically pure 1,7-dibrominated perylene tetracarboxylic acid derivatives. The newly synthesized regioisomerically pure intermediates, namely, 1,7-dibromoperylene-3,4,9,10-tetracarboxylic dibutylester monoanhydride, 1,7-dibromoperylene-3,4,9,10-tetracarboxylic bisanhydride, and 1,7-dibromoperylene monoimide monoanhydride, are ideal starting materials for the synthesis of many different bay-substituted compounds. These compounds have 1,7-bromo substituents and at least one anhydride functionality which allow for a virtually unlimited attachment of substituents both at the peri and bay positions. These intermediates were used in order to synthesize N-(2,6-diisopropylphenyl)-1,7-di(4-methoxyphenoxy)perylene-3,4,9,10-tetracarboxy monoimide dibutylester **3** and 1,7-di(4-methoxyphenoxy)perylene-3,4,9,10-tetracarboxy tetrabutylester **4** (Fig. 2.12). The synthesis of **3** and **4**, illustrated that bromine substitution at the bay position is efficient for all PTCA derivatives. Sengupta et al. (2014) concluded that the reported reactions for the synthesis of **3** and **4** are highly efficient and involve convenient purification processes. According to the photophysical studies, the reactions reported by Sengupta et al. (2014) are suitable for light-harvesting antenna systems.

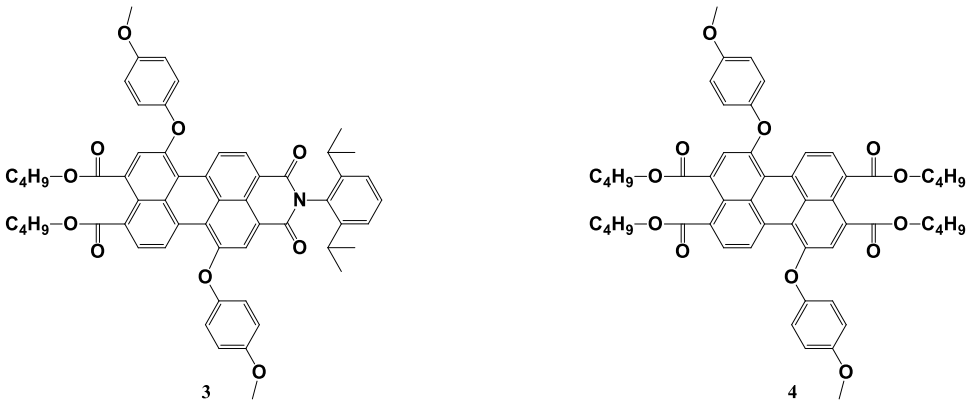

Figure 2.12. Bay-functionalized perylene tetracarboxylic acid derivatives **3** and **4** (Sengupta et al., 2014)**.**

The synthesis and excited-state dynamics of a various light-harvesting antenna molecules were reported by Dubey et al. (2016a) as shown in Figure 2.13. Energy-donors **D1**, **D2**, and **D3** were selected due to their stability, accessibility, high fluorescence, and redox properties to limit electron transfer. Dubey et al. (2016a) demonstrated that the synthesized light-harvesting antenna systems can efficiently harvest solar energy in the spectral range of 350-580 nm. All of the synthesized molecules have great overlap between the donor's emission and acceptor's absorption, which is essential for the Förster mechanism's efficient excited energy transfer (EET). The study concluded that energy transfer from the electron-donor to the electron-acceptor is more successful in solvents with higher polarity, making the antenna molecules with the less electron deficient energy acceptors **A1** and **A2** potential candidates for solar-to-electric and solar-to-fuel devices.

The light-harvesting antenna systems shown in Figure 2.13 are mimicry of the primary processes occurring in natural photosynthesis. The same light-harvesting antenna molecules have been modified by systematic change of molecular structures and by using high polarity solvents such as toluene, chloroform, and benzonitrile. In toluene, it was reported that fast energy transfer and intense acceptor fluorescence were measured for all antenna molecules. Also, photo-induced charge transfer was absent for all antenna molecules in toluene. In chloroform, fast energy transfer and very efficient fluorescence were noticed and the photophysical behavior did not

change when the solvent polarity was increased for the acceptor units **A1** and **A2**. In benzonitrile, the antenna molecules that contain **D1**, which is the weakest donating energy donor, did not sustain photo-induced charge transfer at all. For the other molecules containing **D2** and **D3**, fluorescence quenching was very small, due to a rapid photo-induced charge separation from the excited acceptor. The study concluded that the synthesized antenna molecules are the suitable to be utilized in devices for artificial photosynthesis due to their outstanding antenna behavior such as the fast excitation energy transfer and the absence of charge transfer and other contending processes even in highly polar solvents (Inan et al., 2019).

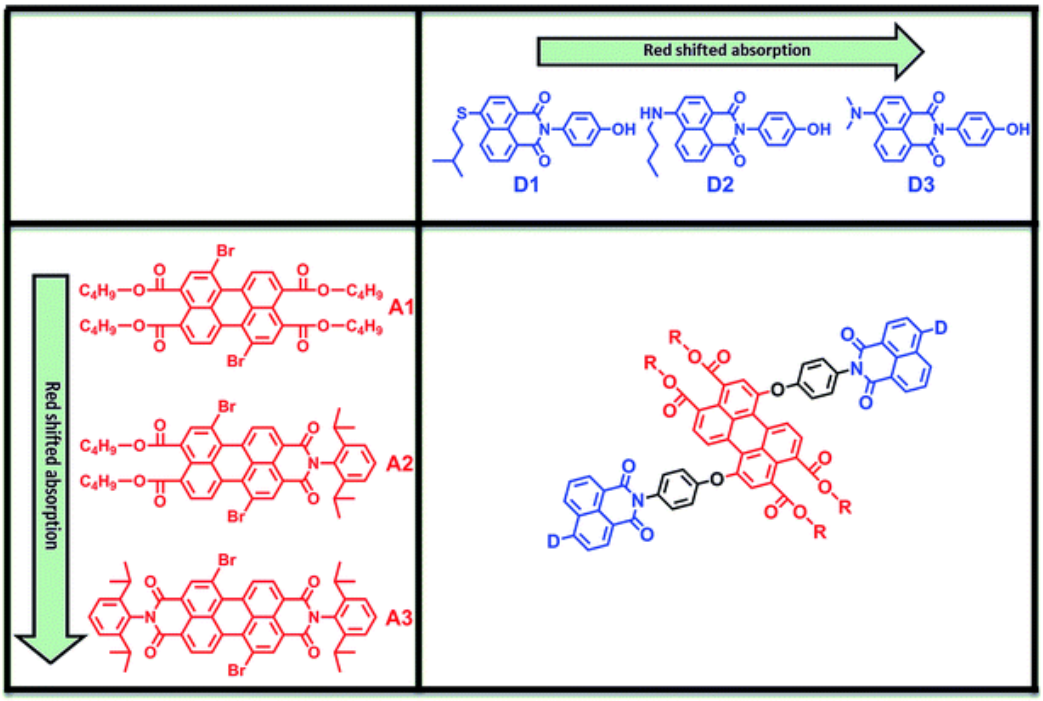

Figure 2.13. Light-harvesting antenna molecules (Dubey et al., 2016a).

Dubey et al. (2016d) synthesized the tetraphenoxy derivative **5** (Fig. 2.14) by two different methods to compare the efficacy of each one of them. Both of the methods utilized incorporate tetrachloroperylene bisimide as the starting material which was reacted with 4-tertbutylphenol. The first method was performed using Cs_2CO_3, and DMF as a solvent at 100ºC for 3 hours. This synthetic method's yield was relatively high (81%). In the second method, the reaction was performed using K_2CO_3, 18-

crown-6, and toluene as a solvent at 100ºC for 24 hours. The yield was very low (30-35%) compared to the first method which concludes that the first method is a promising alternative for this specific reaction. In the same study, electrochemical, absorption, and emission properties of the tetraphenoxy derivative **5** were studied. The study showed that the substitution at the bay-position with phenoxy substituents was not beneficial in terms of electron deficiency when it was compared with a similar tetrachlorinated perylene derivative. Furthermore, the synthesized derivative **5** was proven to have good light absorption on a wide range of the visible light spectrum (350-700 nm), which provides a promising compound to be used as a photo-functional material.

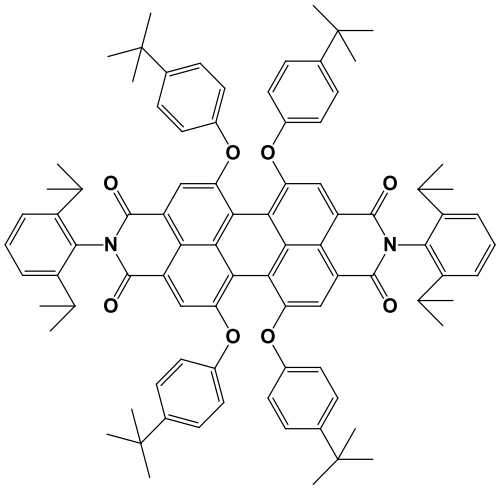

5

Figure 2.14. 1,6,7,12-tetraphenoxyperylene bisimide **5** (Dubey et al., 2016d)

Dubey et al. (2016d) synthesized and studied perylene bisbenzimidazole derivative **6** (Fig. 2.15). Perylene bisbenzimidazole compounds were synthesized with high yields and significantly shorter reaction times by modifying reaction conditions. Similar to **5**, molecule **6** was reported to be capable of absorbing light in a broad range of the solar spectrum (350-700 nm). Furthermore, perylene bisbenzimidazole derivative **6** had a longer fluorescence lifetime compared to **5**, which indicates a low fluorescence rate and high quenching rate as was reported in this study. Both

molecules **5** and **6** exhibited a negative impact on the electron deficiency of the perylene core due to the presence of the four phenoxy substituents at the bay-positons. Nevertheless, the bay-area substitution with tetraphenoxy shifted the absorption band to longer wavelengths by 47-64 nm. This indicates the importance of both peri and bay functionalization to fine-tune optoelectronic properties of perylene derivatives.

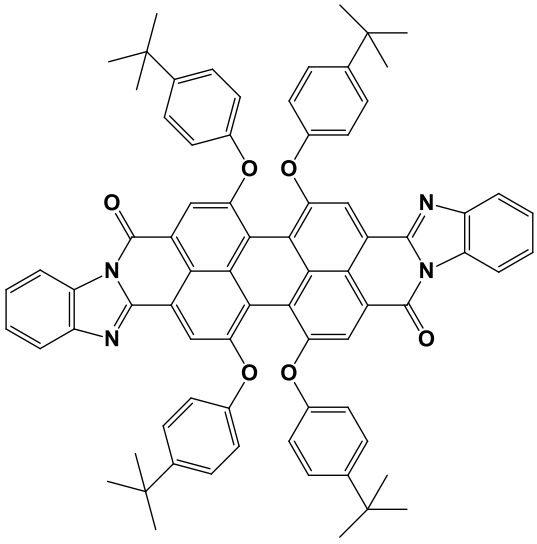

6

Figure 2.15. 1,6,7,12-tetraphenoxyperylene bisbenzimidazole (Dubey et al., 2016d)

Inan et al. (2017) synthesized and studied the photophysical properties of a variety of perylene tetracarboxylic acid derivatives **7**, **8**, and **9** (Fig. 2.16). The research group used 4-methoxyphenoxy groups as electron-donors, which were attached to the 1, 7 bay positions of various PTCA derivatives, namely perylene bisimide (**7)**, perylene monoimide diester (**8)**, and perylene monobenzimidazole monoimide (**9)**. Inan et al. (2017) were aiming to attain good control over the photo-induced charge-transfer process in perylene-based systems by changing the position of energy-donating groups and tuning the electron deficiency of the perylene core. By comparing the mentioned molecules, it was observed that the redox potential of the

compounds becomes more positive when more electron-withdrawing groups are attached at the peri-position (i.e. from **8** to **7**). Furthermore, it was reported that all three compounds **7**, **8**, and **9** are readily soluble in toluene and chloroform. They also have a good absorption at the broad range of the light spectra (425-625 nm). Inan et al. (2017) concluded that the kinetics of charge transfer in highly impacted by the position of the electron-donating groups on the perylene core, and the charge-transfer rates were negatively affected when electron-donors were moved from the bay to peri position.

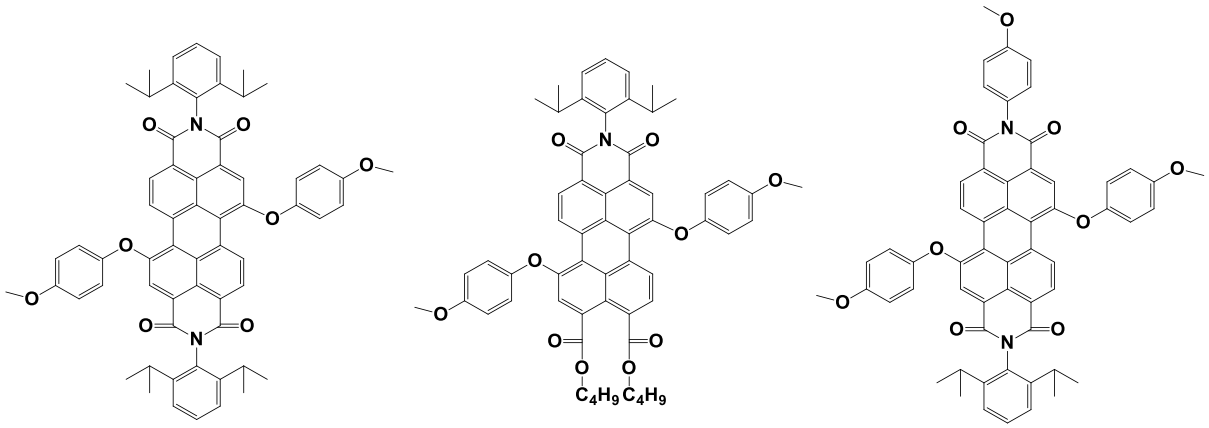

Figure 2.16. Perylene-3,4,9,10-tetracarboxylic Acid Derivatives **7**, **8**, and **9** (Inan et al., 2017)

Dubey et al. (2016b) synthesized perylene-3,4,9,10-tetracarboxylic tetraester-based fluorescent PET probes with aniline receptors attached either at the bay- or the peri-positions (Fig. 2.17). The effect of alternating the position of the aniline receptors was analyzed and the outcome was that the bay-substituted compounds **10b** and **11b** had a significantly higher solubility in organic solvents such as toluene, chloroform, and methanol compared to the peri-substituted compounds. It was reported that both peri- and bay-substituted perylene tetraester-based PET probes exhibit high fluorescence quantum yields. Nevertheless, peri-substituted PTE-based probes have a low fluorescence enchantment compared to the bay-substituted pH probes. The

study concluded that the attachment of spacer receptor units at the bay area is a good strategy to develop highly sensitive perylene-based fluorescent probes.

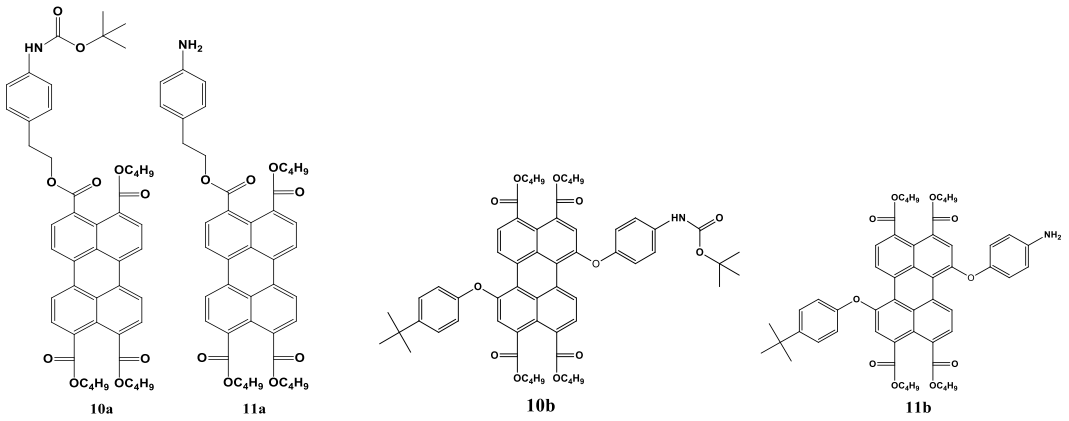

Figure 2.17. Fluorescent PET probes based on perylene-3,4,9,10-tetracarboxylic tetraesters (Dubey et al., 2016b)

Dubey et al. (2016c) demonstrated the synthesis of perylene tetracarboxylic acid derivatives with four different substituents attached to the perylene core (Fig 2.18). The mentioned derivatives, bearing 1,7-diphenoxy, 1,7-dipyrrolidinyl, and two 1-phenoxy-7-pyrrolidinyl groups were synthesized by utilizing 1,7-dibromoperylene-3,4,9,10-tetracarboxylic monoimide dibutylester. The synthesis was carried out in subsequent steps, starting with the nucleophilic substitution reactions with phenols and pyrrolidine, which are always regiospecific and highly efficient reactions, in which the imide-activated bromine at position "7" is substituted. Specific substitution of the remaining bromine at position "1" takes place in a limited number of cases only because the imide-activation of position "7" toward nucleophilic substitution is so pronounced that displacement of the substituent at position "7" may compete with the substitution of the bromine at position "1". If the substituent attached at position "7" is a phenol with poor leaving group ability and the nucleophile is another phenol, the substitution of the bromine at position "1" happens selectively. If the substituent at position "7" is a phenol and the nucleophile is pyrrolidine, substitution occurs at position "7", displacing the phenol without

affecting the bromine at position "1". Following these steps, Dubey et al. (2016c) were able to synthesize several perylene derivatives bearing four different substituents.

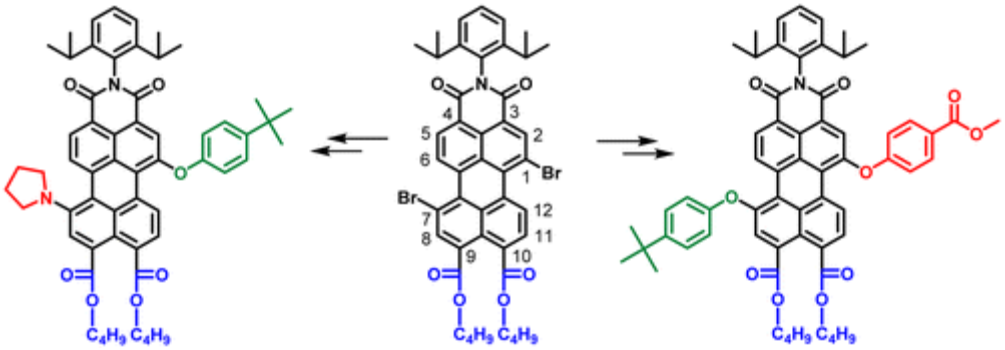

Figure 2.18. PTCA derivatives with four different substituents (Dubey et al., 2016c)

Dubey et al. (2019) made a huge step forward in perylene chemistry by introducing perylene bisimide derivatives with up to five different substituents attached to the perylene core (Fig. 2.19). This method might enable the synthesis of more complex covalent and supermolecular architectures based on perylene bisimide dyes in the future. Dubey et al. (2019) were able to synthesize perylene derivatives based on three different phenoxy groups, which are 4-methoxyphenoxy, 4-tert-butylphenoxy, and 4-methoxycarbonylphenoxy. They achieved regiospecific 7-mono and 7,12-bisphenoxy substitution at the bay positions of 1,6,7,12-tetrachloroperylene monoimide diester in very high yields using mild reaction conditions. It was concluded that this method has many advantages with regards to the synthesis as it produces 7,12-disubstituted perylene bisimide which was never synthesized before. Furthermore, this method is versatile and can be applied to synthesize perylene derivatives with different functional imides and bay substituents. Also, the good control over the subsequential substitutions at the imide and bay positions, which was achieved using the mentioned method, provides allows for the preparation of all regioisomers bearing the same bay substituents. Finally, this method facilitates perylene bisimides with up to six different substituents.

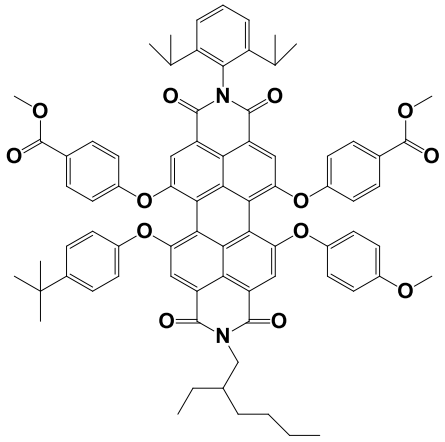

12

Figure 2.19. Perylene bisimide derivative bearing five different substituents (Dubey et al., 2019)

Aydin et al. (2015) synthesized two novel tetrasubstituted perylene tetracarboxylic tetraesters (PTTEs) (**13** and **14),** and perylene monimide diester (PMIDE) (**15)** (Fig. 2.20) derivatives to investigate their behavior as energy acceptors in light-harvesting systems. Those derivatives were produced with reactive ester functionalities which are ready to be utilized in the construction of different functional supermolecular systems, such as light-harvesting dendrimers or biolabels, by employing fast microwave-assisted click chemistry. Steady-state and time-resolved fluorescence studies were performed to assess the efficiency of electronic energy transfer of each light-harvesting system. The author mentioned several important notes to be considered. Among the perylene tetracarboxylic acid derivatives, PTTEs are the weakest electron-acceptors because of the poor orbital interactions between ester carbonyls of PBIs. On the other hand, PMIDEs are stronger electron-acceptors than PTTEs but weaker than PBIs. Consequently, absorption and emission wavelength maxima of the mentioned molecules follow the same trend; PTTE derivatives have the shortest wavelength compared to PMIDEs and PBIs. Aydin et al. (2015) concluded that the synthesized novel dyes can be utilized as donors if a suitable combinations of donor-acceptor system are designed. As assessed by many spectroscopic techniques, excitation energy can be channeled into these novel derivatives when they are employed in light-harvesting systems.

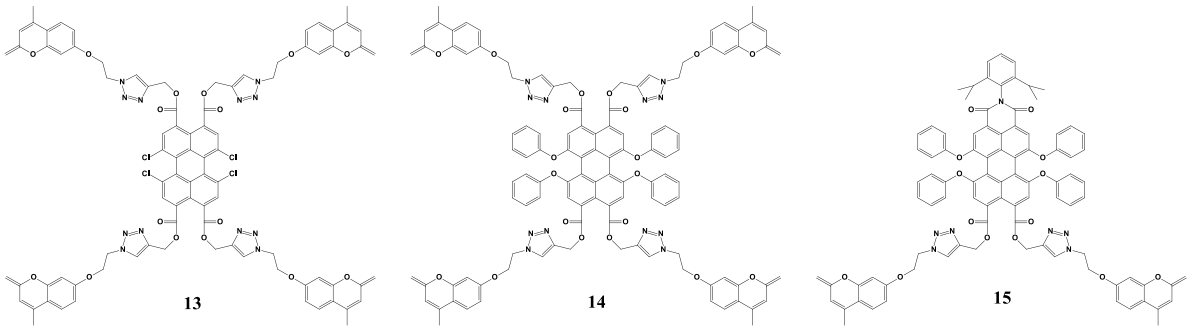

Figure 2.20. Bay-region tetrasubstituted perylene tetracarboxylic acid tetraester and perylene monimide diester (Aydin et al., 2015)

2.5 Fluorene as electron-donor

Fluorene is a derivative of biphenyl with a methylene bridge connecting the 2,2' positions as shown in Figure 2.21. The methylene bridge gives the fluorene molecule exceptional features. The methylene bridge present in fluorene increases the rigidity of the molecule. Due to this, fluorene has a higher quantum efficiency than biphenyl. Furthermore, fluorene molecules have been reported to improve electron charge transfer characteristics due to the electron richness of the fluorene. Fluorene molecules have promising charge-transfer capabilities due to the delocalization of π electrons in the planar configuration of the molecule. Due to these properties, fluorene has been frequently employed as an electron-donor in organic dyes (Yen et al., 2008; Giribabu et al., 2012; Choi et al., 2007; Justin Thomas and Baheti, 2013).

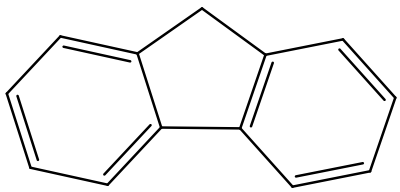

Figure 2.21. Molecular structure of fluorene

Giribabu et al. (2012) designed and synthesized two organic sensitizers based on bis-dimethylfluoreneaniline as electron-donor and cyanoacrylic acid as electron-acceptor. It has been found that the incorporation of dimethylfluoreneaniline

moieties in organic sensitizers ensures greater resistance to degradation when exposed to light and high temperatures as compared to simple arylamine. It has also been reported that the synthesized molecules have improved optical and electrochemical properties due to the electron richness of the bis-dimethylfluoreneaniline unit as it was compared to triphenylamine moiety.

Moreover, Choi et al. (2007) reported two new organic dyes featuring bis-dimethylfluoreneamine as electron-donor and cyanoacrylic acid as an electron-donor. The bis-dimethylefluoreneamine moiety was used to prevent aggregation via molecular staking and to provide better resistance to degradation when exposed to light and high temperatures. It has been concluded that bis-dimethylfluoreneamine is a good electron-donor unit, and it has the potential to be used in DSSCs when coupled with a suitable acceptor.

Justin Thomas and Baheti (2013) reviewed and presented several fluorene-based organic dyes for DSSCs. They demonstrated the special features of using fluorene as a donor element and as a conjugation pathway in organic dyes. It has been concluded that dyes with fluorenylamine based donors provided excellent photons to electricity conversion efficiencies (up to 8.60%) because of the significant donor strength of fluorenylamines, which offered strong donor-acceptor interaction and resulting charge separation.

According to the reviewed literature, Donor-Acceptor (D-A) type dyes are highly efficient and suitable for light-harvesting applications. To produce a potential difference, a fast and efficient energy transfer from the donor to the acceptor should be followed by an efficient energy transfer from the acceptor excited state to other components in the solar cell device. Furthermore, D-A type molecules have a broad absorption range in the visible light region 400-750 nm, which makes them suitable for light-harvesting applications (Sengupta et al., 2014; Dubey et al., 2016a; Inan et al., 2019; Dubey et al., 2020). In addition, the stability of the PTCA core and the versatile synthesis methods reported in the literature provides good control over the substitution at the bay and imide positions (Dubey et al., 2019).

In this work, perylene tetracarboxylic propargyl ester electron-accepting intermediate molecules were synthesized and combined with the electron-donating fluorene unit to obtain bipolar perylene derivatives. The fluorene donor has been employed due to several attractive features. Firstly, the electron richness of fluorene can improve the energy transfer characteristics within the D-A system. Furthermore, incorporating fluorene in organic dyes provides good degradation resistance when exposed to light and high temperatures. On the other hand, the PTCA derivative acceptor exhibit excellent properties such as chemical robustness, thermal, photochemical, and electrochemical stability. Also, the versatility of the PTCA, along with the flexible and scalable synthetic methods offers plenty of opportunities for chemical modifications. These modifications allow a systematic tuning of their optical and electrochemical properties. The combination of the mentioned donor and acceptor groups has a high potential to be used in light-harvesting applications, particularly DSSCs and OLEDs.

CHAPTER 3

EXPERIMENTAL

3.1 Materials and Instruments

The commercially available chemicals and solvents used in this study were reagant grade purity and aquired from Merch Millipore or Sigma-Aldrich. The majority of the chemicals and reagents were utilized as they were supplied, with no further purification required. Solvents used for chromatographic separation such as $CHCl_3$ and DCM were purified by rotary evaporation before they were utilized. Toluene was dried over molecular sieves. Moisture/air-sensitive reactions were carried out in a nitrogen (N_2) atmosphere. For column chromatography, silica gel pore size 60 Å, 70-230 mesh, 63-200 μm was used for purification, and thin-layer chromatography (TLC) was performed on an aluminum TLC plate, silica gel coated with fluorescent indicator F254. Bruker Advance 400 MHz NMR spectrometer was used to measure and record nuclear magnetic resonance (NMR) spectra. FTIR spectra were recorded with a PerkinElmer, Spectrum two spectrometer in the 4000-400 cm^{-1} spectral range in the transmittance mode. UV/VIS measurements were recorded on Perkin Elmer Lambda 950 UV-VIS NIR spectrophotometer and the spectral data was converted into graphs using Origin 2021b software. For emission properties, FS5 Spectrofluorometer of Edinburgh Instruments was used. Lifetime measurements were recorded on FLS 920 Fluorescence Spectrophotometer of Edinburgh Instruments. Electrochemical studies were carried out with a Autolab 204, Metrohm PGSTAT204 by using a three-electrode electrochemical cell configuration. Glassy carbon as the working electrode, Pt wire as the auxiliary electrode and Ag wire as the reference electrode were used. Ferrocene/ferrocenium (CP_2Fe/CP_2Fe_+) redox couple was used as the internal standard and 0.1 M tetrabutylammonium hexafluorophosphate (TBAPF6) in MeCN was used as the supporting electrolyte.

Cyclic voltammograms were obtained at a scan rate of 0.2 V s^{-1}. Thermogravimetric analysis (TGA) measurements were performed by using Sdt Q600 V20 9 Build 20 Thermal Gravimetric (TA Instruments). N_2 gas was used as the inert gas with a flow rate 50 mL/min and heating rate was 10 ^oC/min.

3.2 Synthesis procedure

3.2.1 Synthesis of perylene-3,4,9,10-tetracarboxylic tetrabutylester (P1)

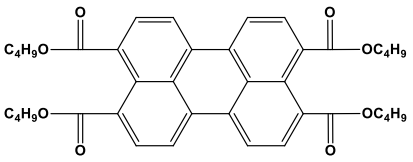

Perylene-3,4,9,10-tetracarboxylic dianhydride (5 g, 12.75 mmol), 1,8-diazabicyclo(5.4.0)undec-7-ene (DBU) (7.6 ml, 4 eq.), n-butanol (9,33 ml, 8 eq.), and 60 ml of dimethylformamide (DMF) were taken into a 2-necked flask. The reaction mixture was stirred at 60^{o}C for 3 hours. 1-bromobutane (11.025 ml, 8 eq.) and 45 ml of DMF were added to the flask. The mixture was stirred for an additional 3 hours at 60^{o}C. The crude product was precipitated in water (350 ml) and the solid was filtered using a Büchner funnel. The crude product was dissolved in a 100 ml solvent mixture of $CHCl_3$:DCM (2:1). Ethanol (140 ml) was added slowly and the precipitate was collected using a Büchner funnel. The precipitate was dried for 10 hours at 80^{o}C under vacuum to afford **P1** as an orange solid (6.96 g, 10.66 mmol, 83.6%). Characterization data for **P1**: IR (ATR): 3147, 2965, 2331, 1731, 1586, 1446, 1305, 1035, 811, 736, 605 cm^{-1}; $\lambda_{max\ CHCl3}$ = 473 nm (ε = 63594, Pearson's r = 0.99, R^2 = 0.98) and 442 nm (ε = 51862, Pearson's r = 0.99, R^2 = 0.98); $\lambda_{max\ DMF}$ = 468 nm (ε = 46068, Pearson's r = 1.00, R^2 = 1.00) and 442 nm (ε = 38617, Pearson's r = 1.00, R^2 = 1.00); and ^{1}H NMR ($CDCl_3$, 400 MHz): 1.05 (t, 12H), 1.54 (m, 8H), 1.82 (m, 8H), 4.38 (t, 8H), 7.81 (d, 4H), 7.84 (d, 4H); ^{13}C NMR ($CDCl_3$, 100 MHz): 13.7, 19.2, 30.8, 65.2, 121.2, 128.2, 128.4, 130.2, 132.3, 168.4.

3.2.2 Synthesis of 1,7-dibromoperylene-3,4,9,10-tetracarboxylic tetrabutylester (P2)

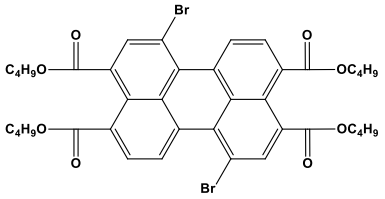

Perylene-3,4,9,10-tetracarboxylic tetrabutylester **P1** (4 g, 6.13 mmol) and K_2CO_3 (2 g, 14.48 mmol) were taken into a 250 ml 2-necked flask. Around 80 ml of DCM was added subsequently to the flask. Bromine (4 ml, 77.6 mmol) was added drop wise to the reaction mixture and stirred at room temperature for 24 hours. Afterward, a saturated solution of sodium metabisulphite ($Na_2S_2O_5$) was added dropwise to quench excess bromine. The organic layer was separated and washed with water (80 ml × 3) and dried over sodium sulphate (Na_2SO_4). The mixture was filtered and the sovent was removed by rotary evaporation to afford crude product (5.3 g) including of a mixture of 1,6 and 1,7-dibromonated isomers. Regioisomerically pure 1,7-dibromo isomer was isolated by crystallization with a solvent mixture of DCM (30 ml)/ acetonitrile (150 ml) to give **P2** (2.48 g, 3.06 mmol, 49.9%). Characterization data for **P2**: IR (ATR): 3578, 3327, 2953, 2871, 2510, 2332, 2085, 1945, 1730, 1588, 1455, 1386, 1302, 1167, 1052, 950, 817, 741, 602 cm^{-1}; $\lambda_{max\ CHCl3}$ = 469 nm (ε = 32364, Pearson's r = 1.00, R^2 = 1.00) and 442 nm (ε = 28718, Pearson's r = 1.00, R^2 = 1.00); $\lambda_{max\ DMF}$ = 467 nm (ε = 31510, Pearson's r = 1.00, R^2 = 1.00) and 440 nm (ε = 28248, Pearson's r = 1.00, R^2 = 1.00); and ^{1}H NMR ($CDCl_3$, 400 MHz): 1.00 (t, 12H), 1.61-1.45 (m, 8H), 1.82-1.76 (m, 8H), 4.33 (t, 8H), 8.07 (d, 2H), 8.29 (s, 2H), 8.92 (d, 2H); ^{13}C NMR ($CDCl_3$, 100 MHz): 13.9, 19.1, 30.7, 65.5, 65.9, 118.6, 126.6, 127.6, 129.1, 130.3, 131.2, 131.6, 136.8, 167.0, 168.1.

3.2.3 Synthesis of 1,7-dibromoperylene-3,4,9,10-tetracarboxylic bisanhydride (P3)

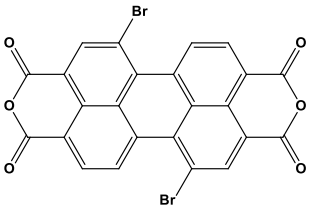

Regioisomerically pure 1,7-dibromoperylene-3,4,9,10-tetracarboxylic tetrabutylester **P2** (1 g, 1.23 mmol), p-toluenesulfonic acid monohydrate (1.17 g, 6.15 mmol), and 20 ml of toluene was taken into a 50 ml 2-necked flask. The reaction mixture was stirred for 48 hours at 100°C. The crude product was filtered using Buchner funnel and washed with methanol (MeOH, 25 ml × 3) and water (25 ml × 3). Afterward, the crude product was dried overnight at 80°C under vacuum. The crude product was then refluxed with a 150 ml solvent mixture of $CHCl_3$:DCM (2:1). The product was collected using a Buchner funnel. The product was dried overnight at 80°C under vacuum to give **P3** as an orange solid (0.604 g, 1.102 mmol, 90.1%). NMR data could not be obtained due to its low solubility. Characterization data for **P3**: IR (ATR): 1767, 1720, 1589, 1282, 1135, 1034, 954, 802, 730, 686 cm^{-1}.

3.2.4 Synthesis of 1,7-dibromoperylene-3,4,9,10-tetracarboxy propargyl ester (P4)

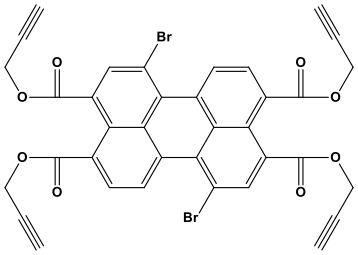

1,7-dibromoperylene-3,4,9,10-tetracarboxylic bisanhydride **P3** (0.40 g, 0.73 mmol) and DMF (15 ml) were transferred into a 50 ml 2-necked flask which was purged with N_2. The mixture was stirred and heated to 60°C. Then, 1,8-Diazabicyclo[5,4,0]undec-7-ene (462 µL, 3.066 mmol) and propargyl alcohol (347 µL, 5.84 mmol) were added to the mixture and stirred for 30 min at 60°C. Afterward, a solution of propargyl bromide (80% in toluene, 655 µL, 5.84 mmol) in 2 ml of DMF was added dropwise and the solution was stirred for 3 hours at 60°C. After the completion of the reaction, the crude product was precipitated onto 100 ml of water, and extraction was done three

times using ethyl acetate. Then, the organic phase was washed with 5% $LiCl_2$ and separated from the water phase. The solvents were removed using the rotary evaporator. Purification by column chromatography was done using a solvent mixture of hexane/ethyl acetate (2:1) to give **P4** (178 mg, 0.241 mmol, 33%) Characterization data for **P4**: IR (ATR): 3287, 2922, 2852, 2129, 1712, 1504, 1393, 1261, 1292, 1155, 1104, 1019, 686, 638, 591 cm^{-1}. ^1H NMR ($CDCl_3$, 400 MHz): 2.61-2.58 (m, 4H), 4.98 (s, 8H), 8.19 (d, 2H), 8.38 (s, 2H), 8.96 (d, 2H).

3.2.5 Synthesis of 2-Azidoflourene (P5)

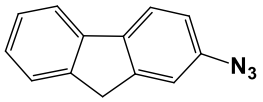

2-aminoflourene (0.18 g, 1 mmol), concentrated HCl (4.5 ml), and 9 ml of H_2O were taken into a 50 ml 2-necked flask. The flask was placed in an ice bath and $NaNO_2$ (96.6 mg, 1.4 mmol) was dissolved in 2.5 ml of water and added to the flask. The reaction mixture was stirred in the ice bath for 1.5 hours. Afterward, NaN_3 (91 mg, 1.4 mmol) was dissolved in 2.5 ml of water and added to the mixture dropwise. The reaction mixture was stirred at room temperature for 2 hours. Upon the completion of the reaction, 25 ml of H_2O was added and the precipitate was filtered and washed with 25 ml of water. After drying for several days at room temperature, the desired product **P5** was obtained (134 mg, 64.7 mmol, 65%). Characterization data for **P5**: IR (ATR): 2112, 1581, 1453, 1291, 1281, 837, 765, 732, 521, 420 cm^{-1}.

3.2.6 Synthesis of P6

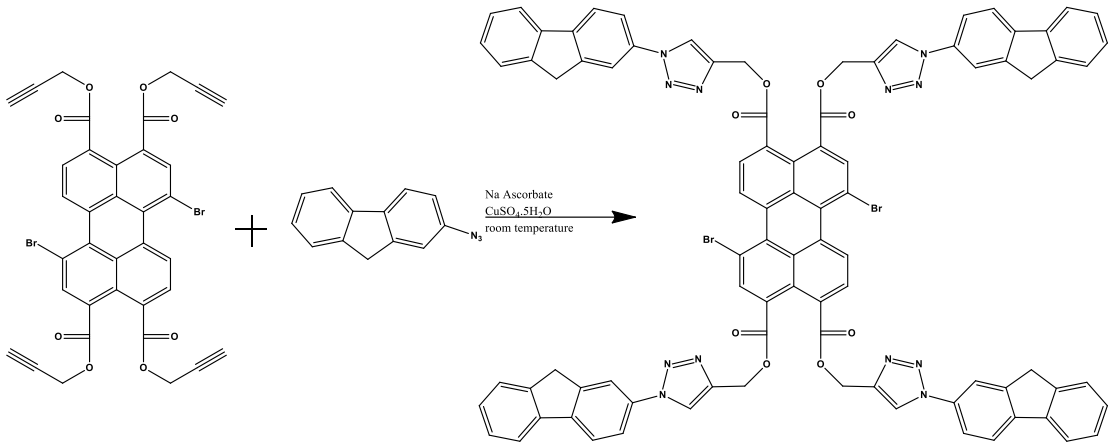

1,7-dibromoperylene-3,4,9,10-tetracarboxylicpropargyl ester **P4** (111 mg, 0.15 mmol), 2-azidofluorene **P5** (126 mg, 0.61 mmol), $CuSO_4.5H_2O$ (8 mg, 0.032 mmol) and sodium ascorbate (15 mg, 0,076 mmol) were dissolved in a solvent mixture of DCM (1.5 ml)/H_2O (1.5 ml). The reaction mixture was stirred for ~16 hours at room temperature. After the completion of the reaction, extraction was done using DCM (150 ml) and H_2O (50 ml). Then, the solvents were evaporated under reduced pressure and a yellow solid was obtained. The crude product was refluxed with DCM (25 ml) for 1 hour to remove trace amounts of starting material. The mixture was cooled overnight in the fridge. The filtration did not work. A small portion of hexane (5-10 ml) was added and the mixture was kept further in the fridge. After a few days, precipitate (yellow solid) was filtered and dried under vacuum at 70°C to give product **P6** (180 mg, 0.115 mmol, 77%). The product was not soluble in common organic solvents, therefore the NMR measurements couldn't be done. Characterization data for **P6**: IR (ATR): 2109, 1726, 1463, 1297, 1272, 1223, 1162, 823, 768, 734, 420 cm^{-1}. A comparision with the IR data from **P4** was done to prove that **P6** was obtained. For **P4**, a peak was observed at 3288 cm^{-1}, which indicates the presence of alkynes. On the other hand, a peak at 2109 cm^{-1} was observed for **P6**, which indicates the presence of azide. It can be concluded that the click reaction was successful and the desired product **P6** was obtained.

3.2.7 Synthesis of P7

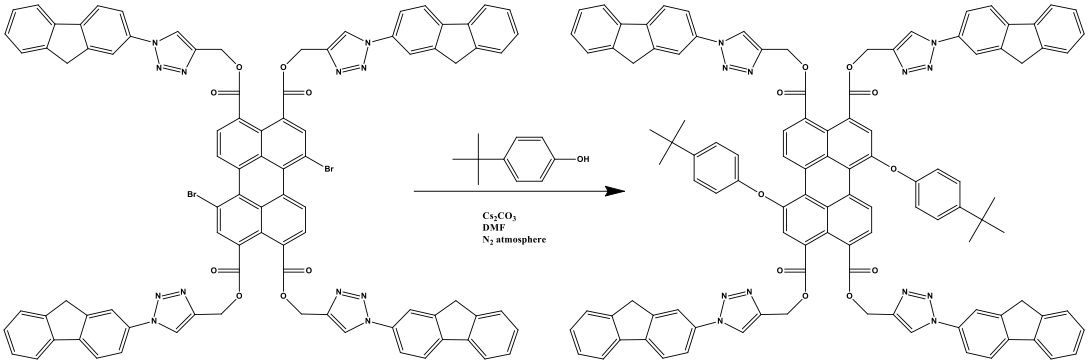

P6 (80 mg, 0.051 mmol), 4-tert-butylphenol (31.5 mg, 0.21 mmol), and Cs_2CO_3 (101 mg, 0.31 mmol) were taken in a dry 10 ml 2-necked flask which was purged with N_2. Then, DMF (3 ml) was added. The reaction mixture was stirred at 130°C for 3 hours. After the completion of the reaction, the mixture was cooled to room temperature. DCM (50 ml) was added and the solid material was filtered (black solid). The organic phase was washed three times with 20 ml of water. Afterward, the organic phase was dried over Na_2SO_4, and the solvents were evaporated on the rotary evaporator. Purification by column chromatography using a solution mixture DCM/MeOH (40:1) was done to obtain **P7** (3.7 mg, 0.002 mmol). The NMR spectrum shows that this compound couldn't be obtained successfully.

3.2.8 Synthesis of 1,7-dibromoperylene-3,4,9,10-tetracarboxylic dibutylester monoanhydride (P8)

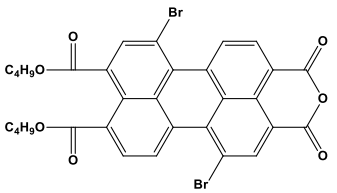

Regioisomerically pure 1,7-dibromoperylene-3,4,9,10-tetracarboxylic tetrabutylester **P2** (1 g, 1.23 mmol), p-toluenesulfonic acid monohydrate (p-TsOH.H_2O) (305 mg, 1.60 mmol), and 3 ml of n-heptane were taken into a 2-necked flask. The reaction mixture was stirred at 90°C for 10 hours. After the completion of the reaction, the reaction mixture was cooled to room temperature, and the product was filtered and washed 3 times with 10 ml of MeOH/H_2O mixture. The filtered product was dried

for 3 hours under vacuum. The dried product was refluxed with 150 ml of MeOH for 2 hours. The refluxed mixture was cooled to room temperature and the residue was filtered. The residue was a mixture of monoanhydride compound **P8**, bisanhydride, and starting material. The mixture was dried and dissolved in 3 ml of DCM to separate the insoluble bisanhydride. Purification by column chromotography using a mixture of chloroform and DCM gave 438 mg of product **P8** (52% yield). Characterization data for **P8**: IR (ATR): 3455, 3059, 2942, 2872, 2726, 2511, 2363, 1783, 1705, 1604, 1457, 1378, 1270, 1169, 1018, 807, 694 cm^{-1}; $\lambda_{max\ CHCl3}$ = 504 nm (ε = 41208, Pearson's r = 1.00, R^2 = 1.00) and 485 nm (ε = 34094, Pearson's r = 1.00, R^2 = 1.00); $\lambda_{max\ DMF}$ = 496 nm (ε = 32016, Pearson's r = 1.00, R^2 = 1.00) and 468 nm (ε = 26756, Pearson's r = 1.00, R^2 = 1.00); Melting point: 205ºC (literature 202ºC); and ^{1}H NMR ($CDCl_3$, 400 MHz): 0.96-0.92 (m, 6H), 1.18 (s, 2H), 1.52-1.39 (m, 6H), 1.77-1.69 (m, 4H), 4.31-4.27 (m, 4H), 8.07 (d, 1H), 8.27 (s, 1H), 8.60 (d, 1H), 8.81 (s, 1H), 9.18 ppm (q, 2H).

3.2.9 Synthesis of N-(2,6-diisopropylphenyl)-1,7-dibromoperylene-3,4,9,10-tetracarboxy monoimide dibutylester (P9)

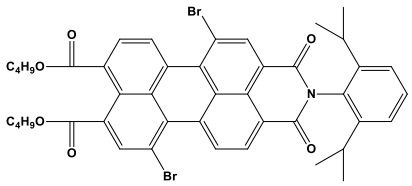

1,7-dibromoperylene-3,4,9,10-tetracarboxylic dibutylester monoanhydride **P8** (32.6 mg, 0,048 mmol), diisopropyl aniline (30 µl, 0,16 mmol), and 2.6 ml of propionic acid were taken into a 25 ml round-bottom flask which was purged with N_2. The reaction mixture was stirred for 46 hours at 90ºC. Afterwards, The mixture was cooled down to room temperature and poured onto 14 ml of water. The yellow precipitate was filtered using 2.5 µm Whatman filter paper. Purification by column chromotography was done using DCM to give pure product **P9** (20 mg, 0.024 mmol, 50%). Characterization data for **P9**: IR (ATR): 2959, 1709, 1669, 1590, 1459, 1378, 1226, 1195, 1064, 805, 748, 548 cm^{-1}; ^{1}H NMR (400 MHz, $CDCl_3$):1.04 (t, 6H), 1.24 (t, 16H), 1.61-1.50 (m, 6H), 1.86-1.81 (m, 4H), 4.39 (t, 4H), 7.29 (s, 2H), 7.38 (d, 2H), 7.53 (t, 1H), 8.19 (d, 1H), 8.38

(s, 1H), 8.76 (d, 1H), 8.98 (s, 1H), 9.29 (q, 2H). ^{13}C NMR (100 MHz, $CDCl_3$): 13.7, 19.1, 23.9, 29.1, 30.5, 65.7, 65.9, 124.0, 128.1, 128.9, 129.2, 130.2, 136.7, 138.1, 145.6, 162.6, 166.8, 167.7 ppm.

3.2.10 Synthesis of N-(2,6-diisopropylphenyl)-1,7-dibromoperylene-3,4,9,10-tetracarboxy monoimide monoanhydride (P10)

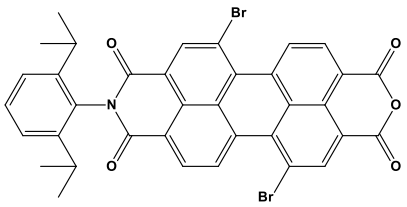

N-(2,6-diisopropylphenyl)-1,7-dibromoperylene-3,4,9,10-tetracarboxy monoimide dibutylester **P9** (303 mg, 0.72 mmol), and p-toluenesulfonic acid monohydrate (685 mg, 3.6 mmol) were taken into a 25 ml 2-necked flask. Toluene (20 ml) was added to the reaction mixture and stirred at 90ºC for 30 hours. The mixture was dried on the rotary evaporator. The residue was washed with a solution mixture of MeOH and H_2O (8 ml × 3). Then, the crude product was filtered and dried at 70ºC for 12 hours. Afterward, the crude product was refluxed with MeOH (50 ml) for 2 hours. The crude product was cooled to room temperature, filtered, and washed with cold MeOH. The side product went to the MeOH phase and pure solid product was obtained **P10** (0.246 g, 0.347 mmol, 96.3%). Characterization data for **P10**: IR (ATR): 3054, 1734, 1378, 1264, 1245, 1046, 732, 703 cm^{-1}. ^{1}H NMR (400 MHz, $CDCl_3$): 1.17 (s, 6H), 1.19 (s, 6H), 2.75-2.68 (m, 2H), 7.36 (d, 2H), 7.51 (t, 1H), 8.76 (d, 1H), 8.76 (d, 1H), 8.80 (d, 1H), 8.98 (s, 1H), 9.02 (s, 1H), 9.58-9.55 (m, 2H). ^{13}C NMR could not be measured because of its low solubility.

3.2.11 Synthesis of N-(2,6-diisopropylphenyl)-1,7-dibromoperylene-3,4,9,10-tetracarboxy monoimide dipropargyl ester (P11)

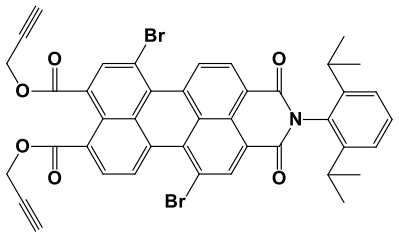

N-(2,6-diisopropylphenyl)-1,7-dibromoperylene-3,4,9,10-tetracarboxy monoimide monoanhydride **P10** (0.24 g, 0.338 mmol), DBU (108.1 mg, 0.71 mmol), and propargyl alcohol (75.68 mg, 1.35 mmol) were taken into a 25 ml 2-necked flask that was flushed with N_2. DMF (4 ml) was added to the reaction mixture and it was stirred for 1 hour at 60°C under N_2 atmosphere. Afterward, propargyl bromide (80% in toluene, 150 µL, 1.35 mmol) was taken in 1 ml DMF and added to the reaction mixture. The reaction mixture was stirred at 60°C for 4 hours. After the completion of the reaction, the crude product was poured onto 30 ml of cold H_2O and kept in the fridge at low temperature for 3 hours. Then, the crude product was filtered and further purification was done by column chromatography using a solvent mixture of hexane:ethyl acetate (2:1) to obtain the desired pure product **P11** (135 mg, 0.023 mmol, 49.7%). Characterization data for **P11**: IR (ATR): 3304, 3279, 2962, 1737, 1718, 1705, 1665, 1590, 1500, 1436, 1379, 1346, 1258, 1228, 1194, 1165, 1106, 1061, 918, 865, 808, 744, 714, 676, 652, 637, 554, 448. ^{1}H NMR ($CDCl_3$, 400 MHz): 1.21 (t, 14H), 1.60 (s, 2H), 2.65-2.62 (m, 2H), 2.79-2.73 (m, 2H), 5.07 (s, 4H), 7.37 (t, 2H), 7.53 (t, 1H), 8.29 (d, 1H), 8.48 (s, 1H), 8.77 (d, 1H), 8.98 (s, 1H), 9.33-9.28 (m, 2H). ^{13}C NMR (100 MHz, $CDCl_3$): 23.9, 29.1, 53.2, 53.4, 75.5, 119.8, 120.1, 122.1, 122.3, 124.0, 126.9, 128.0, 128.3, 129.1, 129.7, 130.2, 130.4, 131.1, 131.4, 131.9, 133.5, 133.9, 137.5, 138.1, 145.5, 162.5, 163.0, 165.8, 166.6 ppm.

3.2.12 Synthesis of P12

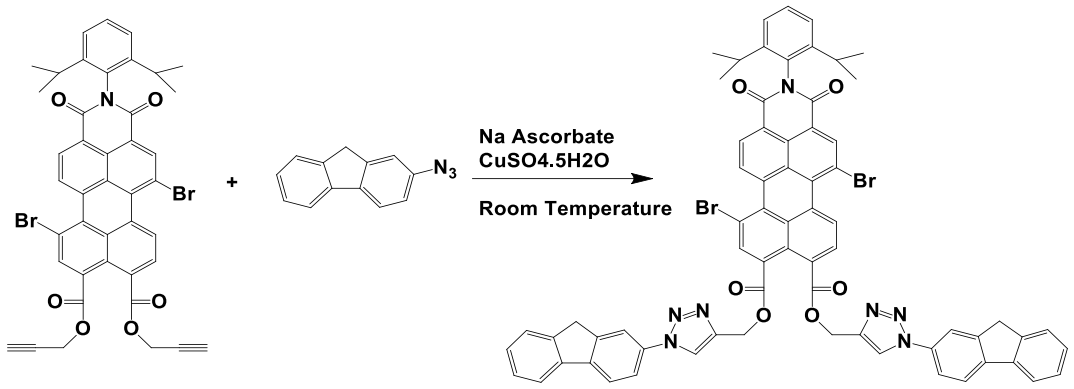

N-(2,6-diisopropylphenyl)-1,7-dibromoperylene-3,4,9,10-tetracarboxy monoimide dipropargyl ester **P11** (277 mg, 0.345 mmol), fluorene azide (157.3 mg, 0.759 mmol), $CuSO_4.5H_2O$ (8.61 mg, 0.0345 mmol) and sodium ascorbate (27.34 mg, 0.138 mmol) were dissolved in a solvent mixture of DCM (8 ml)/H_2O (4 ml)/C_2H_5OH (3 ml). The reaction mixture was stirred for ~26 hours at room temperature. After the completion of the reaction, extraction was done using DCM (15 ml) and H_2O (10 ml). The organic phase was dried over Na_2SO_4. Then, the solvents were evaporated under reduced pressure. The product was purified by column chromatography using $CHCl_3$:MeOH (100:1) as a solvent system. Afterward, recrystallization was done using DCM:$C_6H_{14,}$ and pure product **P12** was filtered and dried (265 mg, 0.22 mmol, 63%). Characterization data for **P12**: IR (ATR): 2963, 1709, 1668, 1591, 1496, 1462, 1380, 1239, 1170, 1152, 1109, 1040, 857, 824, 806, 765, 730, 711, 693, 649, 591, 549, 420 cm^{-1}. ^1H NMR ($CDCl_3$, 400 MHz): 1.19 (d, 12H), 5.63 (s, 4H), 7.42-7.29 (m, 6H), 7.53 (q, 4H), 7.71 (d, 2H), 7.81 (q, 4H), 7.93 (s, 2H), 8.31 (t, 3H), 8.49 (s, 1H), 8.75 (d, 1H), 8.97 (s, 1H), 9.29 (q, 3H).

3.2.13 Synthesis of P13

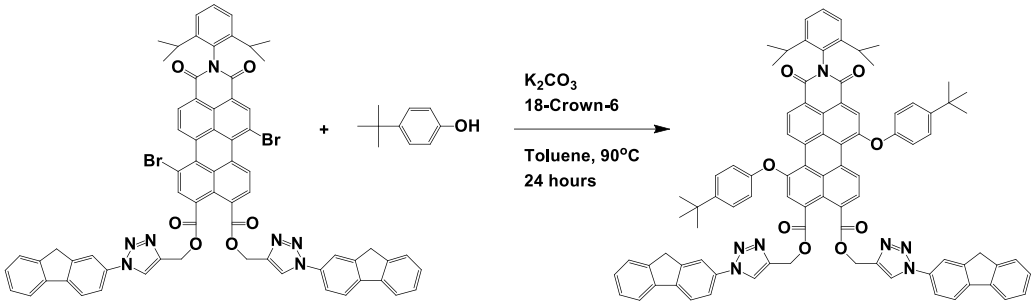

P12 (50 mg, 0.123 mmol), 4-tert butyl phenol (18.48 mg, 0.123 mmol), K_2CO_3 (34 mg, 0.246 mmol), and 18-crown-6 (129.95 mg, 0.492 mmol) were dissolved in dry toluene (10 ml) and stirred for 45 minutes at room temperature. Afterward, P51 (50 mg, 0.04 mmol) was added and the reaction mixture was stirred for 24 hours at 90°C. Upon the completion of the reaction, the mixture was cooled to room temperature and toluene was removed by rotary evaporation. The crude product was washed with water (20 ml x 2 times). Then, it was filtered and washed with cold MeOH (50 ml), a black solid was obtained. Purification by column chromatography was done using $CHCl_3$:MeOH (400:1) as a solvent system. Orange pure product was collected (18 mg, 0.013, 32%). Characterization data for **P13**: IR (ATR): 2962, 1707, 1667, 1591, 1503, 1463, 1350, 1227, 1146, 1104, 1043, 959, 834, 804, 737, 528 cm^{-1}. According to the NMR data, the obtained molecule is not the desired product therefore, an alternative method will be used to synthesize the desired product **P13**.

3.3 Data and calculations

3.3.1 Maximum extinction coefficient (ε_{max})

The maximum extinction coefficient refers to the amount of light absorbed by a substance at a specific wavelength. It is a chemical property that depends on the chemical's concentration and structure. Beer Lambert's law defines the relationship between the maximum extinction coefficient with regards to the concentration, absorbance, and path length of the light.

$$\varepsilon_{\max} = \frac{A}{cL} \qquad \textbf{(3. 1)}$$

Where ε_{max} is the maximum extinction coefficient at a specific wavelength ($M^{-1}. cm^{-1}$), c is the concentration (M), A is the absorbance and L is the path length of the sample (cm).

The molar extinction coefficient (ε) was determined from the plot of absorbance versus concentration at specific wavelengths. Different concentrations of the selected compounds were prepared and their absorbances were recorded by UV-vis spectrophotometer, using $CHCl_3$ as a solvent. The absorbance and concentration were recorded at the two wavelength peaks of each compound, which are presented in Figure A.21– Figure A.29. By analyzing the absorbance versus concentration graphs, the slope, Pearson's correlation coefficient, and R-square were obtained. The slope of the line represents the molar extinction coefficient (ε).

3.3.2 Fluorescence quantum yield ($\boldsymbol{\varphi_f}$)

The ratio of photons absorbed to photons released by fluorescence is known as the fluorescence quantum yield ($\boldsymbol{\varphi_f}$). In addition, the quantum yield indicates the likelihood that the excited state would be deactivated by fluorescence rather than another, non-radiative mechanism.

Figure 3.1 illustrates all the processes involved when light photons are absorbed by a fluorophore, an exited state is created depending of the nature of the molecule and its surrounding. Eventually, the excitaion ends in loss of energy (deactivation) due to emission of photons (fluorescense), vibration relaxation, and the intersystem crossing to the triplet state and subsequent emission of photons by phosphorescence.

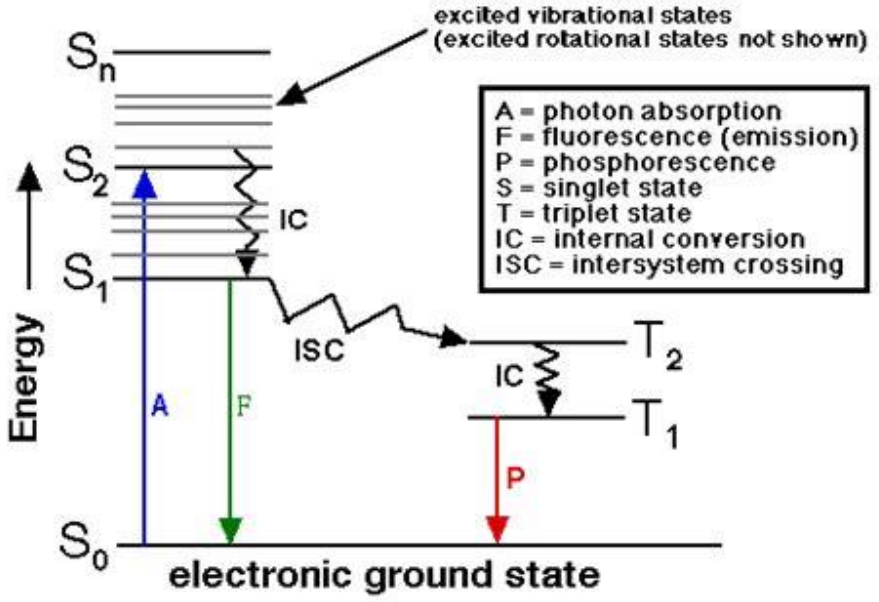

Figure 3.1. Jablonski diagram

For the calculation of the fluorescence quantum yield, the relative method and the following equation was used (Maity et al., 2014):

$$\varphi_s = \varphi_r \frac{I_s A_r n_s^2}{I_r A_s n_r^2} \qquad \textbf{(3. 2)}$$

Where φ_r is the fluorescence quantum yield of the reference. I stands for the integrated area under the emission curves. The subscripts **s** and **r** stand for sample and reference, respectively. A is the absorbance at a particular excitation wavelength. n is the refractive index of the medium. N,N'-bis(2,6-diisopropylphenyl)-perylene-3,4,9,10-tetracarboxydiimide was used as the reference

with $\boldsymbol{\varphi_f = 1}$ in $CHCl_3$. The same solvent ($CHCl_3$) was used as a medium for both the refernce and samples with $\boldsymbol{n}$ = 1.4495.

3.3.3 Fluorescence lifetime (τ)

A molecule's fluorescence lifetime can be defined as the average time a fluorophore spends in the excited state before returning to the ground state. Fluorescence lifetime can range from picoseconds to hundreds of nanoseconds depending on the fluorophore structure. The fluorescence lifetime of the synthesized compounds (**P4**, **P6**, **P11**, and **P12**) are shown in Figure 4.14 – Figure 4.17.

3.3.4 Optical band gap energy (E_g)

The optical band gap energy of compounds (**P4**, **P6**, **P11**, and **P12**) are estimated by identifying the optical tangent line of maximum absorption spectra with the corresponding wavelength using the following equation:

$$\boldsymbol{E_g = \frac{1240\ eV\ nm}{\lambda}} \qquad \textbf{(3. 3)}$$

Where $\boldsymbol{Eg}$ is the band gap energy in eV, and λ is the cut-off wavelength of the absorption band in nm.

From Figure 4.18, λ = 530 nm

Thus, $\boldsymbol{E_g = \frac{1240\ eV\ nm}{530}}$ **= 2.34 eV**

3.3.5 Electrochemical studies

Cyclic voltammetry measurements were performed to investigate the electrochemical properties of the synthesized materials. Reduction (E_{red}) and oxidation (E_{ox}) potentials were determined from the cyclic voltammograms using the maximum peak points $[E_{1/2} = (E_p^a + E_p^c)/2]$ and corresponding HOMO-LUMO

energy levels were calculated. LUMO energy levels were calculated from the reduction potentials by using the equation (3.4), and HOMO energy levels were calculated by using the equation (3.5) which uses the optical bandgap of those materials. The cyclic voltammetry graphs of the synthesized materials are shown in Figure 4.19 – Figure 4.22.

$$E_{LUMO} = -[4.8 - E_{Ferrocene} + E_{1/2(red)}] \quad \textbf{(3. 4)}$$

$$E_{HOMO} = E_{LUMO} - E_{g\,(optical)} \quad \textbf{(3. 5)}$$

3.3.6 Thermogravimetric analysis (TGA)

Thermogravimetric analysis (TGA) is a thermal analytical method that measures the mass of a sample over time as the temperature varies, and it was used to study the thermal properties of the synthesized compounds. This method can be used to measure various physical parameters such as absorption, adsorption, and desorption; as well as chemical parameters involving oxidation, reduction, chemisorption, and thermal decomposition. TGA curves were plotted using the data obtained from the TA instrument as shown in Figure 4.24 – Figure 4.26.

CHAPTER 4

RESULTS AND DISCUSSION

4.1 Chemical synthesis

In this work, commercially available perylene-3,4,9,10-tetracarboxylic dianhydride **PDA** was used as a starting material to produce perylene-3,4,9,10-tetracarboxylic tetrabutylester (**P1)** under mild conditions with a high yield (83.6%). Then, bromination reaction was carried out at room temperature using Br, K_2CO_3, and DCM as a solvent to obtain regioisomerically pure 1,7-dibromoperylene-3,4,9,10-tetracarboxylic tetrabutylester (**P2)** with ~50% yield. Afterwards, the reaction to convert **P2** to 1,7-dibromoperylene-3,4,9,10-tetracarboxylic bisanhydride (**P3)** was carried out at a relatively high temperature (100ºC) using p-toluenesulfonic acid monohydrate and toluene as the solvent. The reaction had a very high yield (90.1%). However, NMR data could not be obtained due to its low solubility. Subsequently, 1,7-dibromoperylene-3,4,9,10-tetracarboxy propargyl ester (**P4)** was produced with a relatively low yield (33%). 2-aminofluorene was converted into its azide derivative (2-azidofluorene, P5, 77% yield) and attached to the P4 by using click chemistry which allowed us to obtain a D-A type material. Due to the very low solubility of the synthesized compound in organic solvents (i.e. DCM, $CHCl_3$, and toluene) and the low electron-accepting ability of perylene tetraester derivative (**P6)**, it was not possible to proceed with the following bay-substitution reaction. A summary of the synthesis procedure is illustrated in Figure 4.1.

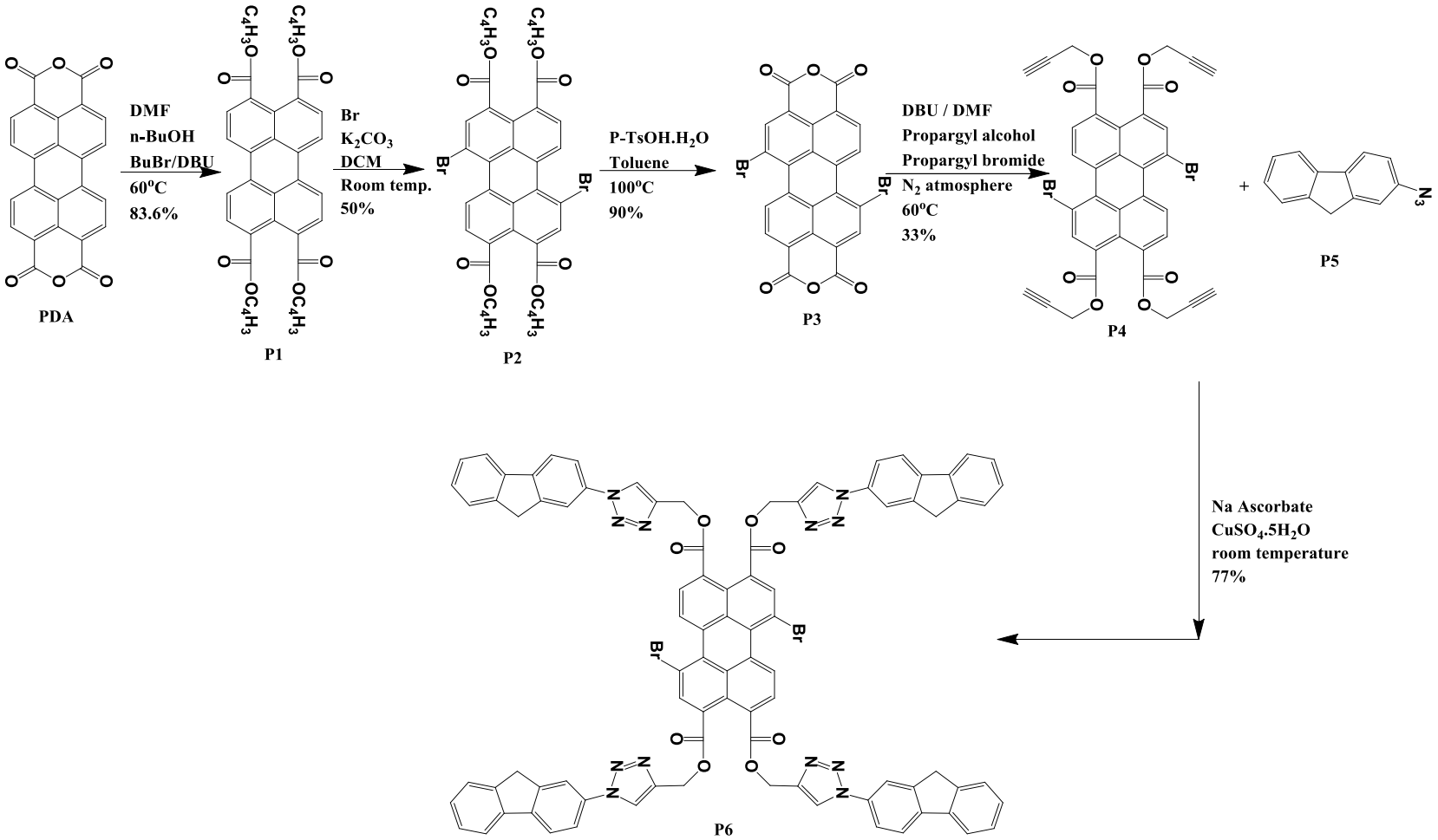

Figure 4.1. Synthesis of bipolar perylene derivative materials 1

Similarly, target molecule **P13** was synthesized from the commercially available **PDA**. The synthesis procedure was the same as demonstrated previously from **PDA** to **P2**. Afterwards, 1,7-dibromoperylene-3,4,9,10-tetracarboxylic dibutylester monoanhydride (**P8)** was synthesized using p-TsOH.H_2O, and heptane as the solvent at 90^oC to afford the desired intermediate **P8** in 52%. In the next step, an imidization reaction was done by using diisopropyl aniline and propionic acid at a relatively high temperature (130^oC) to produce N-(2,6-diisopropylphenyl)-1,7-dibromoperylene-3,4,9,10-tetracarboxy monoimide dibutylester (**P9)** with 50% yield. Then, the conversion of **P9** to N-(2,6-diisopropylphenyl)-1,7-dibromoperylene-3,4,9,10-tetracarboxy monoimide monoanhydride (**P10)** was carried out at 90^oC using p-TsOH.H_2O, and toluene as the solvent, yielding 96.3%. N-(2,6-diisopropylphenyl)-1,7-dibromoperylene-3,4,9,10-tetracarboxy monoimide dipropargyl ester (**P11)** was produced from **P10** under mild reaction conditions and an inert atmosphere with 49.7% yield. Afterwards, click chemistry was applied to react **P11** with **P5** affording **P12** in 63% yield. A summary of the synthesis procedure is illustrated in Figure 4.2.

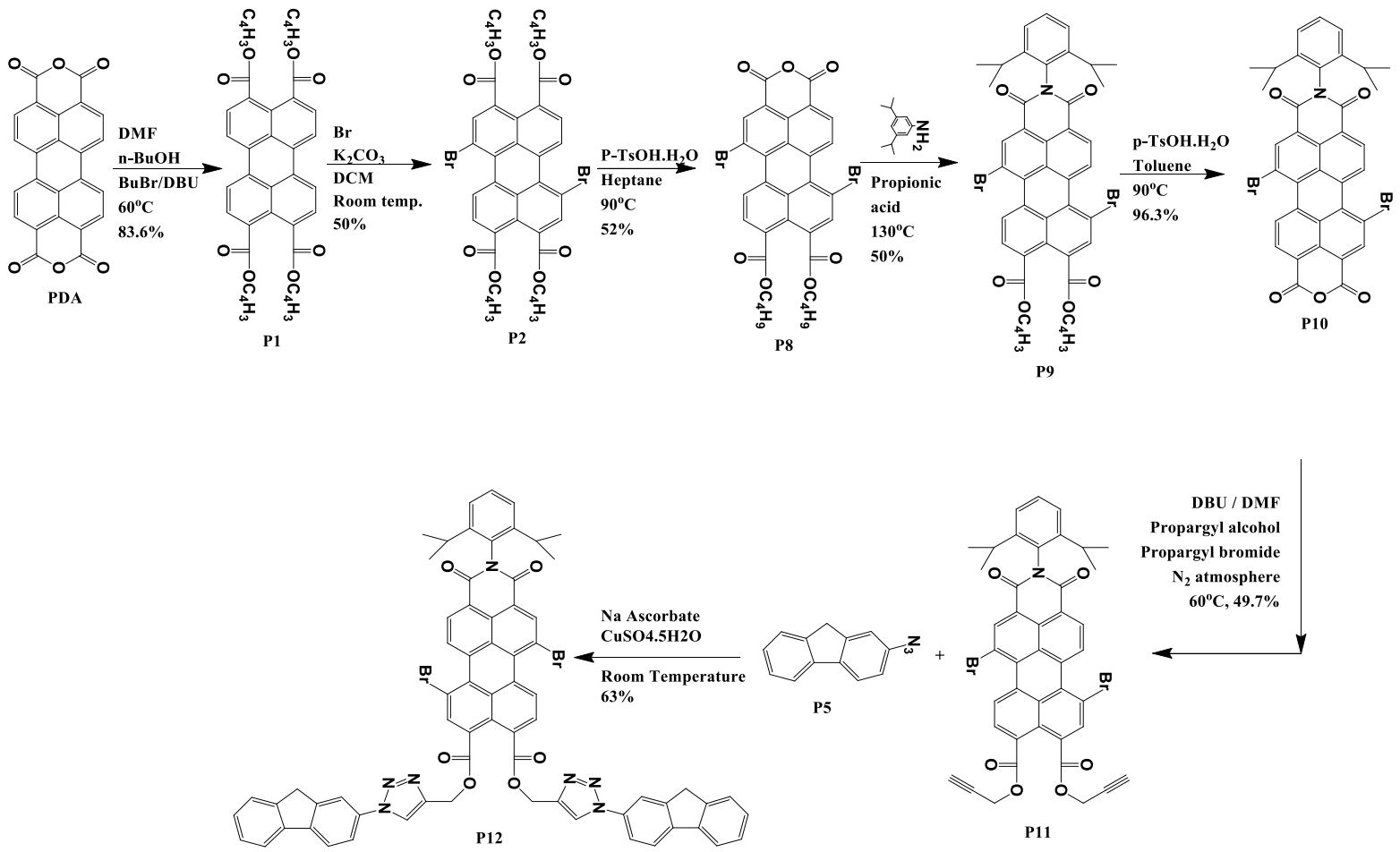

Figure 4.2. Synthesis of bipolar perylene derivative materials 2

4.2 Optical properties

The fluorescence properties of the synthesized compounds (**P4**, **P6**, **P11**, and **P12**) were observed in chloroform under daylight and UV light (254, 302, and 365) nm, which is shown in Figure 4.3 to Figure 4.6. It was observed that compounds **P11** and **P12** are fluorescent while compounds **P4** and **P6** are weakly fluorescent.

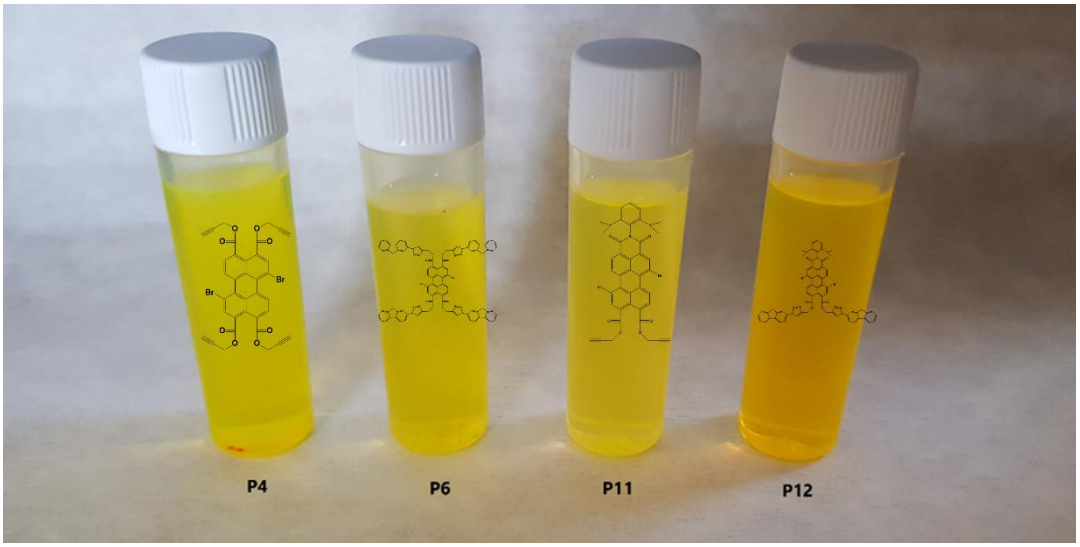

Figure 4.3. Picture of compounds (**P4**, **P6**, **P11**, and **P12**) under daylight

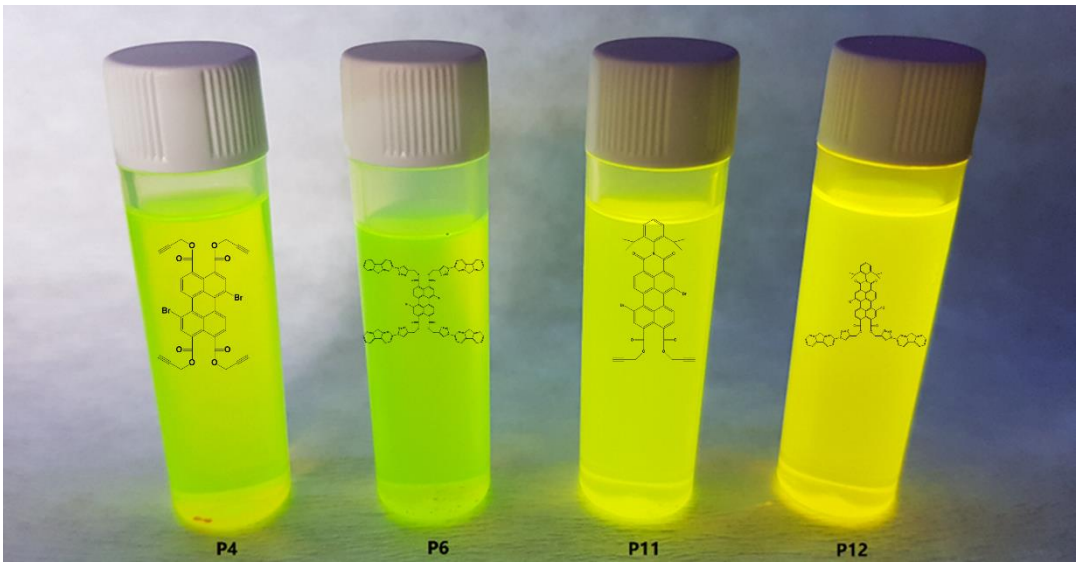

Figure 4.4. Picture of compounds (**P4**, **P6**, **P11**, and **P12**) under 254 nm

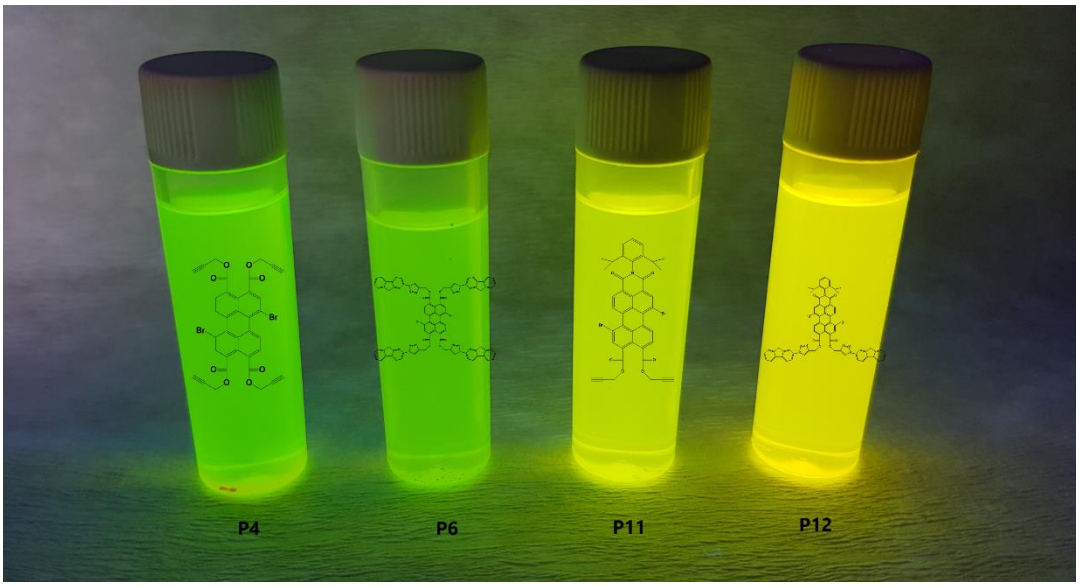

Figure 4.5. Picture of compounds (**P4**, **P6**, **P11**, and **P12**) under 302 nm

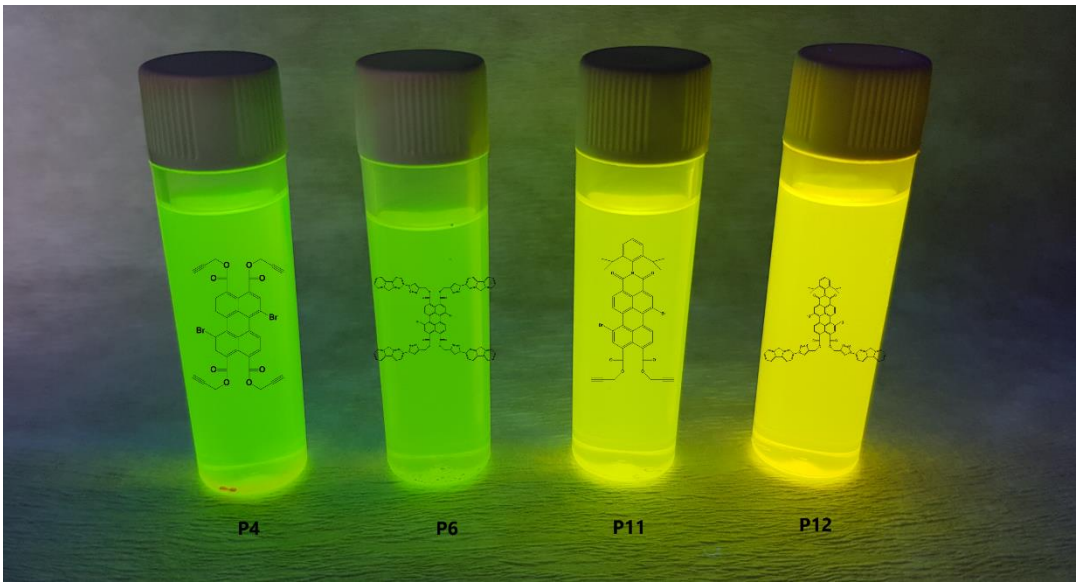

Figure 4.6. Picture of compounds (**P4**, **P6**, **P11**, and **P12**) under 365 nm

The optical properties of the synthesized compounds (**P4**, **P6**, **P11**, and **P12**) in solution were studied by ultraviolet-visible (UV–Vis) and fluorescence spectroscopies. Figure 4.7 shows the absorption spectra of the synthesized compounds recorded in $CHCl_3$. It is shown that the substitution of the alkyne group by the fluorene group at the peri position does not change the absorption properties of the PTCA derivative. On the other hand, altered absorption properties were observed when comparing di-substituted perylene and tetra-substituted perylene at the peri position.

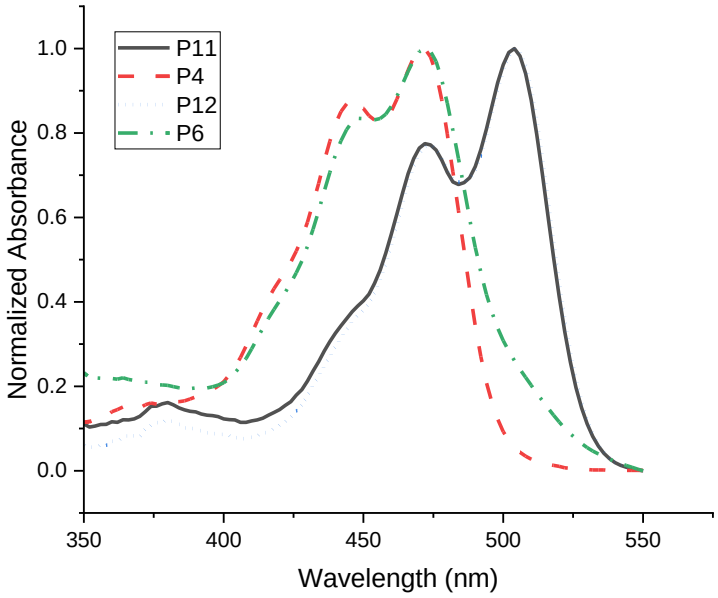

Figure 4.7. Absorption spectra of compounds (**P4**, **P6**, **P11**, and **P12**) in $CHCl_3$

All the compounds exhibit well-defined S_0-S_1 absorption and emission bands in the visible light region, which is a characteristic feature of the aromatic perylene core. Among the compounds (**P4**, **P6**, **P11**, and **P12**), taking 1,7-dibromoperylene-3,4,9,10-tetracarboxy propargyl ester (**P4**) as parent compound (λ_{abs} = 472 nm, λ_{abs} = 446 nm in $CHCl_3$), large bathochromic shifts were observed with perylene monoimde dipropargyl ester (**P11**) (λ_{abs} = 504 nm, λ_{abs} = 472 nm in $CHCl_3$), and perylene monoimide difluorene (**P12**) (λ_{abs} = 504 nm, λ_{abs} = 474 nm in $CHCl_3$), as

32 nm and 26 nm (in case of **P11**), and 32 nm and 28 nm (in case of **P12**) respectively. The attachment of the electron-donating fluorene group did not have a significant change in the case of both compounds **P6** and **P12**.

The synthesized PTCA derivatives, monoimide dipropargyl ester perylene (**P11),** and tetrapropargyl ester perylene (**P4)** were compared to each other in terms of absorbance in the wavelength range of 350-700 nm. Figure 4.8 shows that dipropargyl and tetrapropargyl ester derivatives follow almost the same absorption pattern but dipropargyl ester peaks are further red-shifted than tetrapropargyl ester. Because of the poor perylene-core ester-carbonyls orbital interactions, tetraesters are the weakest of the perylene tetracarboxylic derivatives in terms of electron-withdrawing ability, which corresponds to the electron-withdrawing abilities of ester < imide < anhydride groups (Ozser and Mohiuddin, 2018). As a result, a similar pattern was seen in the absorption and emission wavelength maxima of the synthesized compounds, with perylene tetraesters having the shortest absorption and emission wavelengths and monoimides having the longest. Since the attachment of the fluorene group did not have a significant effect on the absorption properties of the compounds **P6** and **P12**, the absorption pattern was also similar as shown in Figure 4.9. Perylene monoimide difluorene (**P12**) exhibits a red shift when compared to perylene tetrafluorene (**P6**).

The calculated molar absorptivity of the absorption maximum is 28718, 39789, and 41599 M^{-1} cm^{-1} for **P4**, **P11**, and **P12** respectively, and represents the favored high photon absorbing ability within 350-700 nm of the visible light region, making these compounds highly desirable derivatives for the photovoltaic applications.

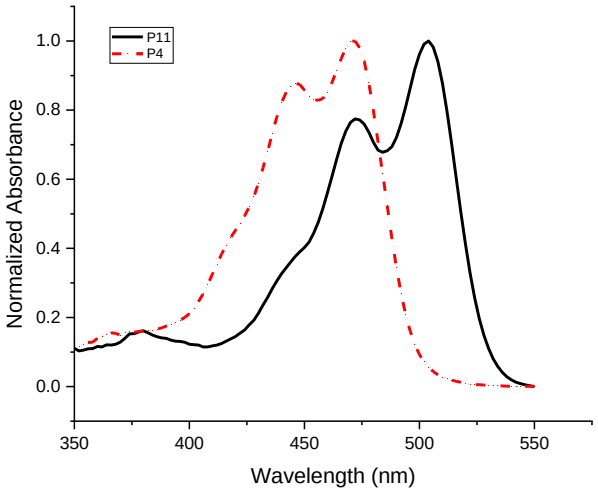

Figure 4.8. Comparison of dipropargyl ester perylene (**P11**) compound with tetrapropargyl ester perylene (**P4**) in $CHCl_3$

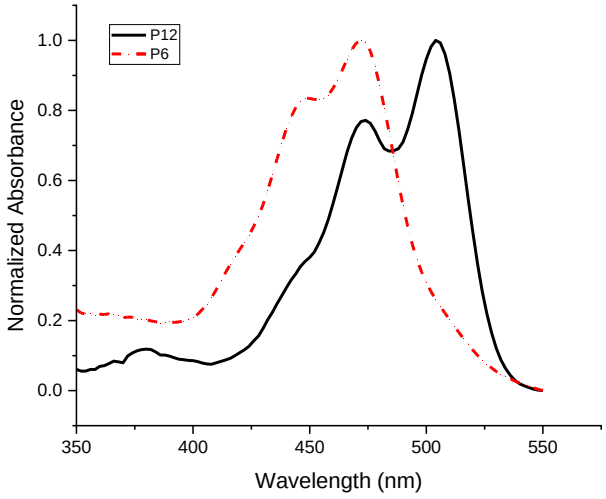

Figure 4.9. Comparison of difluorene perylene (**P12**) compound with tetrafluorene perylene (**P6**) in $CHCl_3$

The emission spectrum of the synthesized compounds (**P4**, **P6**, **P11**, and **P12**) was obtained by fluorescence spectroscopy at specific excitation wavelengths, 472 nm for **P4** and **P6**, and 503 nm for **P11** and **P12**. The normalized absorbance/fluorescence intensity spectra are shown in Figure 4.10 – Figure 4.13. Among the compounds (**P4**, **P6**, **P11**, and **P12**), taking **P4** as parent compound (λ_{ems} = 503 in $CHCl_3$), large bathochromic shifts were observed with **P11** (λ_{ems} = 530 in $CHCl_3$), and **P12** (λ_{ems} = 532 in $CHCl_3$), as 27 nm and 29 nm for **P11** and **P12**, respectively. The attachment of the electron-donating fluorene group did not have a significant change in the emission properties in the case of both compounds **P6** and **P12**.

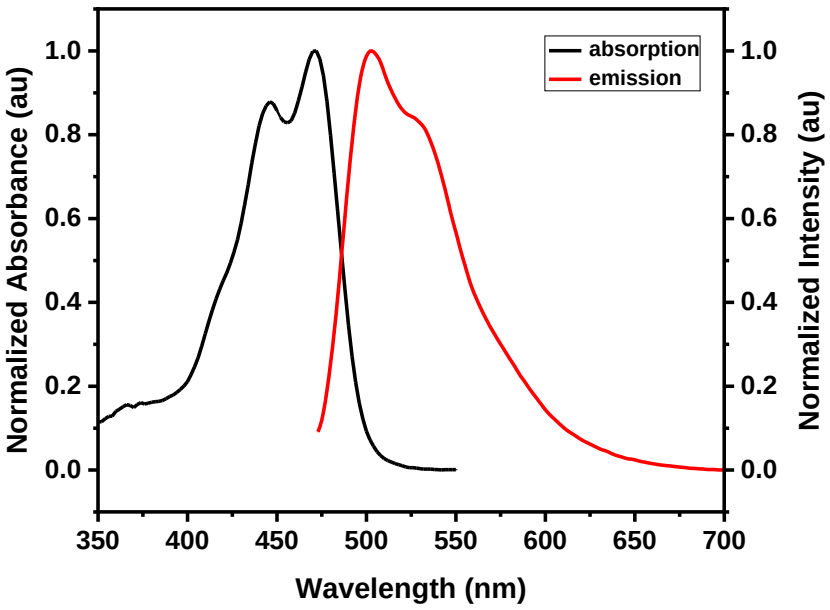

Figure 4.10. Normalized absorption and emission of **P4** in $CHCl_3$

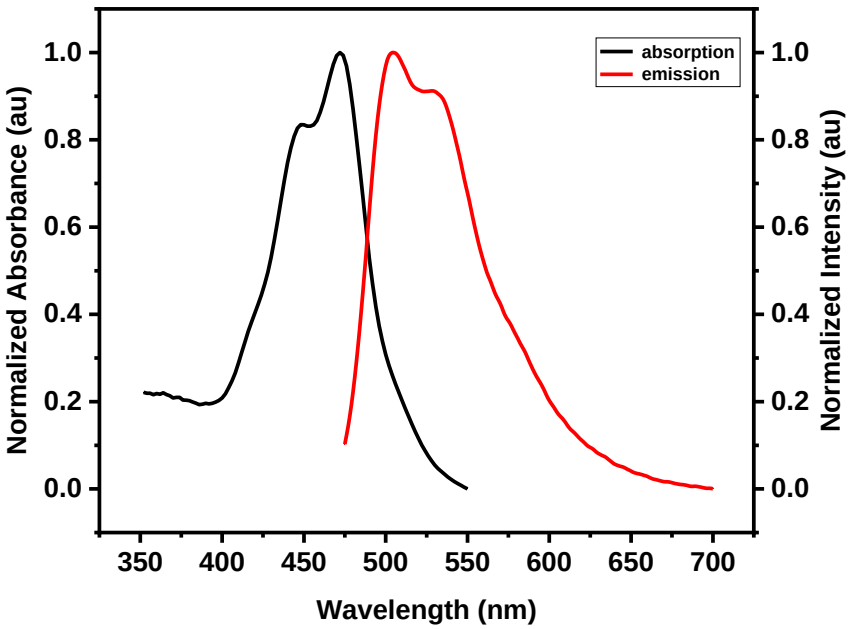

Figure 4.11. Normalized absorption and emission of **P6** in $CHCl_3$

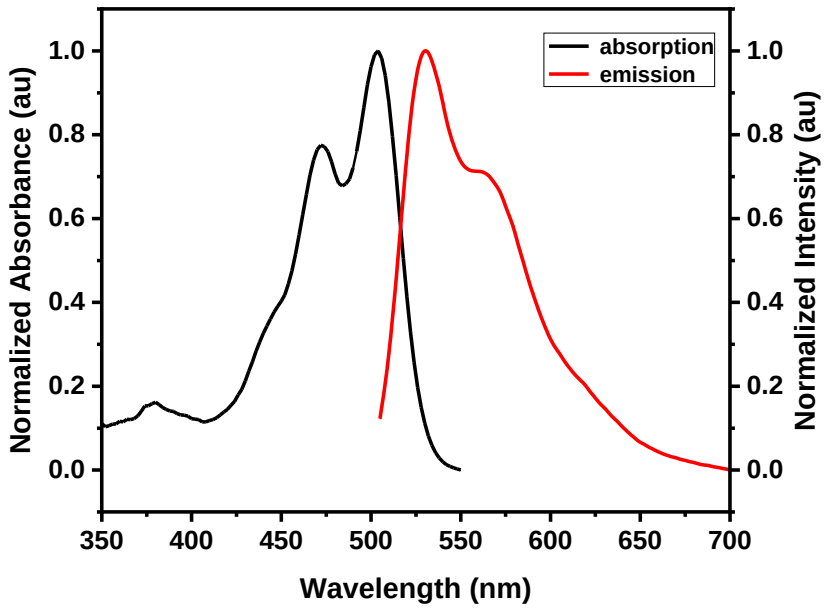

Figure 4.12. Normalized absorption and emission of **P11** in $CHCl_3$

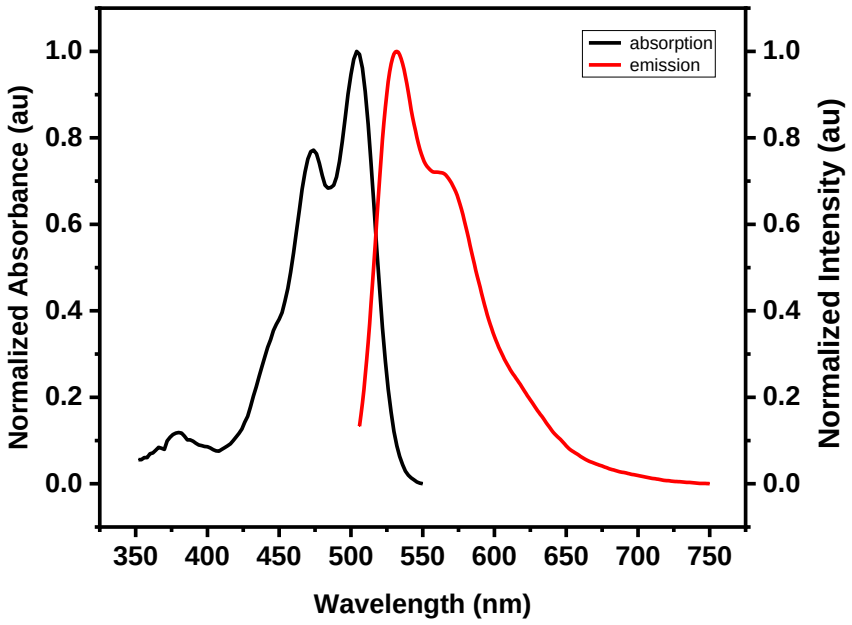

Figure 4.13. Normalized absorption and emission of **P12** in $CHCl_3$

The fluorescence quantum yield for all of the synthesized compounds was calculated using equation (3.2) and the data shown in Table 4.1. For all the compounds, the fluorescence quantum yield ranged from 0.05 to 0.63, which is significantly lower than the similar monoimide and tetraester compounds reported in many studies (>0.70) (Dubey et al., 2016a; Inan et al., 2019). The fluorescence quantum yield is lower for tetraester derivatives **P4** and **P6**, with Φ_f = 0.24 and Φ_f = 0.05, respectively, than for monoimide derivatives **P11** and **P12**, with Φ_f = 0.63 and Φ_f = 0.63, respectively. The fluorescence quantum yield for **P11** and **P12** had the same value despite the attachment of two fluorene groups at the peri positions. Surprisingly, the fluorescence quantum yield of compound **P6** had the lowest value, which can be due to the attachment of four fluorene groups at the peri positions. The higher quantum yield of compounds (**P11** and **P12**) suggests better performance and optoelectronic properties when utilized in OLEDs (Dayneko et al., 2021).

Table 4.1. Fluorescence quantum yield data.

Compound	λ_{max}**(nm)**	λ_{exc}**(nm)**	I_s	I_r	A_s	A_r	Φ_f
P4	472	472	6560437	5131780	0.15	0.028	0.24
P6	472	472	3578118	5131780	0.39	0.028	0.05
P11	503	503	9533748	4270754	0.12	0.034	0.63
P12	504	504	11747369	4236689	0.15	0.034	0.63

The fluorescence lifetime of the synthesized compounds (**P4**, **P6**, **P11**, and **P12**) ranged between 0.5 and 5 ns. The fluorescence lifetime of the tetraester derivatives **P4** and **P6** is 0.82 ns and 1.54 ns, respectively, which is significantly lower compared to the monoimide derivatives **P11** and **P12** having lifetimes 4.00 ns and 4.27 ns, respectively. The fluorescence lifetimes are usually observed between 4-5 ns for perylene monimide diester derivatives and between 1-1.6 ns for perylene tetraester derivatives (Inan et al., 2019; Dubey et al., 2015). The observed increase in the fluorescence lifetime for compounds (**P11** and **P12**) further supports better energy transfer abilities (Dayneko et al., 2021). The lifetime graphs are shown in Figure 4.14 - Figure 4.17.

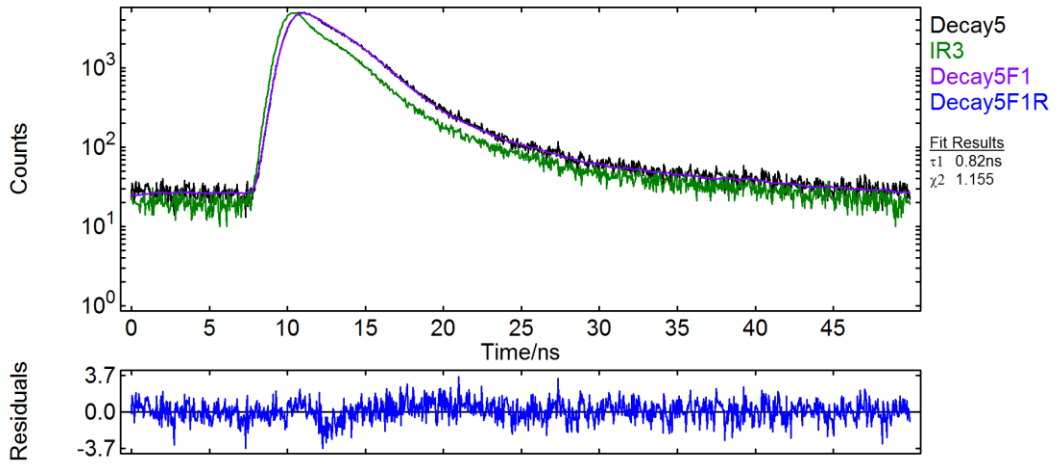

Figure 4.14. The fluorescence lifetime of **P4**

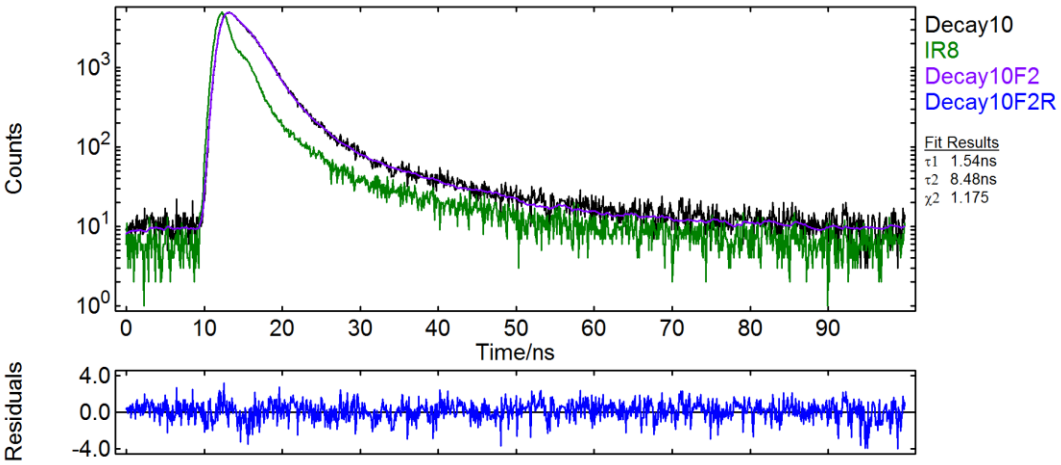

Figure 4.15. The fluorescence lifetime of **P6**

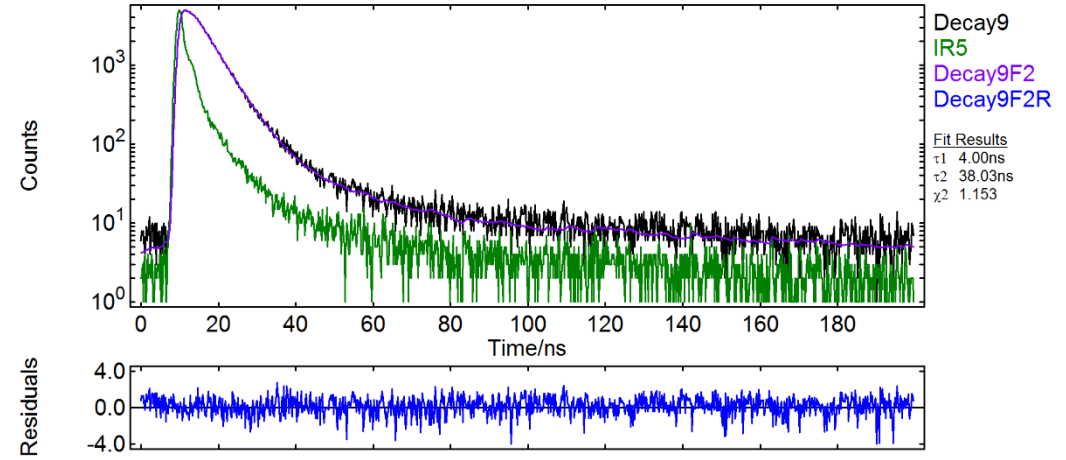

Figure 4.16. The fluorescence lifetime of **P11**

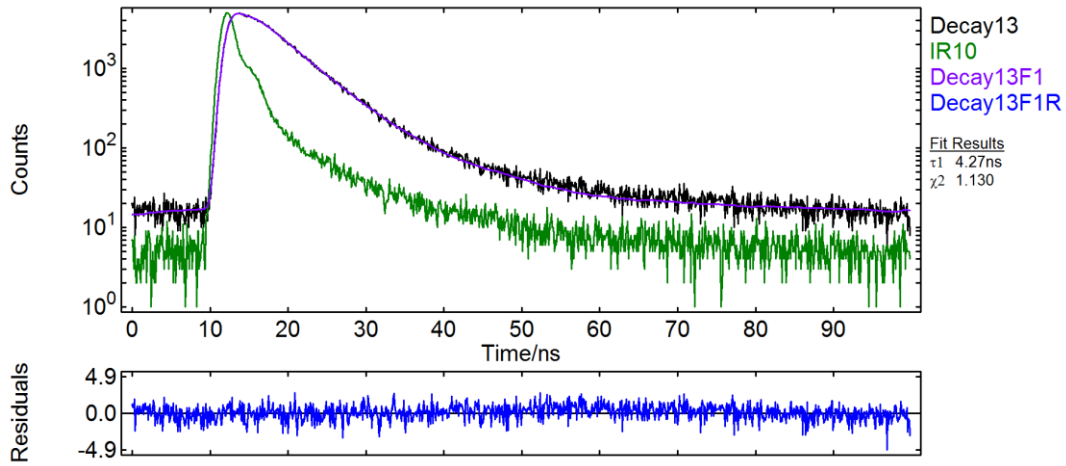

Figure 4.17. The fluorescence lifetime of **P12**

The photophysical data for all the compounds is summarized in Table 4.2.

Table 4.2. Photophysical data of compounds (**P4**, **P6**, **P11**, and **P12**) in $CHCl_3$.

Compound	**λ_{max}(nm) /ε_{max}(M^{-1} cm^{-1})**	φ_f	**λ_{ems}(nm)**	**Stokes shift (nm)**	**τ (ns)**
P4	472 (28718) 446 (25185)	0.24	503	31	0.82
P6	472 448	0.05	505	33	1.54
P11	504 (39789) 472 (30850)	0.63	530	26	4.00
P12	504 (41599) 474 (32112)	0.63	532	25	4.27

4.3 Electrochemical properties

Cyclic voltammetry was used to investigate the electrochemical properties. The cyclic voltammograms of the synthesized compounds are shown in Figure 4.19 – Figure 4.22. The cut-off wavelength of the synthesized compounds was obtained in correspondence to their maximum absorption spectra as shown in Figure 4.18 to calculate the optical bandgap energy (E_g) using equation (3.3) and the results are shown in Table 4.3.

Table 4.3. Optical bandgap energy for compounds (**P4**, **P6**, **P11**, and **P12**)

Compounds	**P4**	**P6**	**P11**	**P12**
$\lambda_{0\rightarrow0}$	505	520	530	535
E_g **(eV)**	2.46	2.38	2.34	2.31

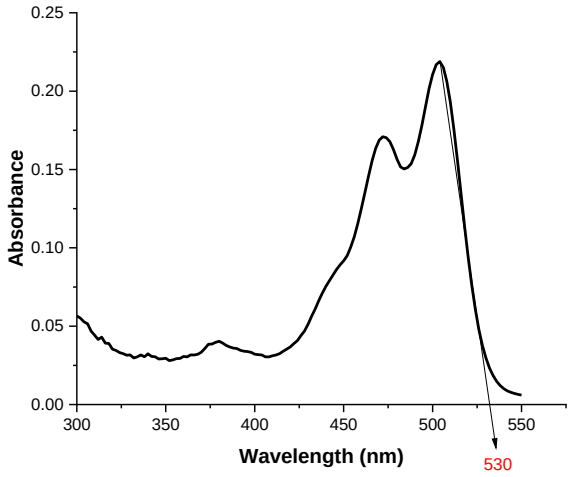

Figure 4.18. The cut-off wavelength for **P11** at 530 nm in $CHCl_3$

The reduction potentials of the synthesized compounds ranged between -0.50 and -0.81 V. Perylene tetraester derivatives (**P4** and **P6)** exhibit lower reduction potential values, which means they are the least electron-deficient compounds. Upon moving to the monoimide derivatives (**P11** and **P12**), the electron deficiency increases due to the presence of an imide group that is more electron-withdrawing than the ester groups. The HOMO-LUMO energy levels were calculated using the mentioned equations (3.4 and 3.5) and the results are summarized in Table 4.4. As illustrated in Figure 4.23, compounds **P6** and **P12**, with fluorene groups attached to the perylene core, exhibit lower values for HOMO and LUMO energy levels compared to their corresponding intermediates **P4** and **P11**, respectively, represents the clear effect of peri substitution on the electronic structure of perylene core (Dubey et al., 2016d).

Table 4.4. Electrochemical properties of compounds (**P4**, **P6**, **P11**, and **P12**).

Compound	**$E_{1/2\ red}$ (V)**	**$E_{1/2\ ox}$ (V)**	**E_{LUMO} (eV)**	**E_{HOMO} (eV)**	**E_g (optical)**
P4	-0.75	0.99	-3.68	-6.14	2.46
P6	-0.81	-	-3.62	-6.00	2.38
P11	-0.50	-	-3.93	-6.27	2.34
P12	-0.52	0.63	-3.91	-6.22	2.31

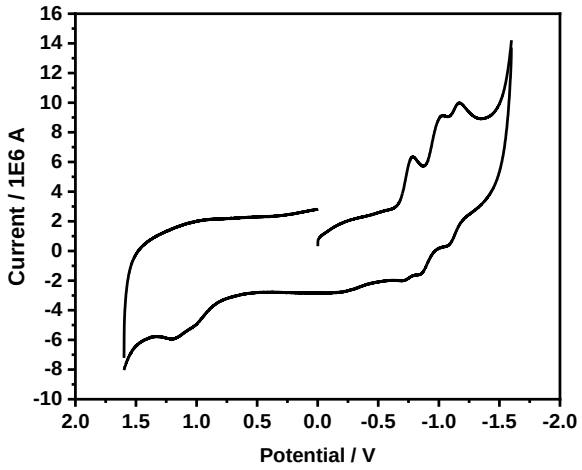

Figure 4.19. Cyclic voltammogram of **P4**

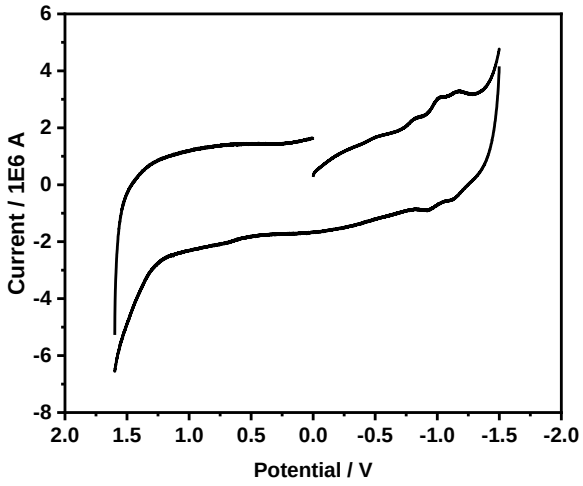

Figure 4.20. Cyclic voltammogram of **P6**

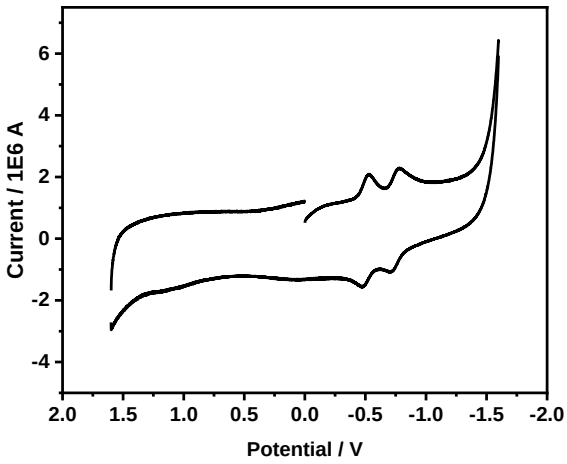

Figure 4.21. Cyclic voltammogram of **P11**

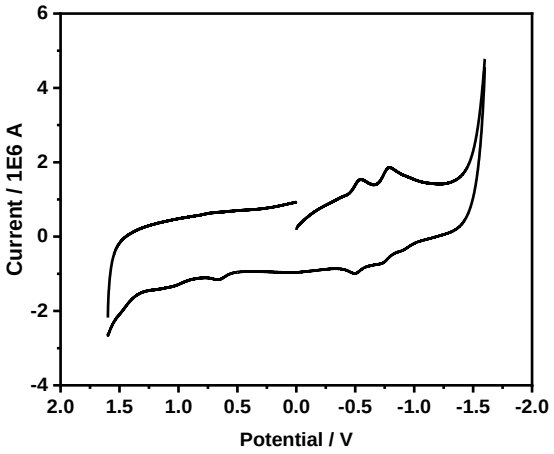

Figure 4.22. Cyclic voltammogram of **P12**

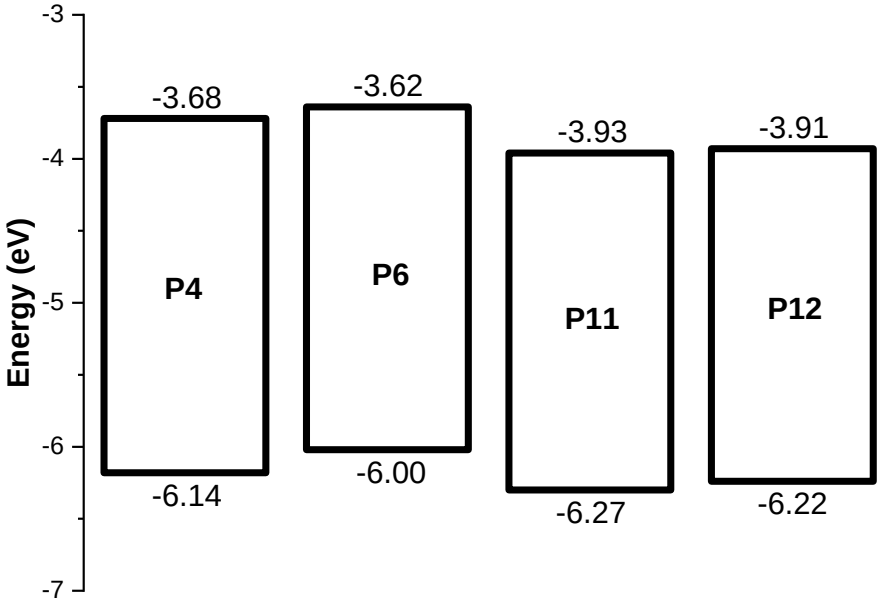

Figure 4.23. The HOMO and LUMO energy levels of the synthesized compounds

4.4 Thermal properties

The thermal properties of the synthesized compounds were determined by thermogravimetric analysis (TGA). The TGA curves of the compounds are shown in Figure 4.24 – Figure 4.26. The results show 5% weight loss temperatures for **P4**, **P11**, and **P12** are 300, 313, and 251 °C, respectively. Compounds **P4**, **P11**, and **P12** retain 60% of their weight at 495, 564, and 642 °C, respectively.

P12 retains 87% of its weight at 279 °C which is matching with the calculated 13% weight loss by losing the N-(2,6-diisopropylphenyl) group at the imide position. The same compound (**P12**) retains 60% of its weight at 642 °C, which is also matching with the calculated 40% weight loss by losing the N-(2,6-diisopropylphenyl) group and two fluorene groups. The thermogravimetric results are summarized in Table 4.5.

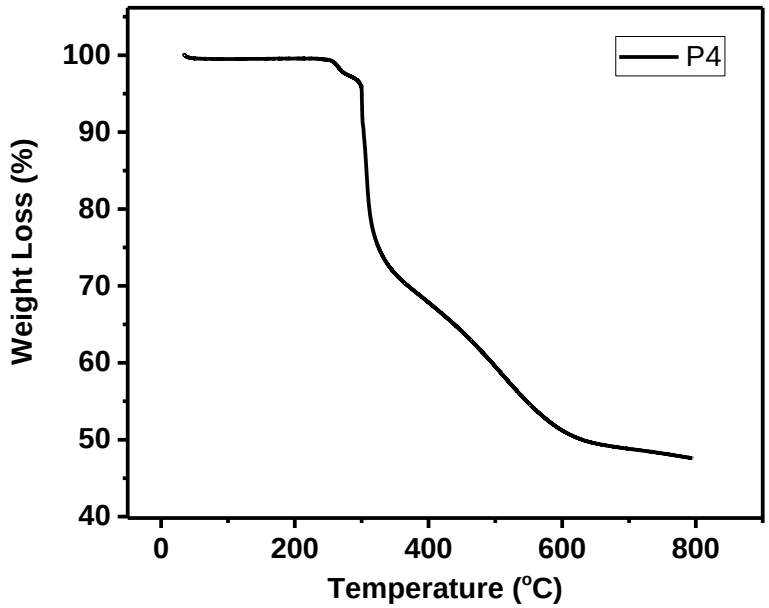

Figure 4.24. TGA curve of **P4**

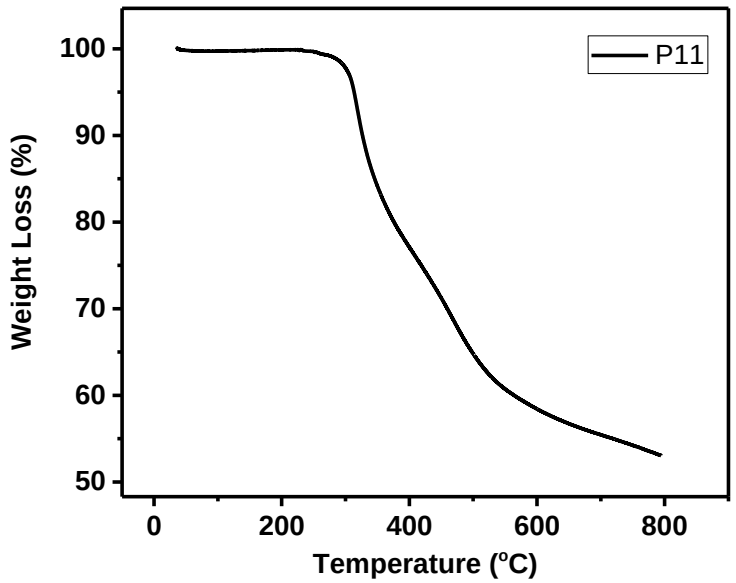

Figure 4.25. TGA curve of **P11**

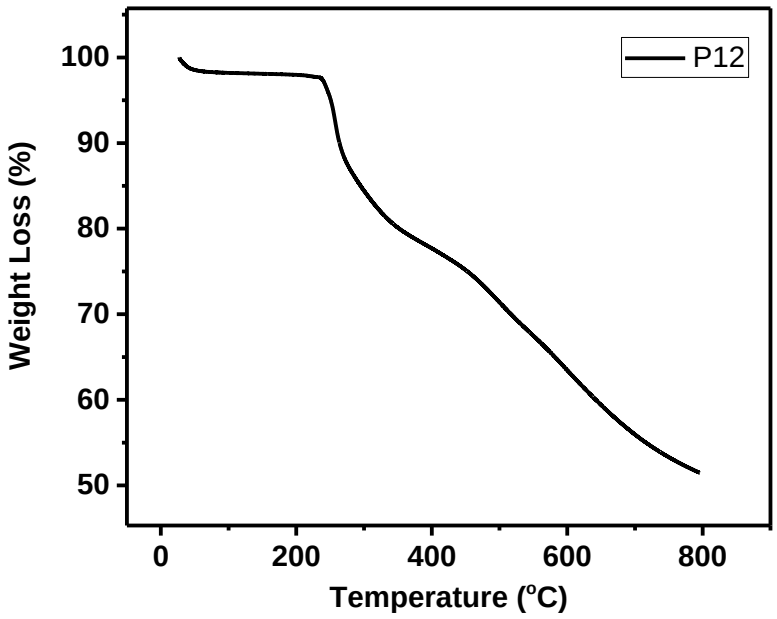

Figure 4.26. TGA curve of **P12**

Table 4.5. Thermogravimetric analysis of the synthesized compounds

Compound	**%5 Weight Loss Temperature (ºC)**	**%40 Weight Loss Temperature (ºC)**	**Carbon res (%) at 795 ºC**
P4	300	495	52
P11	313	564	47
P12	251	642	49

CHAPTER 5

CONCLUSION AND FUTURE WORK

In this study, two isomerically pure perylene tetracarboxy propargyl ester derivatives (**P4** and **P11**) were designed, synthesized, and purified successfully to be used as intermediate compounds for bipolar perylene light-harvesting systems. Afterwards, click chemistry was utilized for further substitution at the peri positions and D-A type bipolar perylene derivatives (**P6** and **P12**) were obtained. Synthesized compounds were characterized by NMR and FTIR spectroscopies and results suggest that the compounds were obtained successfully.

Optical properties were studied by steady-state UV-Vis and fluorescence spectroscopies. Perylene monoimide dipropargyl ester derivatives (**P11** and **P12**) exhibited more red-shifted absorbance and emission, higher fluorescence quantum yields, and longer lifetimes compared to the tetraester derivatives (**P4** and **P6**). Perylene monoimide derivatives have higher molar extinction coefficients and longer lifetimes, which make them better dye alternatives for the DSSC applications. Also, the higher fluorescence quantum yields of the monoimide derivatives make them better alternatives for the OLED applications. On the other hand, perylene tetrapropargyl ester derivative (**P4**) allows further substitution with more substituents compared to dipropargyl ester derivative (**P11**), which may improve their performance, optical, and electrochemical properties. The synthesized intermediates (**P4** and **P11**) are very favorable structures, which can be further derivatized by using click reaction and changing the electron-donor groups at the peri positions. Various donor-acceptor type light-harvesting materials can be obtained in this way. By using more appropriate electron-donor groups, and providing efficient overlap between the donor emission and acceptor absorption,

efficient energy transfer from donor to acceptor may be satisfied which is a desired property for the light-harvesting systems.

The electrochemical properties were studied by cyclic voltammetry and HOMO-LUMO energy levels were determined. All molecules showed reduction bands arise from the electron-accepting perylene tetracarboxylic acid derivatives. Results indicate that monoimide diester derivatives (**P11** and **P12**) have lower reduction potentials compared to the tetraester derivatives (**P4** and **P6**) which is related to the stronger electron-accepting ability of the monoimide diester derivatives. The calculated LUMO energy levels were between -3.62 eV and -3.93 eV and HOMO energy levels were between -6.00 eV and -6.27 eV, which is consistent with the literature.

In the synthesis of the D-A type derivatives, azidofluorene donor group was used as a trial and other electron-donor groups will be used in the future work. The bay substitution with different electron-rich substituents such as tert-butyl-phenoxy derivatives and cyclic amines should be studied to compare their properties to similar bay-brominated compounds. Figures 5.1 and 5.2 show the target molecules (**P7** and **P13**) which could not be obtained successfully within this study. Therefore, new synthetic methods will be applied in future work to synthesize them.

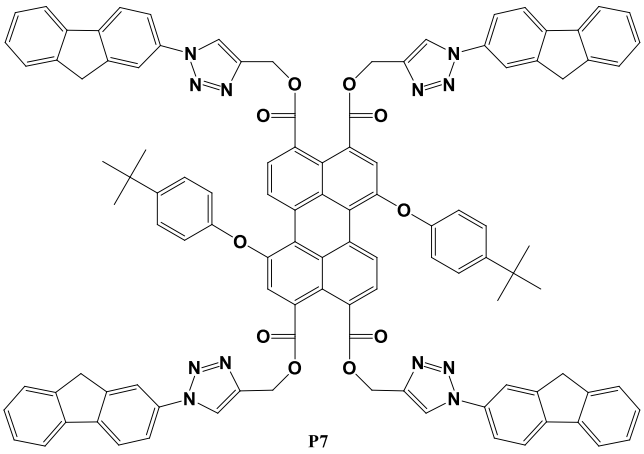

Figure 5.1. Target molecule **P7** for future work

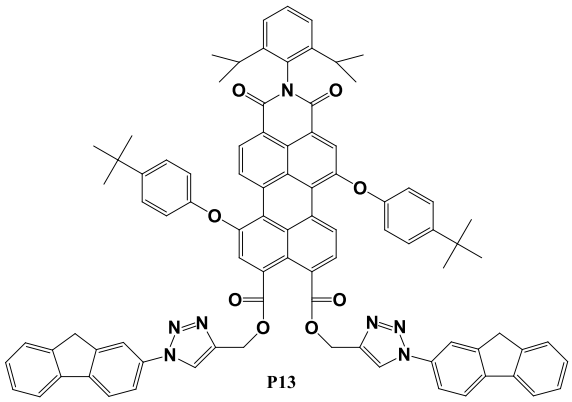

Figure 5.2. Target molecule **P13** for future work

REFERENCES

Aydin, E., Nisanci, B., Acar, M., Dastan, A., Bozdemir, Ö.A., 2015, Synthesis and use of "clickable" bay-region tetrasubstituted perylene tetracarboxylic tetraesters and a perylene monoimide diester as energy acceptors, *New J. Chem.*, 39(1), 548–554pp.

Bala, I., Singh, N., Yadav, R.A.K., De, J., Gupta, S.P., Singh, D.P., Dubey, D.K., Jou, J.H., Douali, R., Pal, S.K., 2020, Room temperature perylene based columnar liquid crystals as solid-state fluorescent emitters in solution-processable organic light-emitting diodes, *J. Mater. Chem. C*, 8(36), 12485–12494pp.

Blakers, A., Zin, N., McIntosh, K.R., Fong, K., 2013, High efficiency silicon solar cells, *Energy Procedia*, 33, 1–10pp.

Blandford, R., Watkins, M., 2009, Bell Labs Demonstrates the First Practical Silicon Solar Cell, *APS News*,

Chiba, Y., Islam, A., Watanabe, Y., Komiya, R., Koide, N., Han, L., 2006, Dye-sensitized solar cells with conversion efficiency of 11.1%, *Japanese J. Appl. Physics, Part 2 Lett.*, 45(7L), L638p.

Choi, H., Lee, J.K., Song, K., Kang, S.O., Ko, J., 2007, Novel organic dyes containing bis-dimethylfluorenyl amino benzo[b]thiophene for highly efficient dye-sensitized solar cell, *Tetrahedron*, 63(15), 3115–3121pp.

Dayneko, S. V., Cieplechowicz, E., Bhojgude, S.S., Van Humbeck, J.F., Pahlevani, M., Welch, G.C., 2021, Improved performance of solution processed OLEDs using N -annulated perylene diimide emitters with bulky side-chains , *Mater. Adv.*, 2(3), 933–936pp.

Dayneko, S. V., Rahmati, M., Pahlevani, M., Welch, G.C., 2020, Solution processed red organic light-emitting-diodes using an: N-annulated perylene diimide fluorophore, *J. Mater. Chem. C*, 8(7), 2314–2319pp.

Dimroth, F., 2006, High-efficiency solar cells from III-V compound semiconductors, *Phys. Status Solidi C Conf.*, 3(3), 373–379pp.

Dubey, R.K., Eustace, S.J., Van Mullem, J.S., Sudhölter, E.J.R., Grozema, F.C., Jager, W.F., 2019, Perylene Bisimide Dyes with up to Five Independently Introduced Substituents: Controlling the Functionalization Pattern and Photophysical Properties Using Regiospecific Bay Substitution, *J. Org. Chem.*, 84(15), 9532–9547pp.

Dubey, R.K., Inan, D., Philip, A.M., Grozema, F.C., Jager, W.F., 2020, Efficacious elimination of intramolecular charge transfer in perylene imide based light-harvesting antenna molecules, *Chem. Commun.*, 56(41), 5560–5563pp.

Dubey, R.K., Inan, D., Sengupta, S., Sudhölter, E.J.R., Grozema, F.C., Jager, W.F., 2016a, Tunable and highly efficient light-harvesting antenna systems based on 1,7-perylene-3,4,9,10-tetracarboxylic acid derivatives, *Chem. Sci.*, 7(6), 3517–3532pp.

Dubey, R.K., Knorr, G., Westerveld, N., Jager, W.F., 2016b, Fluorescent PET probes based on perylene-3,4,9,10-tetracarboxylic tetraesters, *Org. Biomol. Chem.*, 14(5), 1564–1568pp.

Dubey, R.K., Westerveld, N., Eustace, S.J., Sudhölter, E.J.R., Grozema, F.C., Jager, W.F., 2016c, Synthesis of Perylene-3,4,9,10-tetracarboxylic Acid Derivatives Bearing Four Different Substituents at the Perylene Core, *Org. Lett.*, 18(21), 5648–5651pp.

Dubey, R.K., Westerveld, N., Grozema, F.C., Sudhölter, E.J.R., Jager, W.F., 2015, Facile synthesis of pure 1,6,7,12-tetrachloroperylene-3,4,9,10-tetracarboxy bisanhydride and bisimide, *Org. Lett.*, 17(8), 1882–1885pp.

Dubey, R.K., Westerveld, N., Sudhölter, E.J.R., Grozema, F.C., Jager, W.F., 2016d, Novel derivatives of 1,6,7,12-tetrachloroperylene-3,4,9,10-tetracarboxylic acid: Synthesis, electrochemical and optical properties, *Org.*

Chem. Front., 3(11), 1481–1492pp.

Fraas, L.M., Fraas, L.M., 2014, History of Solar Cell Development, in: Low-Cost Solar Electric Power

Giribabu, L., Kanaparthi, R.K., Velkannan, V., 2012, Molecular engineering of sensitizers for dye-sensitized solar cell applications, *Chem. Rec.*, 12(3), 306–328pp.

Grätzel, M., 2003, Dye-sensitized solar cells, *J. Photochem. Photobiol. C Photochem. Rev.*, 4(2), 145–153pp.

Green, M.A., 2016, Commercial progress and challenges for photovoltaics, *Nat. Energy*, 1(1), 1–4pp.

Gupta, R.K., Ulla, H., Satyanarayan, M.N., Sudhakar, A.A., 2018, A Perylene-Triazine-Based Star-Shaped Green Light Emitter for Organic Light Emitting Diodes, *European J. Org. Chem.*, 2018(13), 1608–1613pp.

Hoppe, H., Sariciftci, N.S., 2004, Organic solar cells: An overview, *J. Mater. Res.*, 19(7), 1924–1945pp.

Inan, D., Dubey, R.K., Jager, W.F., Grozema, F.C., 2019, Tailoring Photophysical Processes of Perylene-Based Light Harvesting Antenna Systems with Molecular Structure and Solvent Polarity, *J. Phys. Chem. C*, 123(1), 36–47pp.

Inan, D., Dubey, R.K., Westerveld, N., Bleeker, J., Jager, W.F., Grozema, F.C., 2017, Substitution Effects on the Photoinduced Charge-Transfer Properties of Novel Perylene-3,4,9,10-tetracarboxylic Acid Derivatives, *J. Phys. Chem. A*, 121(24), 4633–4644pp.

Ito, S., Murakami, T.N., Comte, P., Liska, P., Grätzel, C., Nazeeruddin, M.K., Grätzel, M., 2008, Fabrication of thin film dye sensitized solar cells with solar to electric power conversion efficiency over 10%, *Thin Solid Films*, 516(14), 4613–4619pp.

Justin Thomas, K.R., Baheti, A., 2013, Fluorene based organic dyes for dye sensitised solar cells: Structure-property relationships, *Mater. Technol.*, 28(1–2), 71–87pp.

Kabir, E., Kumar, P., Kumar, S., Adelodun, A.A., Kim, K.H., 2018, Solar energy: Potential and future prospects, *Renew. Sustain. Energy Rev.*, 82, 894–900pp.

Kalogirou, S.A., 2004, Solar thermal collectors and applications, *Prog. Energy Combust. Sci.*, 30(3), 231–295pp.

Lee, S.H., 2009, Cost effective process for high-efficiency solar cells, *Sol. Energy*, 83(8), 1285–1289pp.

Lewis, N.S., 2007, Toward cost-effective solar energy use, *Science (80-.).*, 315(5813), 798–801pp.

Maity, B., Chatterjee, A., Seth, D., 2014, The photophysics of 7-(diethylamino)coumarin-3-carboxylic acid N-succinimidyl ester in reverse micelle: Excitation wavelength dependent dynamics, *RSC Adv.*, 4(7), 3461–3471pp.

Mathew, S., Yella, A., Gao, P., Humphry-Baker, R., Curchod, B.F.E., Ashari-Astani, N., Tavernelli, I., Rothlisberger, U., Nazeeruddin, M.K., Grätzel, M., 2014, Dye-sensitized solar cells with 13% efficiency achieved through the molecular engineering of porphyrin sensitizers, *Nat. Chem.*, 6(3), 242–247pp.

Nelson, J., 2003, The Physics of Solar Cells, The Physics of Solar Cells

Newell, R.G., Raimi, D., Aldana, G., 2019, Global Energy Outlook 2019: The Next Generation of Energy, *Resour. Futur.*, (July), 46p.

Ozser, M.E., Mohiuddin, O., 2018, Synthesis, photophysical, structural and electronic properties of novel regioisomerically pure 1,7-disubstituted perylene-3,4,9,10-tetracarboxylic monoimide dibutylester derivatives, *J. Mol. Struct.*, 1158, 145–155pp.

Quaschning, V., 2014, Understanding renewable energy systems, Understanding Renewable Energy Systems

Ranabhat, K., Patrikeev, L., Revina, A.A. evna, Andrianov, K., Lapshinsky, V., Sofronova, E., 2016, An introduction to solar cell technology, *J. Appl. Eng. Sci.*, 14(4), 481–491pp.

Sengupta, S., Dubey, R.K., Hoek, R.W.M., Van Eeden, S.P.P., Gunbasç, D.D., Grozema, F.C., Sudhölter, E.J.R., Jager, W.F., 2014, Synthesis of regioisomerically pure 1,7-dibromoperylene-3,4,9,10- tetracarboxylic acid derivatives, *J. Org. Chem.*, 79(14), 6655–6662pp.

Sharma, K., Sharma, V., Sharma, S.S., 2018, Dye-Sensitized Solar Cells: Fundamentals and Current Status, *Nanoscale Res. Lett.*, 13(1), 1–46pp.

United States Environmental Protection Agency, 2019, Global Greenhouse Gas Emissions Data | Greenhouse Gas (GHG) Emissions | US EPA, *United States Environ. Prot. Agency*,

Wu, M., Lin, X., Wang, T., Qiu, J., Ma, T., 2011, Low-cost dye-sensitized solar cell based on nine kinds of carbon counter electrodes, *Energy Environ. Sci.*, 4(6), 2308–2315pp.

Yen, Y.S., Hsu, Y.C., Lin, J.T., Chang, C.W., Hsu, C.P., Yin, D.J., 2008, Pyrrole-based organic dyes for dye-sensitized solar cells, *J. Phys. Chem. C*, 112(32), 12557–12567pp.

APPENDICES

A. FTIR, NMR, and UV-vis spectra for the synthesized compounds

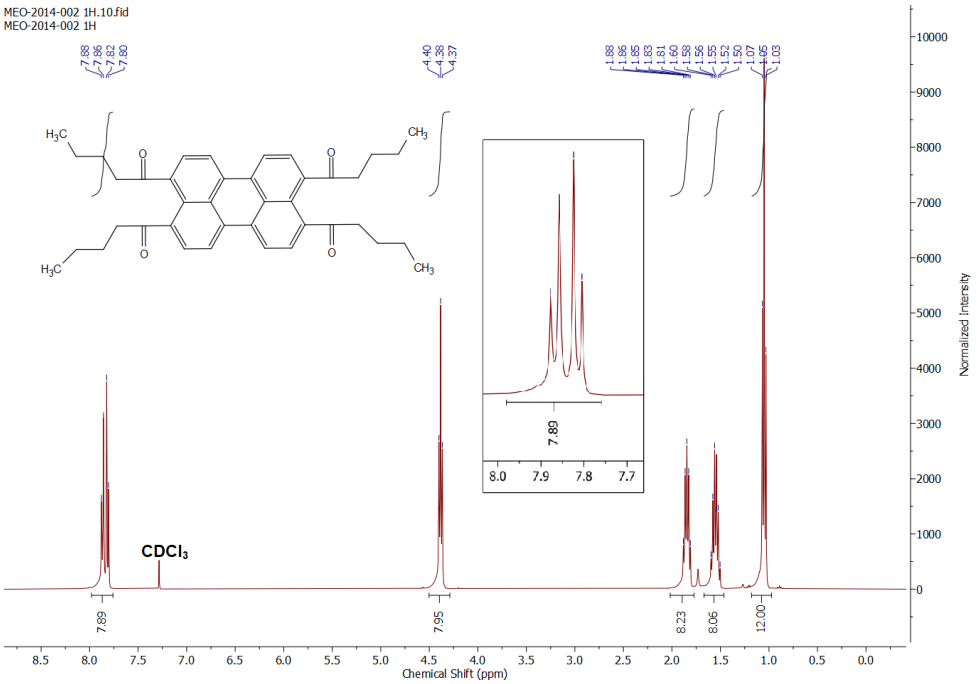

Figure A. 1. ^{1}H-NMR spectrum of **P1**.

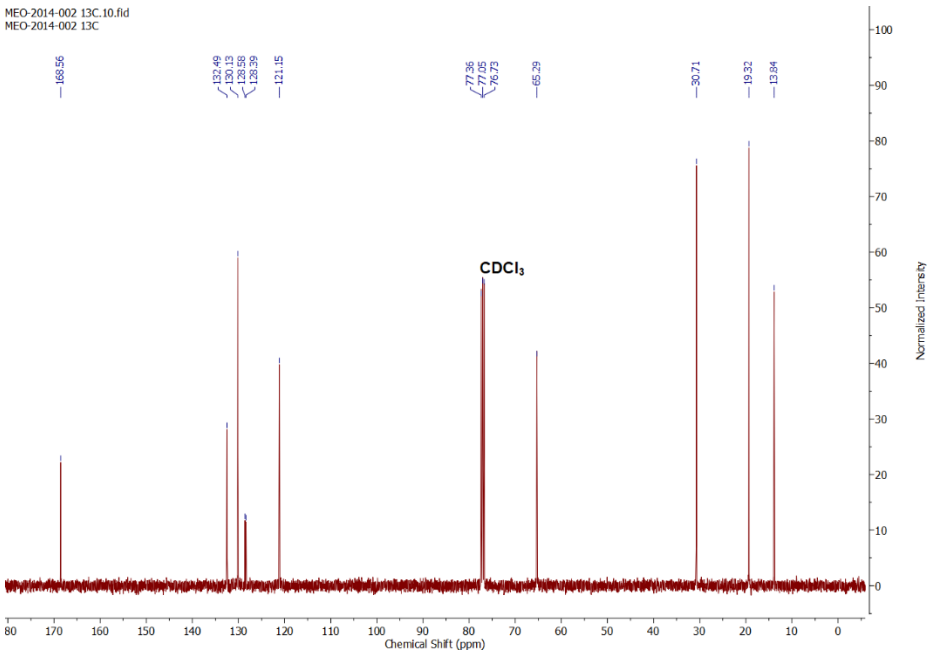

Figure A. 2. ^{13}C-NMR spectrum of **P1**.

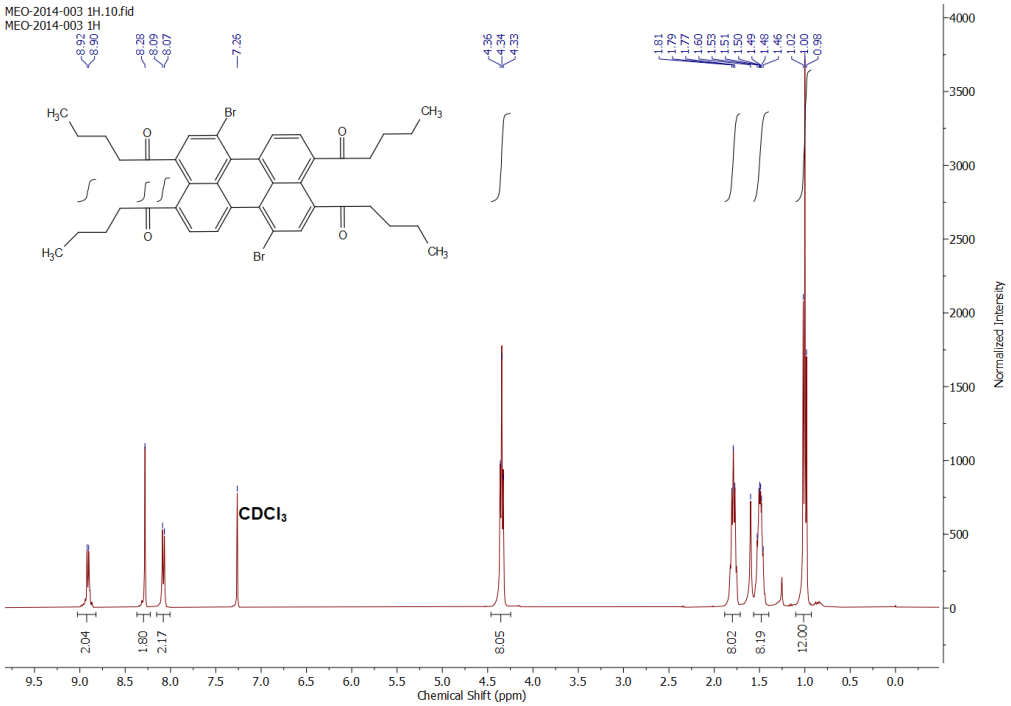

Figure A. 3. ^{1}H-NMR spectrum of **P2**.

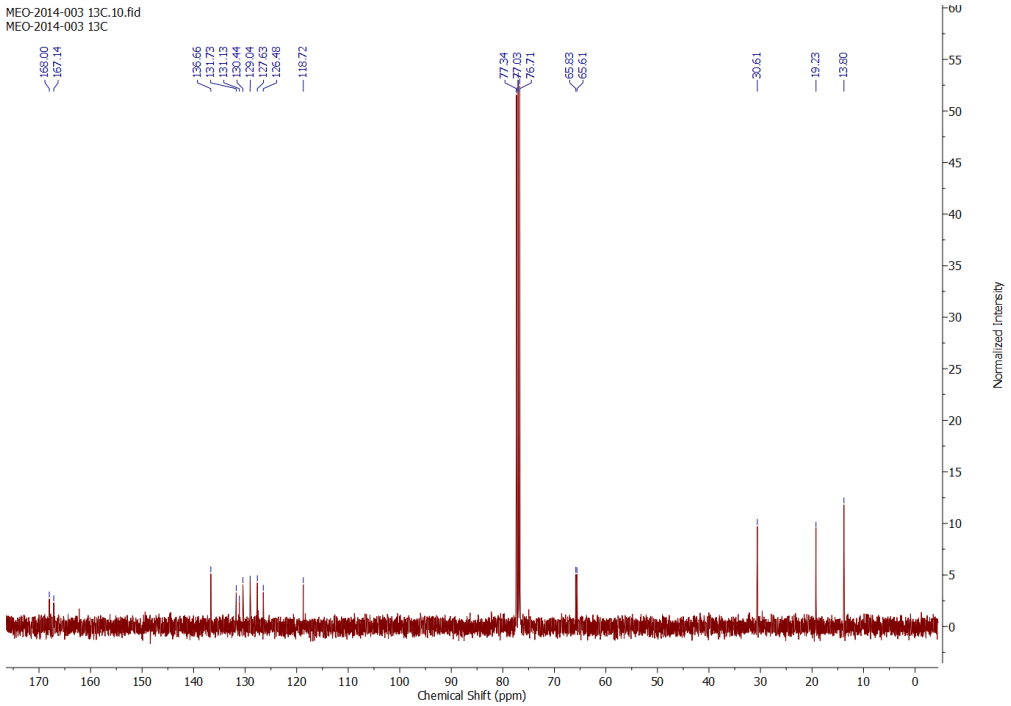

Figure A. 4. ^{13}C-NMR spectrum of **P2**.

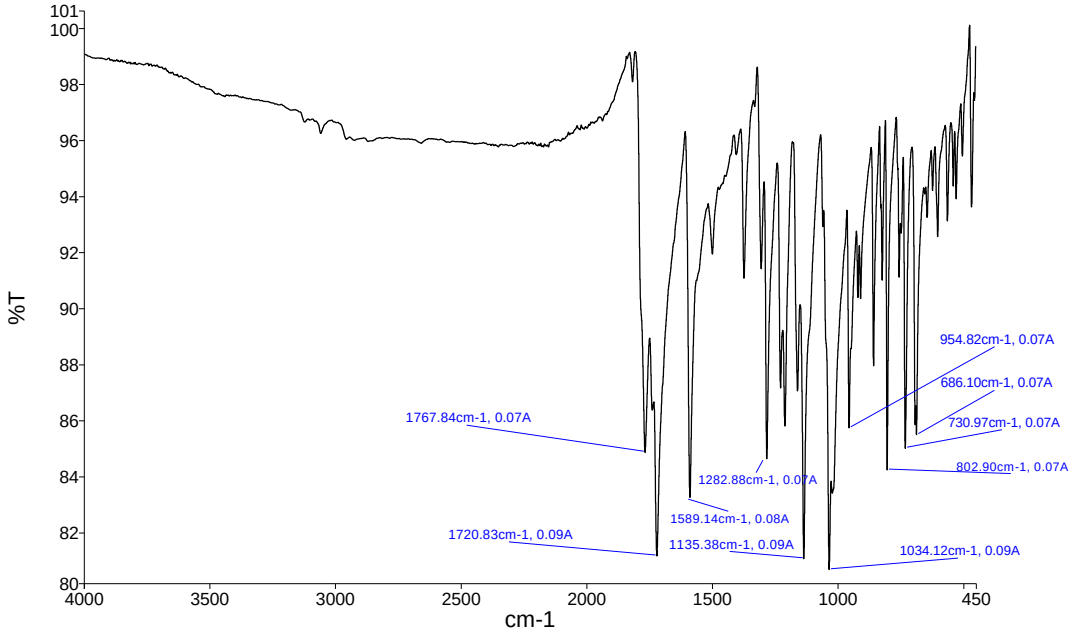

Figure A. 5. FTIR spectrum of 1,7-dibromoperylene-3,4,9,10-tetracarboxylic bisanhydride **P3**

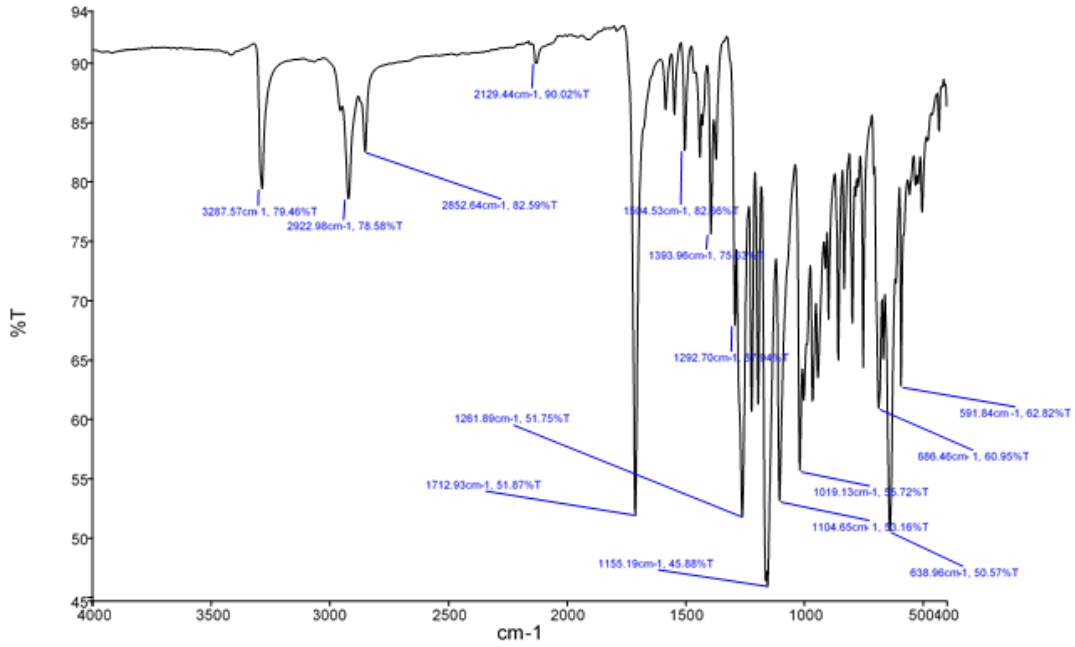

Figure A. 6. FTIR spectrum of 1,7-dibromoperylene-3,4,9,10-tetracarboxylicpropargyl ester **P4**

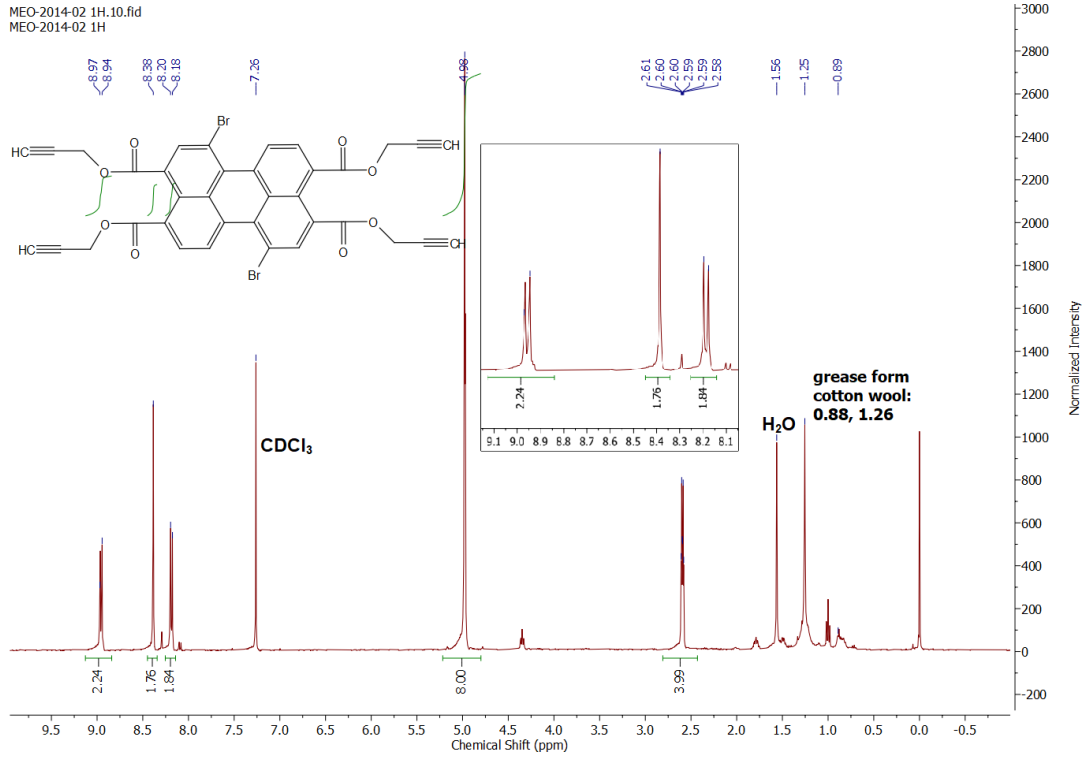

Figure A. 7. ^{1}H-NMR spectrum of **P4**.

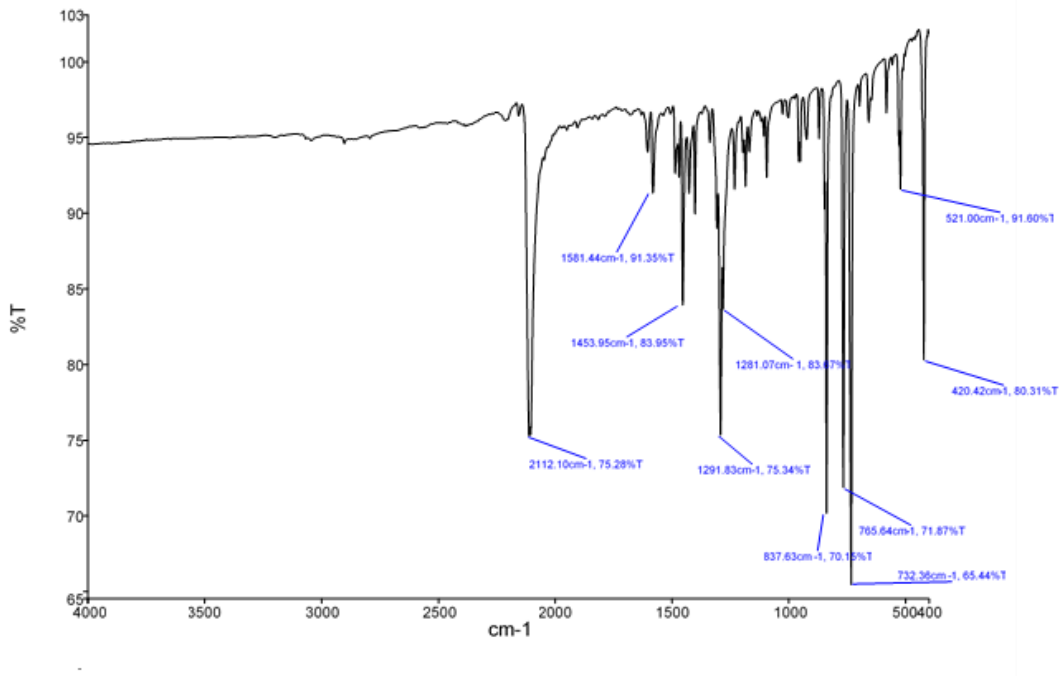

Figure A. 8. FTIR spectrum of 2-azidoflourene **P5**

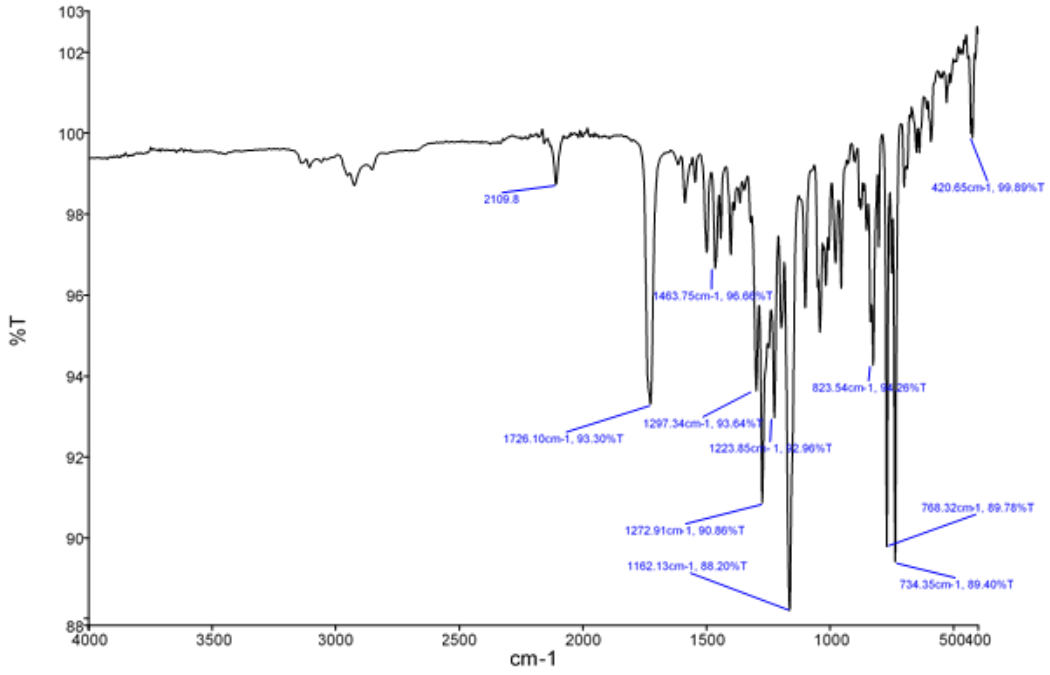

Figure A. 9. FTIR spectrum of **P6**

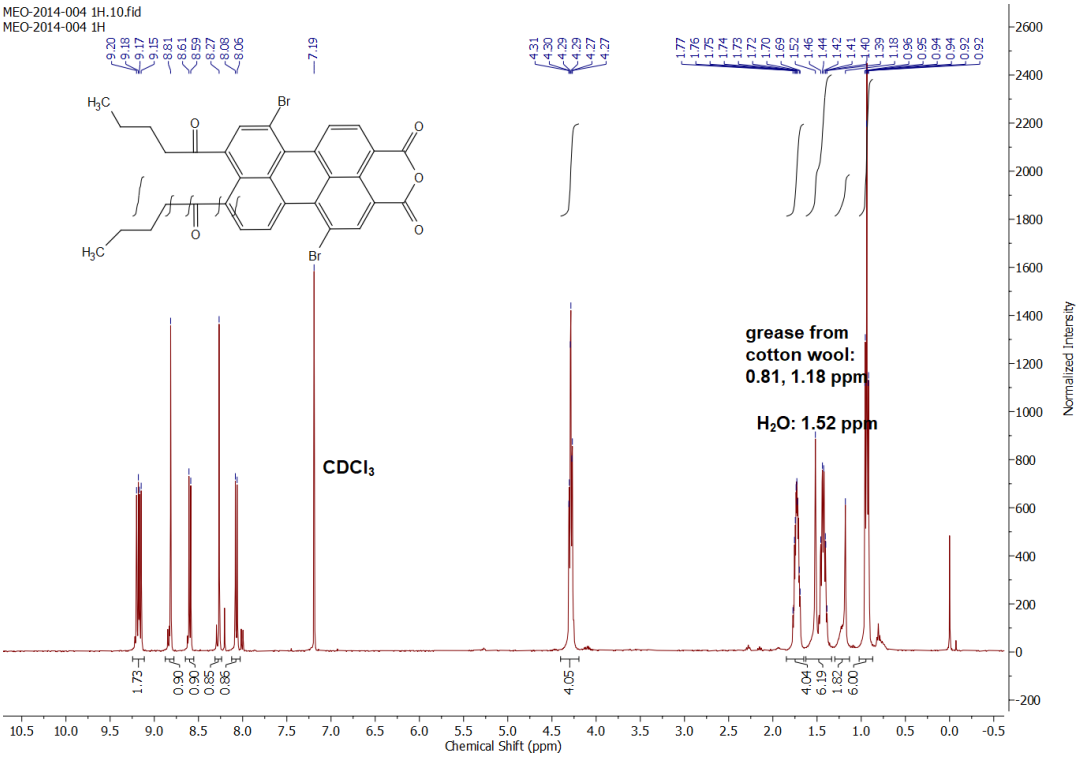

Figure A. 10. ^{1}H-NMR spectrum of **P8**.

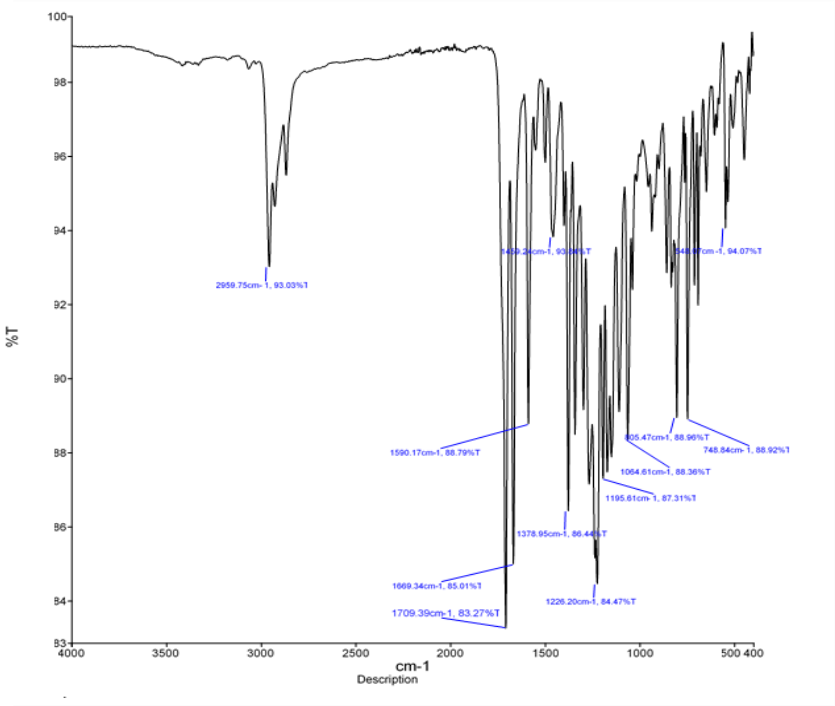

Figure A. 11. FTIR spectrum of N-(2,6-diisopropylphenyl)-1,7-dibromo-perylene-3,4,9,10-tetracarboxy monoimide dibutylester **P9**

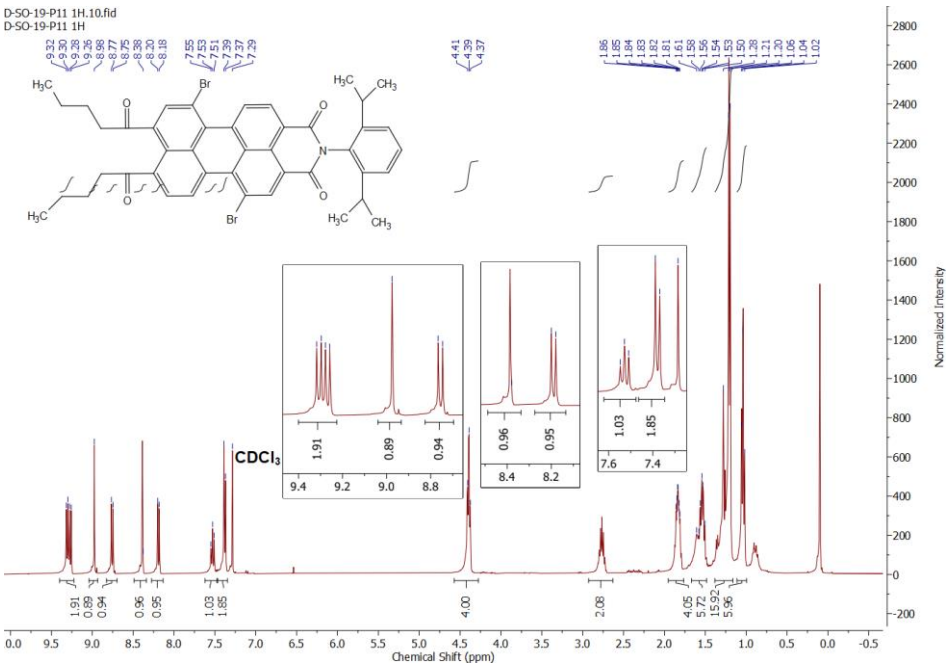

Figure A. 12. ^{1}H-NMR spectrum of **P9**.

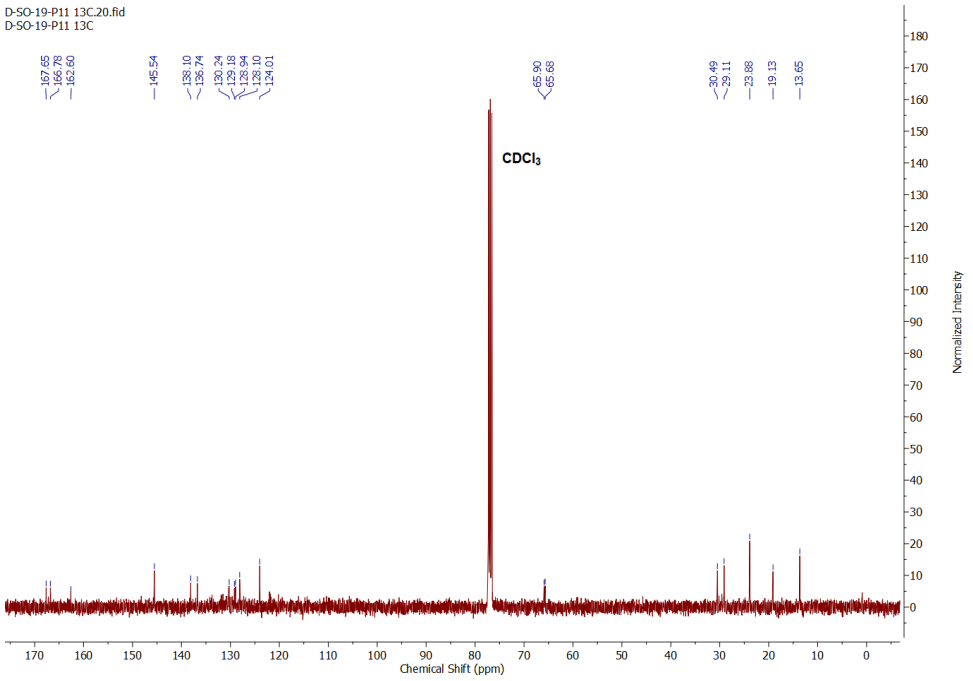

Figure A. 13. ^{13}C-NMR spectrum of **P9**.

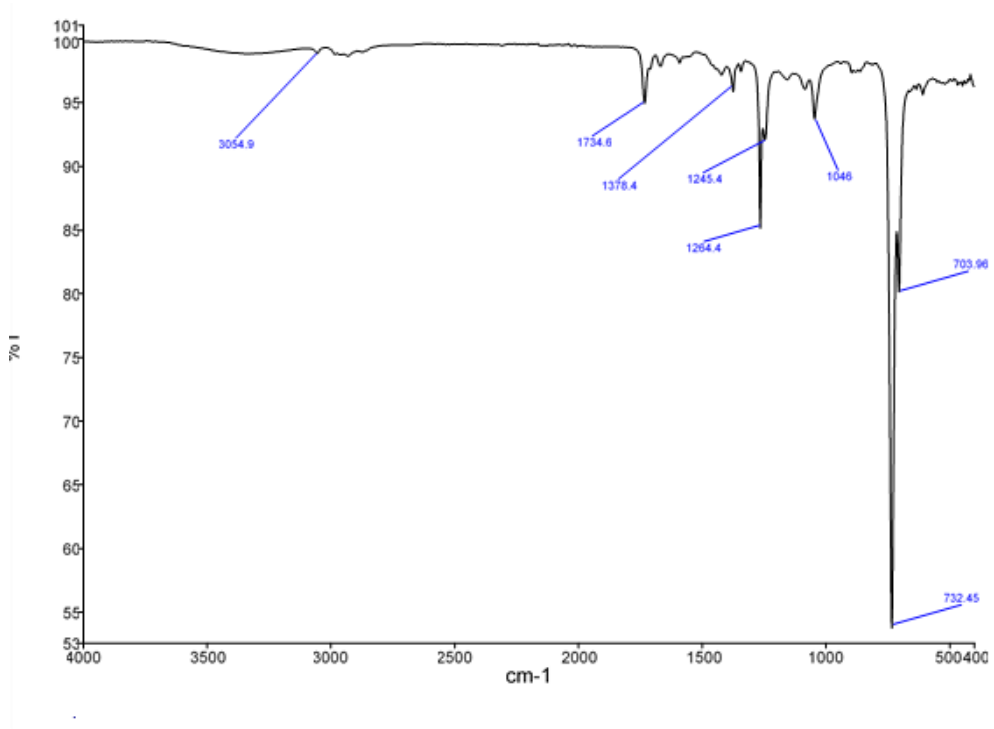

Figure A. 14. FTIR spectrum of 1,7-dibromoperylene monoimide monoanhydride **P10**

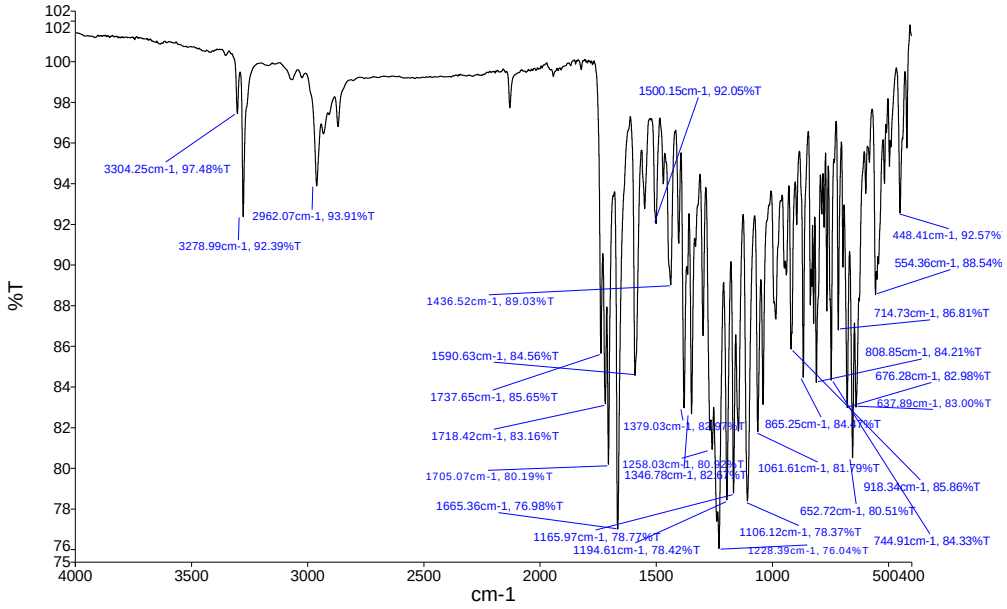

Figure A. 15. FTIR spectrum of N-(2,6-diisopropylphenyl)-1,7-dibromoperylene-3,4,9,10-tetracarboxy monoimide dipropargyl ester **P11**

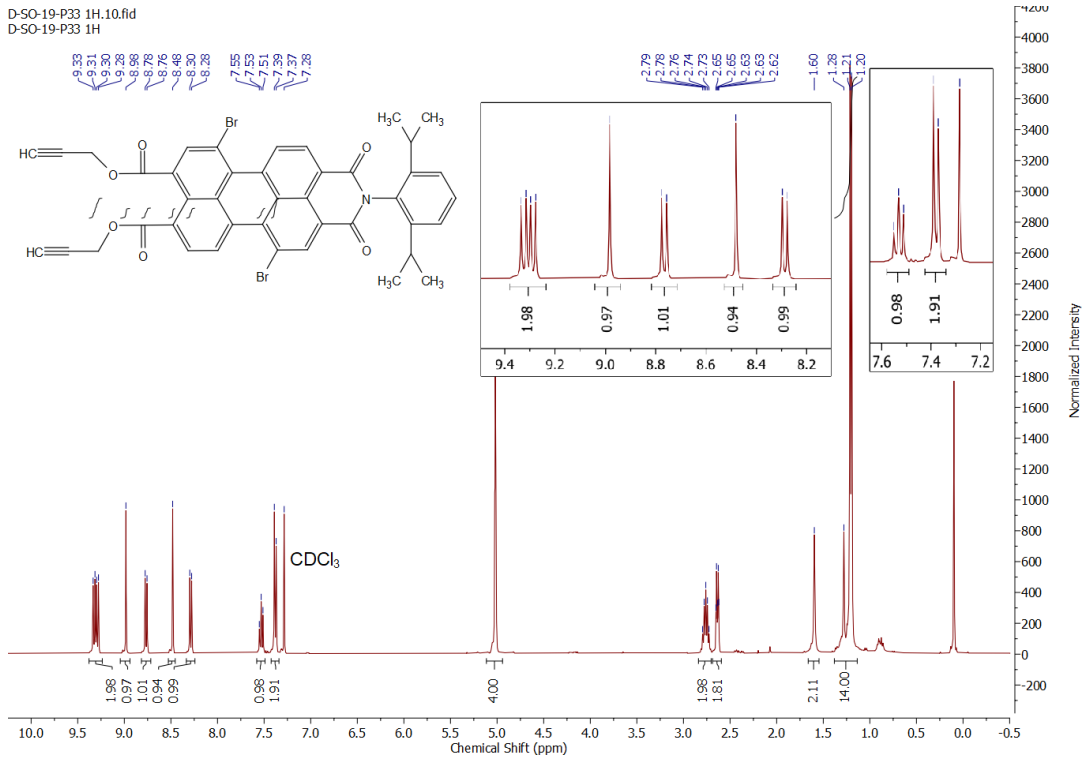

Figure A. 16. ^{1}H-NMR spectrum of **P11**.

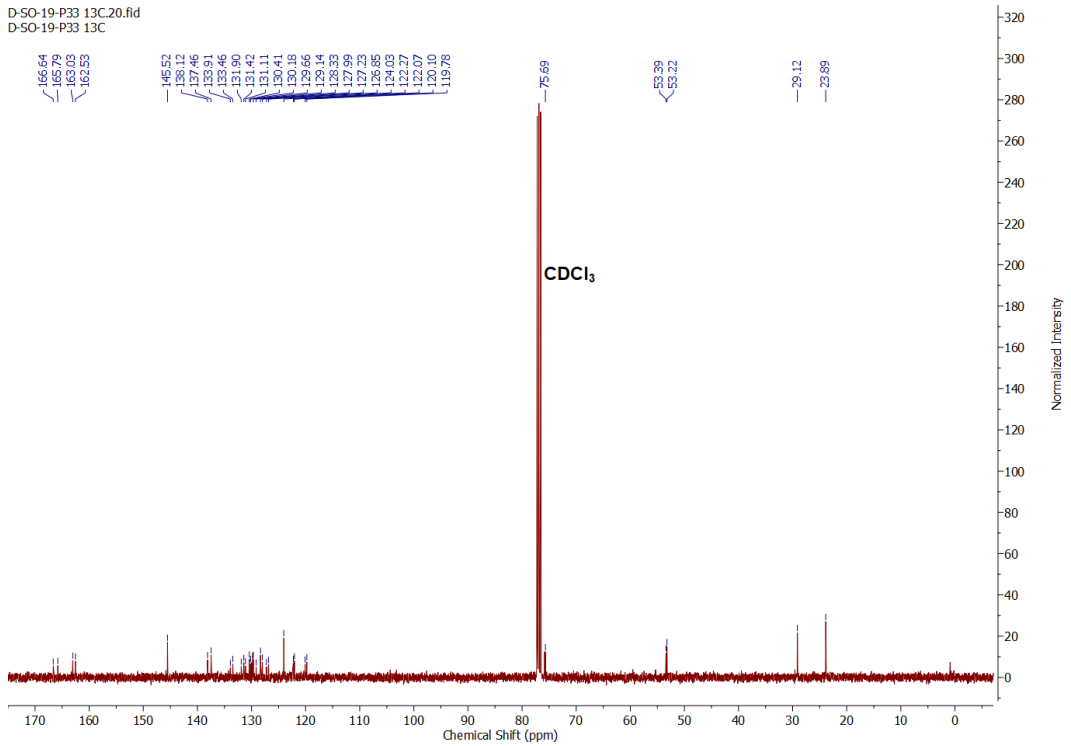

Figure A. 17. ^{13}C-NMR spectrum of **P11**.

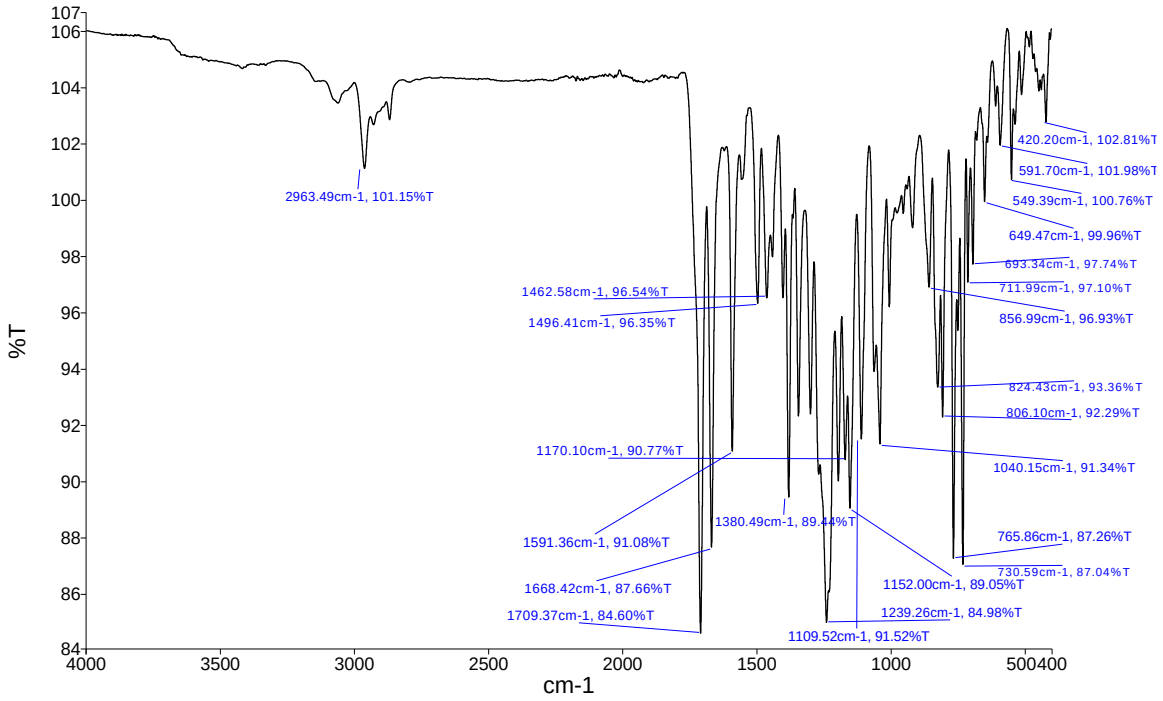

Figure A. 18. FTIR spectrum of **P12**

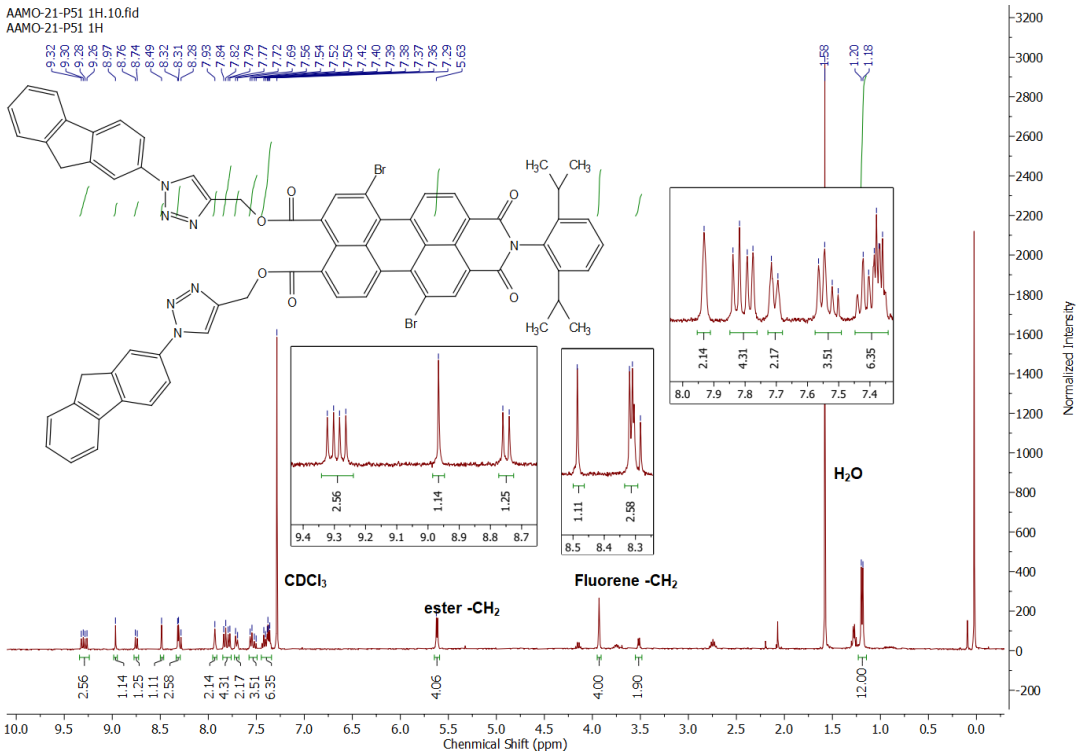

Figure A. 19. ^{1}H-NMR spectrum of **P12**.

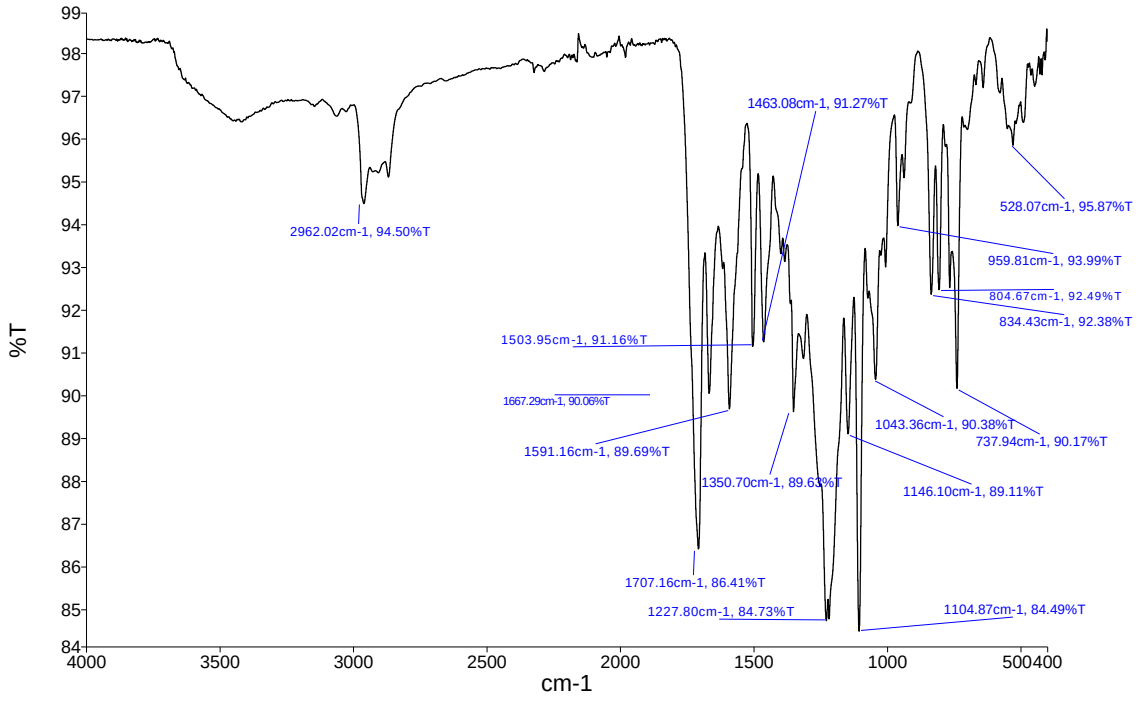

Figure A. 20. FTIR spectrum of **P13**

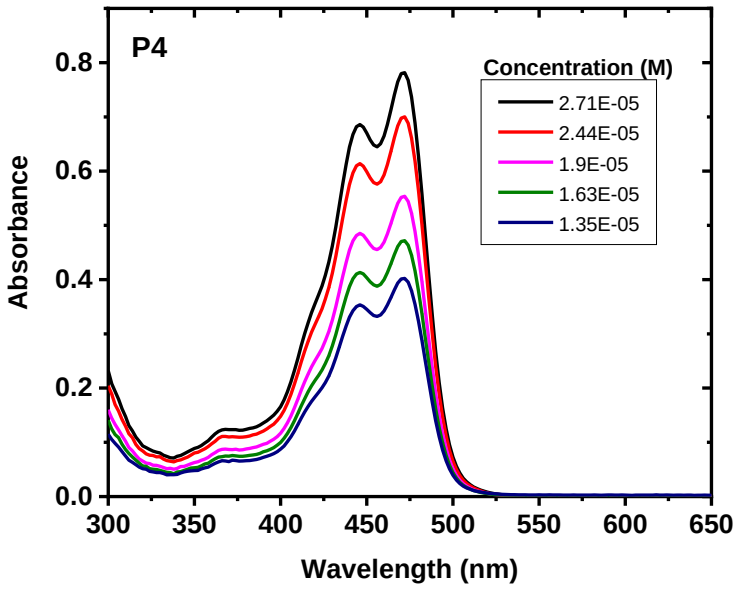

Figure A. 21. Absorption spectra of **P4** in $CHCl_3$

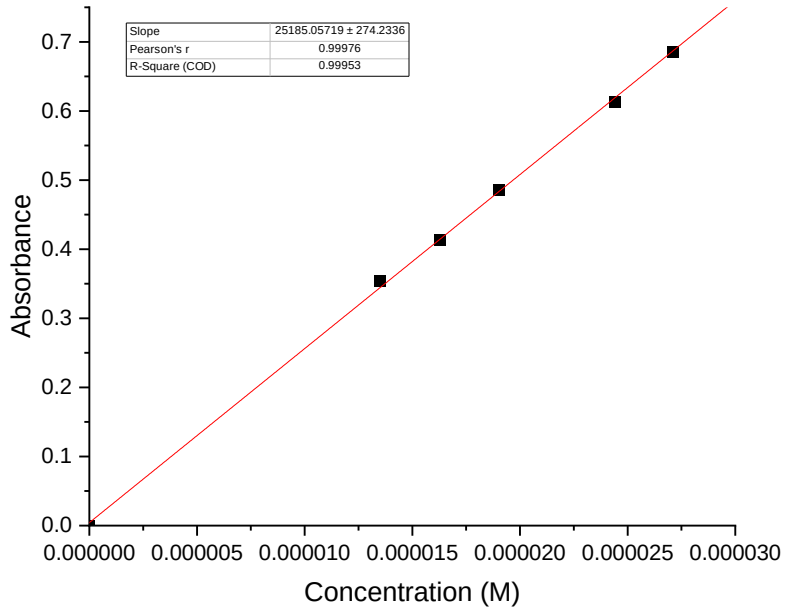

Figure A. 22. Absorbance vs. concentration graph of **P4** at 446 nm in $CHCl_3$

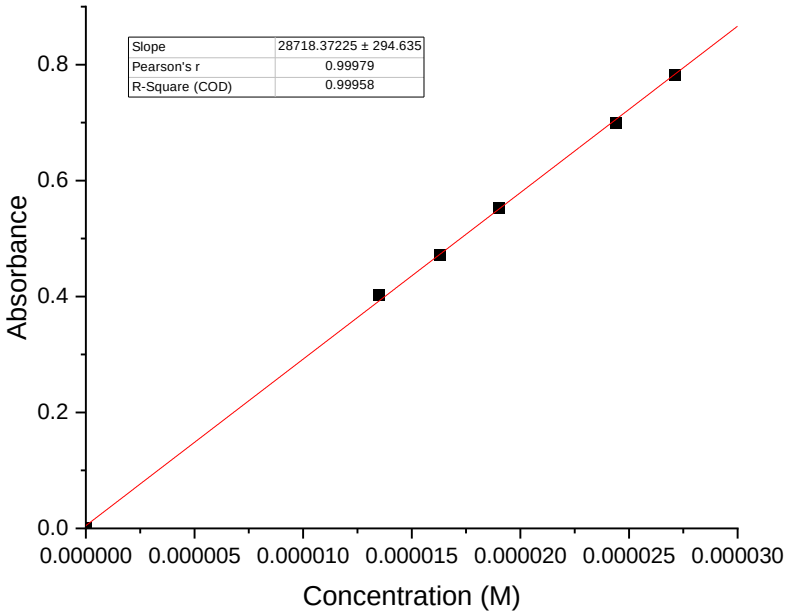

Figure A. 23. Absorbance vs. concentration graph of **P4** at 472 nm in $CHCl_3$

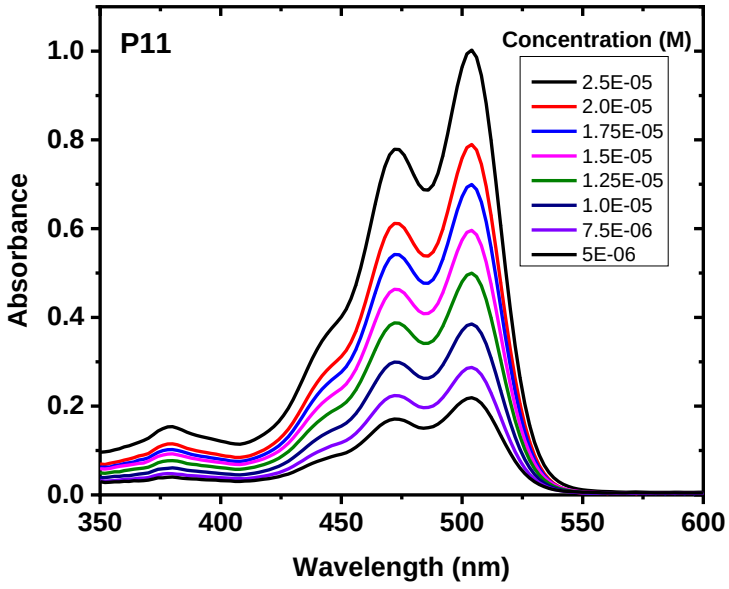

Figure A. 24. Absorption spectra of **P11** in $CHCl_3$

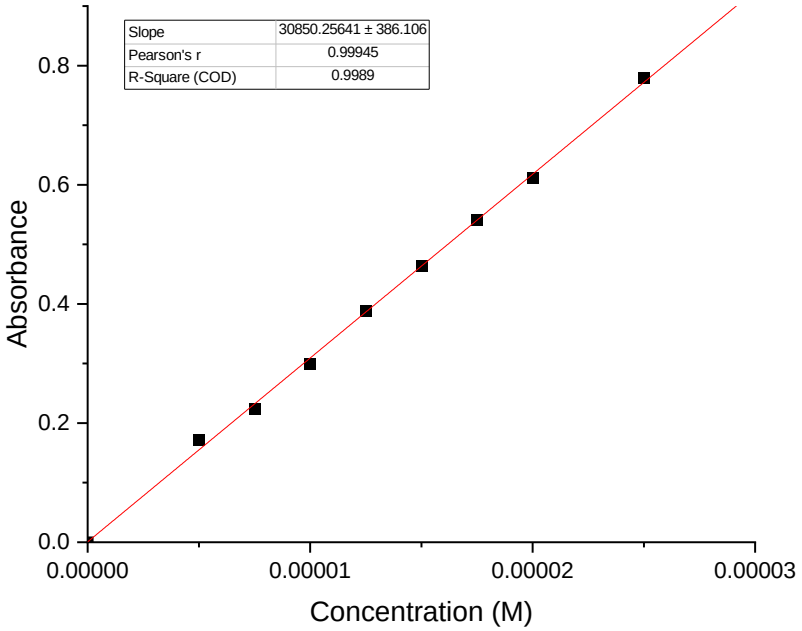

Figure A. 25. Absorbance vs. concentration graph of **P11** at 472 nm in $CHCl_3$

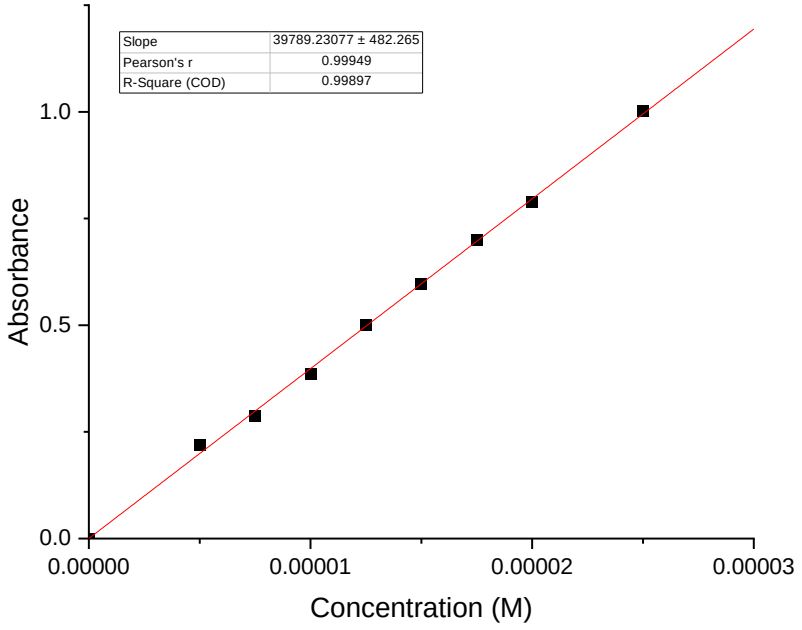

Figure A. 26. Absorbance vs. concentration graph of **P11** at 504 nm in $CHCl_3$

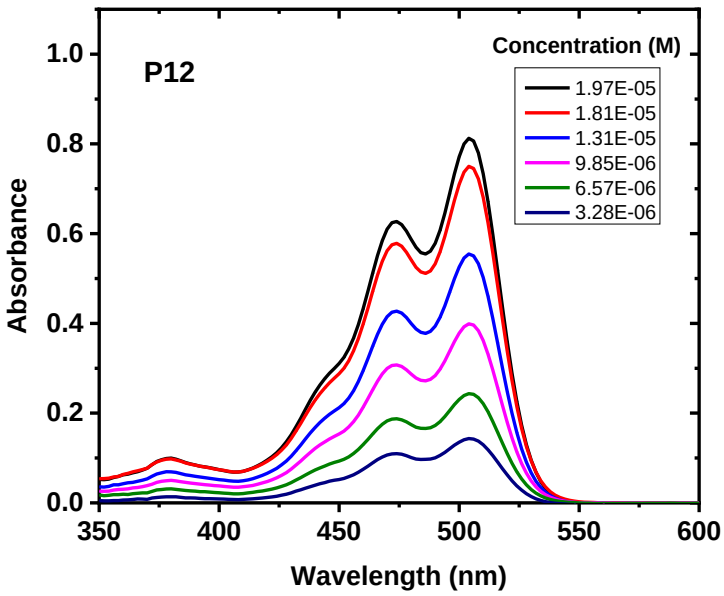

Figure A. 27. Absorption spectra of **P12** in $CHCl_3$

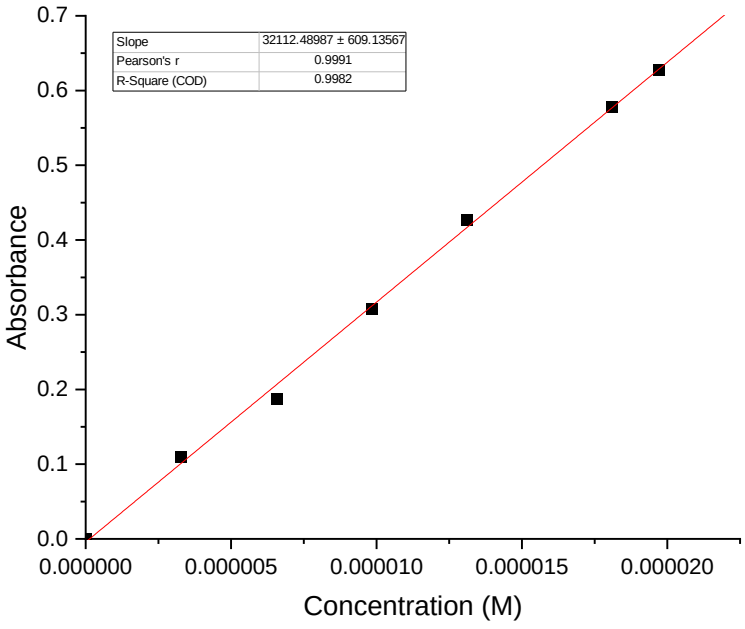

Figure A. 28. Absorbance vs. concentration graph of **P12** at 474 nm in $CHCl_3$.

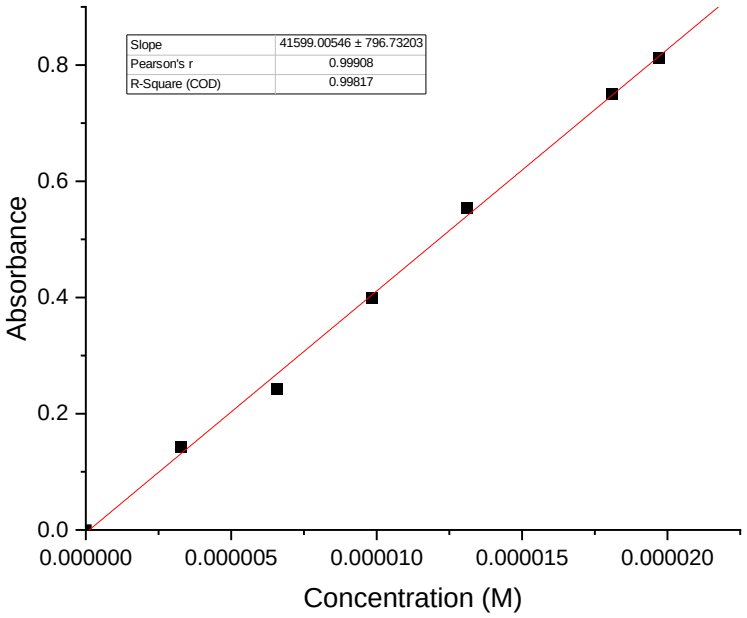

Figure A. 29. Absorbance vs. concentration graph of **P12** at 504 nm in $CHCl_3$.